



## Early Pleistocene obliquity-scale pCO<sub>2</sub> variability at ~1.5 million years ago

Kelsey A. Dyez<sup>1\*</sup><sup>a</sup>, Bärbel Hönlisch<sup>1,2</sup>, Gavin A. Schmidt<sup>3</sup>

<sup>1</sup>Lamont-Doherty Earth Observatory, Columbia University, Palisades, NY, USA. Department of Earth and Environmental Sciences of Columbia University, New York, NY, USA <sup>3</sup>NASA Goddard Institute for Space Studies, New York, NY, USA

\* Corresponding author: Kelsey Dyez (kdyez@umich.edu)

<sup>a</sup> Now at University of Michigan, Ann Arbor, MI, USA. Department of Earth and Environmental Sciences.

### Key points:

1. Early Pleistocene pCO<sub>2</sub> roughly varied with obliquity cycles.
2. Interglacial pCO<sub>2</sub> was similar in the early and late Pleistocene; glacial pCO<sub>2</sub> declined over the mid-Pleistocene transition.
3. Discrepancies between  $\delta^{11}\text{B}$  values and corresponding pCO<sub>2</sub> estimates from *G. ruber* and *T. sacculifer* are observed and may indicate evolving vital effects.

This article has been accepted for publication and undergone full peer review but has not been through the copyediting, typesetting, pagination and proofreading process which may lead to differences between this version and the Version of Record. Please cite this article as doi: 10.1029/2018PA003349

## Abstract

In the early Pleistocene, global temperature cycles predominantly varied with ~41-kyr (obliquity-scale) periodicity. Atmospheric greenhouse gas concentrations likely played a role in these climate cycles; marine sediments provide an indirect geochemical means to estimate early Pleistocene CO<sub>2</sub>. Here we present a boron isotope-based record of continuous high-resolution surface ocean pH and inferred atmospheric CO<sub>2</sub> changes. Our results show that, within a window of time in the early Pleistocene (1.38-1.54 Ma), pCO<sub>2</sub> varied with obliquity, confirming that, analogous to late Pleistocene conditions, the carbon cycle and climate co-varied at ~1.5 Ma. Pairing the reconstructed early Pleistocene pCO<sub>2</sub> amplitude ( $92 \pm 13 \mu\text{atm}$ ) with a comparably smaller global surface temperature glacial/interglacial amplitude ( $3.0 \pm 0.5 \text{ K}$ ), yields a surface temperature change to CO<sub>2</sub> radiative forcing ratio of  $S_{[\text{CO}_2]} \sim 0.75 (\pm 0.5) \text{ }^\circ\text{C}/\text{Wm}^{-2}$ , as compared to the late Pleistocene  $S_{[\text{CO}_2]}$  value of  $\sim 1.75 (\pm 0.6) \text{ }^\circ\text{C}/\text{Wm}^{-2}$ . This direct comparison of pCO<sub>2</sub> and temperature implicitly incorporates the large ice sheet forcing as an internal feedback and is not directly applicable to future warming. We evaluate this result with a simple climate model, and show that the presumably thinner, though extensive, northern hemisphere ice sheets would increase surface temperature sensitivity to radiative forcing. Thus, the mechanism to dampen actual temperature variability in the early Pleistocene more likely lies with Southern Ocean circulation dynamics or antiphase hemispheric forcing. We also compile this new carbon dioxide record with published Pliocene δ<sup>11</sup>B records using consistent boundary conditions and explore potential reasons for the discrepancy between Pliocene pCO<sub>2</sub> based on different planktic foraminifera.

## 1. Introduction

The Pleistocene Epoch was characterized by a sequence of glacial/interglacial climate oscillations that are recorded in geochemical records from deep-sea sediments, continental deposits, and ice cores [e.g., *Imbrie et al.*, 1984; *Lüthi et al.*, 2008; *Joannin et al.*, 2010].

These records show that Earth's surface temperature covaried with the dominant periodicities of Earth's orbit around the Sun: orbital precession, obliquity and/or eccentricity.

Nevertheless, understanding how the climate system responds to and amplifies the initial orbital insolation forcing is a long-standing problem in the field of paleoclimatology [*Hays et al.*, 1976; *Hansen et al.*, 1984; *Imbrie et al.*, 1992; *Hansen et al.*, 2005]. High-resolution records of temperature and greenhouse gas concentrations are of paramount value to elucidate the pattern and drivers of global climate change, yet continuous high-resolution ice core records of trapped ancient air are thus far restricted to the late Pleistocene (0.8 Ma to present) [e.g., *Lüthi et al.*, 2008]. Ancient air inclusions in late Pleistocene ice-cores suggest that the partial pressure of atmospheric CO<sub>2</sub> (pCO<sub>2</sub>) lagged an initial temperature perturbation [*Fischer et al.*, 2010] such that radiative greenhouse gas forcing at most amplified the orbital pacing of Pleistocene climate, via carbon cycle feedbacks, deep-sea carbon storage and release, and radiative forcing [*Anderson et al.*, 2009; *Shakun et al.*, 2012]. During the early Pleistocene (2.6-1.0 Ma), obliquity set the dominant tempo of climate, and cold glacial intervals were shorter and less extreme [e.g., *Lisiecki and Raymo*, 2005; *Huybers*, 2007]. The presence of North American glacial tills indicates that early Pleistocene ice sheets at glacial maxima extended as far south as 39°N [*Roy et al.*, 2004; *Balco and Rovey*, 2010].

In the early Pleistocene, both tropical [e.g., *Herbert et al.*, 2010] and extratropical [e.g., *Lawrence et al.*, 2009; *Martínez-García et al.*, 2010] sea-surface temperature (SST) records reveal long-term cooling in both glacial and interglacial intervals (i.e., 2 K cooler in tropics and 3-4 K cooler in high latitudes). At the same time, the glacial-interglacial amplitude of surface temperature increased from ~3 K to ~5 K from the early to late Pleistocene, as glacial temperatures cooled [*Lawrence et al.*, 2009; *Herbert et al.*, 2010; *Martínez-García et al.*, 2010]. The gradual cooling of the early Pleistocene glacials culminated in the mid-Pleistocene transition (MPT) when surface temperature and benthic  $\delta^{18}\text{O}$  records shifted from a dominant 41-kyr periodicity to ~100-kyr pacing, albeit without an obvious corresponding change in the periodicity of incoming solar radiation [*Ruddiman et al.*, 1989; *Clark et al.*, 2006]. Mechanisms put forward to explain this shift in climate response at the MPT include

the exposure of crystalline bedrock and thus a more solid foundation for the Laurentide ice sheet [e.g. *Clark and Pollard, 1998*], changing ocean dynamics that provide increased precipitation available to build larger northern hemisphere ice sheets [*Tziperman and Gildor, 2003; McClymont et al., 2008*], or the consequence of long-term cooling and glacial CO<sub>2</sub> drawdown as a result of iron fertilization and/or reduced ocean ventilation which sequestered more carbon in the deep ocean [*Köhler and Bintanja, 2008; Hönisch et al., 2009; Chalk et al., 2017*]. Filling in the early Pleistocene pCO<sub>2</sub> data gaps with orbitally-resolved records will help to evaluate these hypotheses.

While efforts to extend the continuous ice-core pCO<sub>2</sub> record to the early Pleistocene are being actively pursued [*Fischer et al., 2013; Higgins et al., 2015; Witze, 2015; Bibby et al., 2016*], such records are not yet available. However, marine sediments provide an opportunity to estimate pCO<sub>2</sub> changes from earlier and warmer periods of Earth history. One leading method for estimating atmospheric pCO<sub>2</sub> from marine sediments is via the boron isotope ratio ( $\delta^{11}\text{B}$ ) recorded in the shells of planktic foraminifera. Shell  $\delta^{11}\text{B}$  is primarily controlled by seawater acidity (i.e., pH). CO<sub>2</sub> exchanges between the atmosphere and the surface ocean depend on the partial pressure in each medium after Henry's law. Higher atmospheric pCO<sub>2</sub> results in more CO<sub>2</sub> dissolved in seawater and thereby lowers surface ocean pH. The pH dependency of the relative abundance and isotopic signature of the two main species of boron in seawater (borate ion and boric acid) permits the  $\delta^{11}\text{B}$  value of marine carbonates to reflect such changes in ocean pH (see Methods). Several studies have validated this proxy relative to ice core pCO<sub>2</sub> in the late Pleistocene [*Hönisch and Hemming, 2005; Henehan et al., 2013; Chalk et al., 2017*] and presented estimates of pCO<sub>2</sub> throughout portions of the Pliocene and Pleistocene [*Hönisch et al., 2009; Bartoli et al., 2011; Henehan et al., 2013; Martínez-Botí et al., 2015a; Chalk et al., 2017*]. Here we present estimates of pCO<sub>2</sub> based on new  $\delta^{11}\text{B}$  measurements in planktic foraminifera shells within a time window spanning Marine Isotope Stages (MIS) 44-52 (1.38-1.54 Ma).

Published estimates of early Pleistocene pCO<sub>2</sub> are as high as 410 ( $\pm 50$ )  $\mu\text{atm}$  as recorded at ODP Site 999 at 2.37 Ma [*Martínez-Botí et al., 2015a*] and as low as 167 ( $\pm 19$ )  $\mu\text{atm}$  at 0.65 Ma [*Hönisch et al., 2009*]. *Bartoli et al.* [2011] observed that atmospheric pCO<sub>2</sub> decreased in a step-wise fashion at  $\sim 2.7$  Ma, although that particular study did not measure a temperature proxy alongside each of the boron isotope analyses, and used modeled estimates of the

carbonate ion concentration,  $[\text{CO}_3^{2-}]$ , as the second parameter of the carbonate system to translate pH into reconstructed pCO<sub>2</sub>. Here we present new high-resolution data from ODP 668B in the eastern tropical Atlantic, revise the dataset of *Bartoli et al.* [2011] with new temperature and geochemical constraints, and compile these records in a consistent manner with other published datasets of early Pleistocene pCO<sub>2</sub>. By minimizing the differences in the way boundary conditions are treated among these records, we are able to compare the combined  $\delta^{11}\text{B}$  and pCO<sub>2</sub> records and to describe coherent features of the pCO<sub>2</sub> decline from the late Pliocene through the Pleistocene.

## 2. Materials and Methods

The primary materials for this study come from ODP Site 668B in the eastern tropical Atlantic (4.77°N, 20.93°W, water depth 2693 m, average sedimentation rate 1.5 cm/kyr, Figure 1). The modern surface ocean at this location is near equilibrium with the atmosphere with respect to CO<sub>2</sub> [*Takahashi et al.*, 2009], and previously published late Pleistocene boron isotope data from this site show good agreement with ice core pCO<sub>2</sub> over the past 0.8 Ma [*Hönisch and Hemming*, 2005; *Hönisch et al.*, 2009], making this a promising location for extending the reconstruction of paleo-pCO<sub>2</sub>. Sediment samples were taken from core 668B every 5 cm (3.3 kyr) and were selected to include glacial and interglacial extrema in planktic  $\delta^{18}\text{O}$  [*Hönisch et al.*, 2009]. Samples were washed and picked for the planktic foraminiferal species *Globigerinoides ruber* (300-355  $\mu\text{m}$  size fraction) and *Trilobatus* (formerly *Globigerinoides*) *sacculifer* (>500  $\mu\text{m}$  size fraction), which both live in the surface mixed layer [*Spero et al.*, 2003].

### 2.1 $\delta^{11}\text{B}$ -based pCO<sub>2</sub> estimates

Tests of *T. sacculifer* from the >500  $\mu\text{m}$  size fraction have been validated to reflect surface ocean conditions for pH and pCO<sub>2</sub> estimates [*Hönisch and Hemming*, 2004; 2005; *Hönisch et al.*, 2009]. Although partial dissolution has the potential to lower foraminiferal  $\delta^{11}\text{B}$  in corrosive bottom water, this effect is more pronounced in smaller foraminiferal test size classes [*Hönisch and Hemming*, 2004; *Edgar et al.*, 2015]. The samples in this study come from the largest size fraction and from relatively shallow (2693 modern m depth) waters that are oversaturated with respect to calcite ( $\Omega_{\text{calcite}} = 1.5$ ,  $\Delta[\text{CO}_3^{2-}] \sim 35 \mu\text{mol/kg}$ ). This depth is well above the regional lysocline and partial dissolution is unlikely [*Regenberg et al.*, 2006]. For each  $\delta^{11}\text{B}$  sample, ~30-50 *T. sacculifer* shells were picked, gently crushed and cleaned by

repeated sonication in MilliQ water and methanol, oxidation in a buffered H<sub>2</sub>O<sub>2</sub> solution to remove organic material, and a final weak acid leach [Barker *et al.*, 2003]. Cleaned material was rinsed in MilliQ water, dried to determine the calcite mass after cleaning, and finally dissolved in 2N hydrochloric acid just before analysis. All  $\delta^{11}\text{B}$  samples were measured at the Lamont-Doherty Earth Observatory using a TRITON thermal ionization mass spectrometer in negative mode (N-TIMS). Aliquots of the sample solution containing  $\geq 1$  ng boron were loaded onto outgassed zone-refined rhenium filaments, along with 1  $\mu\text{l}$  of boron-free seawater to enhance ionization (see Hönisch *et al.* [2009] for details). Although analysis of boron isotopes in marine carbonates by the N-TIMS method yields  $\sim 1\%$  higher  $\delta^{11}\text{B}$  values compared to the alternative MC-ICP-MS technique, the relative variability between different samples is similar between the two methods and yield equivalent pH and pCO<sub>2</sub> results when technique-specific  $\delta^{11}\text{B}_{\text{foraminifera}}$  vs.  $\delta^{11}\text{B}_{\text{borate}}$  calibrations are applied [Foster *et al.*, 2013; Farmer *et al.*, 2016]. To minimize analytical uncertainty, each sample analysis was replicated 3-10 (average of 7) times. Of those replicates, individual analyses were rejected if excessive fractionation ( $\delta^{11}\text{B} > 1\%$ ) occurred over the 40 minutes of data acquisition; 14% of analyses were rejected on this basis. The majority of samples yielded 5 or more replicates that met the acceptance criteria. Only one sample, at 1.436 Ma, could not be replicated due to low abundance of *T. sacculifer* shells. Uncertainty in the  $\delta^{11}\text{B}$  measurement was determined as the larger of either: (1) the standard error in valid replicate analyses (i.e.,  $2\sigma = 2 \times \text{standard deviation} / \sqrt{N}$ , where N is the number of accepted replicates) or (2) the  $2\sigma$  uncertainty of an equal number of repeat measurements of an in-house standard of NIST 951 precipitated in CaCO<sub>3</sub> matrix (vaterite). Average  $2\sigma$  uncertainty of all  $\delta^{11}\text{B}$  measurements is  $\pm 0.26\%$ .

The relative abundance of the two aqueous species of boron in seawater, borate ion (B(OH)<sub>4</sub><sup>-</sup>) and boric acid (B(OH)<sub>3</sub>), is pH dependent [Dickson, 1990; Hemming and Hanson, 1992]. The isotopic fractionation between <sup>11</sup>B (natural abundance  $\sim 80\%$ ) and <sup>10</sup>B ( $\sim 20\%$ ) generates a constant  $\delta^{11}\text{B}$  offset between these two aqueous boron species, such that  $\delta^{11}\text{B}$  of borate increases with the relative abundance of borate at higher pH. Since the borate ion is the primary species incorporated into foraminiferal calcite [e.g., Hemming and Hanson, 1992; Branson *et al.*, 2015], *in-situ* seawater pH can be estimated from the  $\delta^{11}\text{B}$  of foraminiferal calcite. The boron isotopic composition of seawater ( $\delta^{11}\text{B}_{\text{sw}}$ ) must also be known; in the modern ocean  $\delta^{11}\text{B}_{\text{sw}}$  is  $39.61 (\pm 0.04)\%$  [Foster *et al.*, 2010]. While this value likely increased over the Cenozoic through shifts in weathering and/or volcanic emissions

[Lemarchand *et al.*, 2000], attempts to reconstruct  $\delta^{11}\text{B}_{\text{sw}}$  over the past 5 million years have yielded disparate results. The combined evidence, whether from benthic foraminiferal  $\delta^{11}\text{B}$  alongside modeled ocean pH [Raitzsch and Hönisch, 2013] or paired  $\delta^{11}\text{B}$  measurements in the water column coupled with assumptions about water column pH gradient [Pearson and Palmer, 2000; Greenop *et al.*, 2017], shows no clear indication of a trend in  $\delta^{11}\text{B}_{\text{sw}}$  over the past 5 Ma (Figure S1). As the residence time of boron in seawater is long (11-17 My), the maximum rate of change over this time period is likely  $<0.1\%$  per million years [Lemarchand *et al.*, 2000]; hence, we apply the modern  $\delta^{11}\text{B}_{\text{sw}}$  value (39.61‰) to all Plio-Pleistocene samples and increase the uncertainty of this assumed value at a constant rate of  $0.1\%/Myr$  (Figure S1). Ocean pH is then determined via:

$$\text{pH} = \text{p}K_{\text{B}}^* - \log\left[-(\delta^{11}\text{B}_{\text{sw}} - \delta^{11}\text{B}_{\text{borate}}) / \{\delta^{11}\text{B}_{\text{sw}} - ({}^{11-10}K_{\text{B}} * \delta^{11}\text{B}_{\text{borate}}) - 1000 * ({}^{11-10}K_{\text{B}} - 1)\}\right] \quad (\text{Eq. 1})$$

where  $\text{p}K_{\text{B}}^*$  is the dissociation constant for boric acid at *in situ* temperature, salinity and pressure [Dickson, 1990; Millero, 1995], and the aqueous boron isotope fractionation factor is  ${}^{11-10}K_{\text{B}} = 1.0272 (\pm 0.0006)$  [Klochko *et al.*, 2006]. Application of the boron isotope proxy also requires an understanding of any physiological or vital effects on the pH of the foraminiferal microenvironment, which have been documented for a variety of species. Here we use a calibration specifically established for *T. sacculifer*, which includes culture and core top sediment samples of *T. sacculifer* measured via N-TIMS at LDEO and Stony Brook [Sanyal *et al.*, 2001; Hönisch and Hemming, 2004; 2005; Hönisch *et al.*, 2009]. Values measured at Stony Brook have been cross-calibrated with N-TIMS [Hönisch *et al.*, 2009] and a constant offset of  $-1.1\%$  has been applied to all data measured in Stony Brook to shift them onto data measured on the N-TIMS at LDEO. A linear York fit [York *et al.*, 2004] calculated for laboratory cultured specimens grown across a range of pH values includes uncertainties in the  $\delta^{11}\text{B}_{\text{calcite}}$  measurement and the  $\delta^{11}\text{B}_{\text{borate}}$  calculation for experimental seawater. This regression is then adjusted by a constant intercept offset of  $-0.84\%$  so as to pass through the average of core top *T. sacculifer*  $\delta^{11}\text{B}_{\text{calcite}}$  data and the corresponding preindustrial  $\delta^{11}\text{B}_{\text{borate}}$  (Figure 2 and Table S1). The offset accounts for the difference between cultured and sedimentary specimens, which is likely due to the gametogenic calcite crust that *T. sacculifer* secretes at greater water depths in the ocean [Bé, 1980]. The resulting calibration for *T. sacculifer* in the  $>500 \mu\text{m}$  size fraction (measured on N-TIMS), including  $2\sigma$  uncertainty, is:

$$\delta^{11}\text{B}_{\text{borate}} = [\delta^{11}\text{B}_{T. \text{sacculifer N-TIMS}} - 6.42 (\pm 1.64)] / 0.73 (\pm 0.08) \quad (\text{Eq. 2})$$

In comparison, the published calibration for *T. sacculifer* using the MC-ICP-MS technique [Martínez-Botí *et al.*, 2015b] is:

$$\delta^{11}\text{B}_{\text{borate}} = [\delta^{11}\text{B}_{T. \text{sacculifer MC-ICP-MS}} - 3.60 (\pm 0.72)] / 0.83 (\pm 0.04) \quad (\text{Eq. 3})$$

While the slope of the MC-ICP-MS  $\delta^{11}\text{B}_{\text{borate}}$  calibration is steeper (0.83 vs. 0.73), the additional culture data points in our N-TIMS calibration (5 instead of 3) allow for a more precise calibration. The primary difference between these technique-specific calibrations is the intercept value, which is the most important factor in aligning pH estimates from N-TIMS and MC-ICP-MS  $\delta^{11}\text{B}$  analyses [Foster *et al.*, 2013].

## 2.2 Temperature, salinity, and pressure estimates

Here we present new Mg/Ca-based estimates of SST using *G. ruber* from Site 668B and *T. sacculifer* from Site 999A. Due to the limited availability of large *T. sacculifer* tests from Site 668B, tests of *G. ruber* (*sensu stricto*, white) were used to estimate surface ocean temperature for this site. *Globigerinoides ruber* shares the near-surface ocean habitat of large *T. sacculifer* specimens [Ravelo and Fairbanks, 1992; Spero *et al.*, 2003; Farmer *et al.*, 2007]. For Site 668B, 40-60 *G. ruber* tests were picked from the 300-355  $\mu\text{m}$  size fraction. For Site 999A, 40 shells of *T. sacculifer* were picked from the 425-500  $\mu\text{m}$  size fraction, the same species and size fraction of planktic foraminifera as the original  $\delta^{11}\text{B}$  data [Bartoli *et al.*, 2011]. Shells were then gently broken and cleaned following established protocol including both the oxidative and reductive steps [Boyle and Keigwin, 1985; Mashiotto *et al.*, 1999]. Inclusion of the reductive step is generally preferred for Mg/Ca analysis as it is more effective at removing high-Mg contaminants such as authigenic metals precipitated after deposition in the sediment, even though it has been shown to lower Mg/Ca values beyond their original value [Martin and Lea, 2002; Weldeab *et al.*, 2006]. Because the Mg/Ca-temperature calibration we use [Anand *et al.*, 2003] is based on sediment trap samples and therefore did not apply reductive cleaning, we account for reductive cleaning bias by adding 10% to the measured Mg/Ca ratio of our samples [Martin and Lea, 2002]. Mg/Ca ratios were measured via ICP-MS (iCAP-Q) at the Lamont-Doherty Earth Observatory. The  $2\sigma$  standard error for repeated

measurements of internal foraminifer reference standards is  $\pm 2.2\%$ , or  $\sim \pm 0.08$  mmol/mol. This SST calibration carries a larger uncertainty ( $\pm 2.4$  K,  $2\sigma$ ) than that of the Mg/Ca measurement uncertainty ( $\sim \pm 0.24$  K) and we adopt the larger calibration uncertainty for seawater temperature estimates. As our samples are derived from a time period when the Mg/Ca value of seawater ( $\text{Mg}/\text{Ca}_{\text{sw}}$ ) was likely lower than the modern value of 5.2 mmol/mol, a correction is needed for this change in seawater constituents [Delaney *et al.*, 1985; Fantle and DePaolo, 2005; 2006; Medina-Elizalde *et al.*, 2008; O'Brien *et al.*, 2014; Evans *et al.*, 2016]. To facilitate this correction,  $\text{Mg}/\text{Ca}_{\text{sw}}$  values are taken from reported pore fluid chemistry and numerical modeling [Figure S7, Fantle and DePaolo, 2006]. This  $\text{Mg}/\text{Ca}_{\text{sw}}$  dataset is within the uncertainty of  $\text{Mg}/\text{Ca}_{\text{sw}}$  values estimated from fluid inclusions in marine evaporites, the most recent of which is Messinian in age (5-6 Ma,  $\text{Mg}/\text{Ca}_{\text{sw}} \sim 3.6$  mmol/mol) [Horita *et al.*, 2002; Brennan *et al.*, 2013]. If data from marine evaporite fluid inclusions were considered alone, and  $\text{Mg}/\text{Ca}_{\text{sw}}$  values are linearly extrapolated from 5.5 Ma to present, the resulting SST would be  $\sim 0.7$  K lower and calculated  $\text{pCO}_2$  would be  $\sim 5$   $\mu\text{atm}$  higher. The SST calibration we use includes the power-law modification suggested by Evans and Müller [2012] and the *T. sacculifer* exponential H-value of 0.41 [Delaney *et al.*, 1985; Evans and Müller, 2012]:

$$\text{SST } (^{\circ}\text{C}) = \ln\left[\frac{(\text{Mg}/\text{Ca})_{\text{calcite}} * ((\text{Mg}/\text{Ca})_{\text{sw}}^{t=0})^H}{0.38 * ((\text{Mg}/\text{Ca})_{\text{sw}}^t)^H}\right] / 0.09$$

(Eq. 4)

where  $(\text{Mg}/\text{Ca})_{\text{sw}}^t$  is the Mg/Ca ratio of seawater at time  $t$ . This approach is commonly used to reconstruct temperature in this time period [e.g., Martínez-Botí *et al.*, 2015a; Chalk *et al.*, 2017]. The correction for dissolution with depth [Dekens *et al.*, 2002] is omitted for all records in this study, as all study sites are well above the regional tropical Atlantic lysocline (4200 m water depth), and bottom water is saturated with respect to calcium carbonate [Key *et al.*, 2004; Regenberg *et al.*, 2006]. Hönisch *et al.* [2013] have demonstrated that adjusting Mg/Ca data from sediments above the lysocline effectively overestimates actual calcification temperatures.

Pleistocene salinity was calculated as a function of relative mean sea level (RMSL) as determined via a numerical ice-ocean model [Bintanja and van de Wal, 2008]. The change in

local salinity is approximately proportional to the change in global average salinity due to glacial-interglacial sea level change. The equation used is

$$\text{Salinity}_{668B} = 35.8\text{‰} + \text{RMSL} / 3800 \text{ m} * 34.8\text{‰} \quad (\text{Eq. 5})$$

where 35.8‰ is the modern salinity of the mixed layer (50 m water depth) at Site 668B [Zweng *et al.*, 2013], 3800 m is the average depth of the ocean and 34.8‰ is the average salinity of the modern ocean. These estimates agree (within uncertainty) with local salinity estimates derived from using Mg/Ca-based SST and calcite  $\delta^{18}\text{O}$  to estimate the  $\delta^{18}\text{O}$  of seawater ( $\delta^{18}\text{O}_{\text{sw}}$ , Figure 3) [Bemis *et al.*, 1998; Legrande and Schmidt, 2006].

*In situ* seawater pressure is also required and is a function of the foraminiferal calcification depth. Here we assume a calcification depth for both *G. ruber* and *T. sacculifer* of 50 m [Schiebel and Hemleben, 2005; Farmer *et al.*, 2007] and a corresponding seawater pressure of 50 decibars. The pressure effect on equilibrium constants is small; an uncertainty of  $\pm 50$  m water depth results in an uncertainty in calculated pH of  $\pm 0.002$  and  $\text{pCO}_2$  of  $\pm 1 \mu\text{atm}$ .

### 2.3 Alkalinity estimates

In order to calculate the partial pressure of  $\text{CO}_2$  in seawater, a second variable of the ocean carbonate system is required [e.g., Zeebe and Wolf-Gladrow, 2001]. Here, alkalinity is estimated from the modern local alkalinity-to-salinity relationship following the ‘constant alkalinity’ scenario of previous studies, which assumes that total alkalinity in the ocean remained constant in the past [Hönisch and Hemming, 2005; Hönisch *et al.*, 2009]. The local alkalinity-to-salinity relationship was developed using WOCE and GLODAP databases [Schlitzer, 2000; Key *et al.*, 2004] covering the area 0-10°N and 10-20°W [Hönisch and Hemming, 2005; Hönisch *et al.*, 2009].

$$\text{Total Alkalinity}_{668B} = 65.62 * \text{Salinity}_{668B} + 22.84 \quad (\text{Eq. 6})$$

Over long timescales (tens to hundreds of thousands of years) the local alkalinity-to-salinity relationship could deviate from the modern relationship as a function of the Canadian Shield silicate weathering contribution to global weathering rates, where increased weathering would have added alkalinity to the ocean [Clark *et al.*, 2006]. Even though the relative

contribution of such differential weathering is weakly constrained, the absolute impact on paleo-alkalinity is relatively small. Models show that varying the contribution of Canadian Shield weathering to the total ocean alkalinity budget of between 0 and 8% (Figure S2) only change the total ocean alkalinity in the Pleistocene by  $\sim 50 \mu\text{mol/kg}$  [Clark *et al.*, 2006]. To account for the potential effect of differential weathering on the local alkalinity-to-salinity ratio for past time periods, we include an alkalinity uncertainty of  $\pm 100 \mu\text{mol/kg}$  for the past 1.8 Ma.

## 2.4 Calculation of $p\text{CO}_2$

Aqueous  $\text{CO}_2$  (differentiated as  $\text{PCO}_2$ ) values are calculated from estimates of pH (total scale), alkalinity, salinity, temperature, and pressure using CO2SYS [version 2.3, Pierrot *et al.*, 2006]. Within this program, we selected the recommended default values of  $pK_1$  and  $pK_2$  from Lueker *et al.* [2000],  $\text{KHSO}_4$  from Dickson [1990],  $\text{KHF}$  from Perez and Fraga [1987], and  $[\text{B}]_T$  from Lee *et al.* [2010]. As described above, aqueous  $\text{PCO}_2$  at site 668B is in equilibrium with the atmosphere in the modern ocean [Takahashi *et al.*, 2009] and comparison of boron isotope estimates with ice core records suggests it was also in equilibrium over the past 800 kyr [Hönisch and Hemming, 2005; Hönisch *et al.*, 2009]. We therefore interpret our aqueous paleo- $\text{PCO}_2$  estimates from Site 668B as equivalent to atmospheric paleo- $p\text{CO}_2$ . In order to directly compare with  $\delta^{11}\text{B}$  records from Site 999A, we translate  $\delta^{11}\text{B}$ -based aqueous  $\text{PCO}_2$  records from Site 999 to atmospheric  $p\text{CO}_2$  by subtracting the annual average pre-industrial disequilibrium value ( $21 \mu\text{atm}$ ) as justified by Henehan *et al.* [2013] who accounted for the modern seasonal  $\Delta p\text{CO}_2$  difference and a small correction for pre-industrial  $\text{PCO}_2$  [Gloor *et al.*, 2003; Takahashi *et al.*, 2009].

## 2.5 Uncertainty

Uncertainty in the pH estimate is a function of the propagated  $2\sigma$  uncertainties in the  $\delta^{11}\text{B}$  measurement on  $\delta^{11}\text{B}_{\text{borate}}$ , the uncertainty in  $\delta^{11}\text{B}_{\text{sw}}$ , and the effect of temperature and salinity uncertainties on the dissociation constants of boric and carbonic acid in seawater. We report uncertainty in pH as the root-mean-square error of the effect each parameter uncertainty has on pH: the  $\delta^{11}\text{B}$  measurement and  $\delta^{11}\text{B}_{\text{borate}}$  calibration ( $\pm 0.03$  pH units,  $\sim 80\%$  coming from analytical uncertainty), the estimate of  $\delta^{11}\text{B}_{\text{sw}}$  ( $\pm 0.01$  pH units at 1.5 Ma), the temperature constraints (calibration uncertainty equates to  $\pm 0.02$  pH units) and salinity ( $\pm 0.01$  pH units). Uncertainty is calculated on a sample-by-sample basis; average total pH uncertainty of the

Site 668B data is  $\pm 0.043$  ( $2\sigma$ ). Uncertainty in the  $p\text{CO}_2$  calculation is likewise a function of uncertainty in the overall input parameters: the  $\delta^{11}\text{B}$  measurement and calibration ( $\pm 23$   $\mu\text{atm}$ ), alkalinity ( $\pm 12$   $\mu\text{atm}$ ), and the effects of temperature ( $\pm 19$   $\mu\text{atm}$ ) and salinity ( $\pm 3$   $\mu\text{atm}$ ). Uncertainty in  $\text{PCO}_2$  is similarly calculated on a sample-by-sample basis; average total  $\text{PCO}_2$  uncertainty is  $\pm 33$   $\mu\text{atm}$  ( $2\sigma$ ) for the newly estimated  $\text{PCO}_2$  values at  $\sim 1.5$  Ma.

## 2.6 Chronology

The age model for ODP Site 668B was initially constructed from microfossil occurrence data and estimates of the depths of geomagnetic reversals [*Shipboard Scientific Party*, 1988]. This initial chronology was later tuned through the alignment of glacial-interglacial cycles in the high-resolution planktic (*G. ruber*)  $\delta^{18}\text{O}$  values of Site 668B [*Bird and Cali*, 1998; 2002; *Hönisch et al.*, 2009] with the well-dated planktic  $\delta^{18}\text{O}$  values of ODP Site 677 [*Shackleton et al.*, 1990] and the LR04 benthic  $\delta^{18}\text{O}$  stack [*Lisiecki and Raymo*, 2005]. In order to resolve planktic  $\delta^{18}\text{O}$  mismatches between Sites 668B and 677 during MIS 48-52 (1.45-1.53 ka), we used AnalySeries software [*Paillard et al.*, 1996] to add tie points which refine the planktic  $\delta^{18}\text{O}$  alignment. All ages younger than 1.3 Ma (19 m core depth) are unchanged from the previously published age model [*Hönisch et al.*, 2009]. The revised age model for the period prior to 1.3 Ma (core depths 19-26 m) improves the planktic  $\delta^{18}\text{O}$  correlation coefficient (Pearson  $R^2$ ) between Sites 677 and 668B from  $\sim 0.31$  to  $\sim 0.40$  and reconstructed ages are up to 15% younger than previously estimated (Figure S3). The updated age model also conforms to the original ODP geomagnetic constraints, which placed the top of the Olduvai reversal (1.78 Ma) at 2.725 m core depth [*Shipboard Scientific Party*, 1988], just beyond the oldest available  $\delta^{18}\text{O}$  values from Site 668B (Figure S3). Unfortunately, the age uncertainty of the underlying benthic  $\delta^{18}\text{O}$  stack is  $\pm 6$  kyr in the early Pleistocene [*Lisiecki and Raymo*, 2005]; this age uncertainty prevents the determination of leads or lags that are shorter than this confidence interval.

## 2.7 Comparison with other $\delta^{11}\text{B}$ -based $\text{PCO}_2$ records

For comparison between this new record and other previously published Pleistocene  $\delta^{11}\text{B}$ -based  $\text{PCO}_2$  records, we compile  $\text{PCO}_2$  estimates from  $\delta^{11}\text{B}$  data from Site 668B and Site 999A in the tropical Atlantic. These two sites present a good comparison as ocean-atmosphere disequilibrium is small at both locations. In order to rule out methodological differences, we calculated  $\text{PCO}_2$  from each published record using equivalent input

parameters and technique-specific calibrations. The original Site 668B  $\delta^{11}\text{B}_{T. \text{sacculifer}}$  data [Hönisch *et al.*, 2009] are used to recalculate pH and  $\text{PCO}_2$  using the above methods (Section 2.1-2.6). The  $\delta^{11}\text{B}$  calibration for this dataset is updated (Eq. 2) and  $\delta^{11}\text{B}_{\text{sw}}$  is assumed to be 39.61‰ throughout. Temperature is calculated via the same Anand *et al.* [2003] calibration, after correcting for changes in seawater Mg/Ca (Eq. 4).

The  $\delta^{11}\text{B}_{T. \text{sacculifer}}$  data of ODP 999A [Bartoli *et al.*, 2011] were also revised using similar methods described above. To do so, we first generated new Mg/Ca data from the same or adjacent samples used for  $\delta^{11}\text{B}$  analysis (see section 2.2). In the original study, SST was interpolated from *T. sacculifer* Mg/Ca values [Groeneveld, 2005] with a different temporal resolution than the  $\delta^{11}\text{B}$  samples; our new temperature data reduce the interpolation of temperature estimates. Furthermore, the original SST record used the depth-based dissolution correction of Dekens *et al.* [2002], along with an outdated modern  $\text{Mg}/\text{Ca}_{\text{sw}}$  value of 4.96 mmol/mol. Due to omission of the depth correction, the SST estimated for this record is on average 1.8 K cooler than SST in the original publication (Figure S4) which places interglacial SST in agreement with modern SST at this location, whether taken from an annual average of modern direct measurements (27.7 °C) [Locarnini *et al.*, 2013] or estimated from core top Mg/Ca values (28.2 °C) [Henehan *et al.*, 2013]. Site 999A (water depth 2839 m) is situated well above the regional lysocline (4200 m) and *T. sacculifer* shells are not subject to preferential high-Mg calcite dissolution at this water depth [Regenberg *et al.*, 2006]. Taken together, the omission of the depth correction thus appears well justified.

Additionally, Bartoli *et al.* [2011] used modeled surface ocean  $[\text{CO}_3^{2-}]$  estimates as the second parameter of the carbonate system and paired them with their  $\delta^{11}\text{B}$ -pH estimates and to calculate  $\text{PCO}_2$ . Because pH and  $[\text{CO}_3^{2-}]$  are closely related in carbonate equilibria, pairing them in carbon system calculations produces large variations in the calculated parameters. For instance, the pH and  $[\text{CO}_3^{2-}]$  estimates of Bartoli *et al.* [2011] combine to yield glacial-interglacial total alkalinity variations of up ~800  $\mu\text{mol}/\text{kg}$  (Figure S5). Such a large change in ocean alkalinity is unlikely over these timescales as alkalinity is stabilized by the distribution of calcium carbonate accumulation and dissolution (carbonate compensation) in the deep sea on scales of thousands of years [Broecker, 1971; Broecker and Peng, 1987; Boyle, 1988]. Extrapolating from LGM estimates of alkalinity and lysocline depth, an 800  $\mu\text{mol}/\text{kg}$  decrease in alkalinity would correspond to a >2 km shallower lysocline, which is difficult to

reconcile with observations of relatively small changes (<0.5 km) in lysocline depth over the Pleistocene [Farrell and Prell, 1991]. Geochemical models also suggest smaller alkalinity adjustments, e.g. <400  $\mu\text{mol/kg}$  over the past 10 million years [Figures 3d and 4d of Tyrrell and Zeebe, 2004] and <250  $\mu\text{mol/kg}$  over the past 2.6 Ma [Clark et al., 2006]. We therefore revise the  $\text{PCO}_2$  record of Bartoli et al. [2011] by using estimates of total alkalinity as the second carbonate system parameter; pH, salinity, and temperature are calculated in the same manner as for Site 668B (Sections 2.2, 2.4). Here alkalinity is calculated via the same regional relationship with salinity that was previously established for Site 999A [Foster, 2008].

$$\text{Total Alkalinity}_{999\text{A}} = 59.19 * \text{Salinity}_{999\text{A}} + 229.08 \quad (\text{Eq. 7})$$

To account for the potential impact of differential weathering on the local alkalinity-to-salinity ratio for these older samples, we increase the alkalinity uncertainty to  $\pm 175 \mu\text{mol/kg}$  for all samples older than 1.8 Ma. Older time periods ( $> \sim 2$  Ma) are less well constrained and so larger uncertainty estimates are used. In contrast to Chalk et al. [2017] who used constant alkalinity and therefore assumed the larger 175  $\mu\text{mol/kg}$  uncertainty throughout, our uncertainty estimates are superimposed on the alkalinity changes based on sea level, and are therefore even more conservative than those used by Chalk et al. [2017].

Published boron isotope data are also available from *G. ruber* from Site 999A [Foster, 2008; Seki et al., 2010; Henehan et al., 2013; Martínez-Botí et al., 2015a; Chalk et al., 2017].

Boron-based  $\text{PCO}_2$  reconstructions from both *T. sacculifer* and *G. ruber* have been extensively calibrated and both species provide convincing  $\text{PCO}_2$  estimates compared to ice core records. Here we apply minor revisions to the published  $\delta^{11}\text{B}_{G. ruber}$ -based  $\text{PCO}_2$  calculations (namely, using a common SST calibration and assuming a constant  $\delta^{11}\text{B}_{\text{sw}}$  over the past 5 Ma) with the goal of ensuring compatible comparisons among the results. All the published  $\delta^{11}\text{B}_{G. ruber}$  values are translated to  $\delta^{11}\text{B}_{\text{borate}}$  using the established species- and instrument-specific calibration of Henehan et al. [2013]:

$$\delta^{11}\text{B}_{\text{borate}} = [\delta^{11}\text{B}_{G. ruber \text{ MC-ICP-MS}} - 8.87 (\pm 1.52)] / 0.60 (\pm 0.09) \quad (\text{Eq. 8})$$

In each case *G. ruber* specimens are from the 300-355  $\mu\text{m}$  size fraction so any additional offset for size fraction is not required [Henehan *et al.*, 2013].

The other parameters needed (temperature, salinity,  $\delta^{11}\text{B}_{\text{sw}}$ , and alkalinity) are estimated consistently with Sections 2.1-2.6. *In situ* temperature is determined from Mg/Ca values as described by equation 4, except for the record of *Seki et al.* [2010] in which the alkenone unsaturation index is used for temperature reconstruction as in the original publication; alkenone-based temperatures are indistinguishable from Mg/Ca-based SST at this location. In all cases salinity is assessed from the modeled sea level estimates of *Bintanja and van de Wal* [2008], similar to equation 5, with modern salinity of the mixed layer (50 m water depth) at Site 999A of 36.2‰.

$$\text{Salinity}_{999\text{A}} = 36.2\text{‰} + \text{RMSL} / 3800 \text{ m} * 34.8\text{‰} \quad (\text{Eq. 9})$$

For samples older than 3 Ma, the limit of the RMSL data set [*Bintanja and van de Wal*, 2008], the oldest value ( $S_{t=3.0 \text{ Ma}} = 36.2\text{‰}$ ) is used. An alternate method for calculating salinity used by previous publications is via the  $\delta^{18}\text{O}$  and Mg/Ca values of planktic calcite to find local  $\delta^{18}\text{O}_{\text{sw}}$  and then translate  $\delta^{18}\text{O}_{\text{sw}}$  to a salinity estimate. In practice, this method would result in average salinity  $\sim 0.4$  lower than estimated above (Eq. 9), pH  $\sim 0.0002$  lower, and  $\text{PCO}_2 \sim 1 \mu\text{atm}$  higher. Equations for this alternative salinity estimate can be found in the supplemental material.

### 3. Results

The ODP Site 668B boron-based  $\text{PCO}_2$  record for the interval 1.38-1.54 Ma is presented in Figure 3. Within this time period  $\delta^{11}\text{B}_{T. \text{ sacculifer}}$  values range between a maximum of 22.19 ( $\pm 0.21$ )‰ (1.502 Ma) and a minimum of 20.26 ( $\pm 0.25$ )‰ (1.402 Ma) with an average  $\delta^{11}\text{B}$  value of 21.14 ( $\pm 0.16$ )‰. Calculated  $\text{PCO}_2$  ranges between 183 ( $\pm 21$ )  $\mu\text{atm}$  (at 1.502 Ma) and 327 ( $\pm 61$ )  $\mu\text{atm}$  (at 1.408 Ma) with an average  $\text{PCO}_2$  value of 258 ( $\pm 29$ )  $\mu\text{atm}$ . The average amplitude of minimum glacial to maximum interglacial  $\text{PCO}_2$  is 92 ( $\pm 34$ )  $\mu\text{atm}$  (average of 4 interglacial maxima (304 ( $\pm 46$ )  $\mu\text{atm}$ ) minus average of 5 glacial minima (212 ( $\pm 23$ )  $\mu\text{atm}$ ); these uncertainties are based on the average uncertainty of the data points in question)).

The measured  $\delta^{11}\text{B}_{T. \textit{sacculifer}}$  value is the dominating parameter for the calculated  $\text{PCO}_2$  record (Figure S6). To evaluate the respective effects of temperature, alkalinity, and salinity on the calculated  $\text{PCO}_2$ , we performed a simple sensitivity study in which  $\delta^{11}\text{B}$  was held constant at the average value (21.15‰) while all other factors (temperature, alkalinity, salinity) varied as evaluated previously. When  $\delta^{11}\text{B}_{T. \textit{sacculifer}}$  is held constant, the secondary driver of the  $\text{PCO}_2$  calculation is local SST, although even the full range of local SST (3.1 K) can only account for a maximum glacial-interglacial  $\text{PCO}_2$  range of 24  $\mu\text{atm}$  (Figure S6). Thus, the calculation of paleo- $\text{PCO}_2$  is driven primarily by changes in surface ocean pH as reflected in the raw  $\delta^{11}\text{B}$  data; temperature, salinity, and alkalinity exert only a minor additional influence on the pH and  $\text{PCO}_2$  estimates. This is in contrast to the potentially dominant effects other environmental parameters (i.e.  $[\text{B}(\text{OH})_4^-]$ ,  $[\text{HCO}_3^-]$ ) can have on B/Ca-based estimates of carbonate parameters [Tripathi *et al.*, 2011; Allen *et al.*, 2012].

Published records of  $\delta^{11}\text{B}$ -based  $\text{PCO}_2$  were revised to be consistent with the given methodology above. Each parameter revision was tested individually to determine which parameter caused the greatest resulting  $\text{PCO}_2$  shift from the original publication. In each instance, *T. sacculifer*  $\delta^{11}\text{B}$  has been measured via N-TIMS and *G. ruber*  $\delta^{11}\text{B}$  via MC-ICP-MS. For the longer (0-1.8 Ma) Site 668B *T. sacculifer* dataset, average  $\text{PCO}_2$  is +2  $\mu\text{atm}$  higher than the published record [Hönisch *et al.*, 2009]. This difference is composed of the assumption that  $\delta^{11}\text{B}_{\text{sw}}$  was 39.61‰ rather than 39.5‰ (+6  $\mu\text{atm}$ ), the updated  $\delta^{11}\text{B}_{\text{borate}}$  calibration (Eq. 2, -16  $\mu\text{atm}$ ), updated SST calibration (Eq. 4, +3  $\mu\text{atm}$ ), and alkalinity calculated via the ‘constant alkalinity scenario’ (Eq. 6, +14  $\mu\text{atm}$ ). For Site 999A (0-26 ka), average  $\text{PCO}_2$  is also +12  $\mu\text{atm}$  higher than the published record [Henehan *et al.*, 2013], primarily due to the revised salinity and alkalinity estimations (Eq. 7 and 9). For Site 999A (0-1.24 Ma), average  $\text{PCO}_2$  is +12  $\mu\text{atm}$  higher than the published record [Chalk *et al.*, 2017] also due to the revised salinity and alkalinity estimates. For the Site 999A study of Seki *et al.* [2010] (0-2.6 Ma), the revised average  $\text{PCO}_2$  is +26  $\mu\text{atm}$  higher than the published record [Seki *et al.*, 2010], due to the updated calibration for the boron isotope proxy in *G. ruber* [Henehan *et al.*, 2013]. For the Plio-Pleistocene (2.3-3.3 Ma) Site 999A *G. ruber* dataset, average  $\text{PCO}_2$  is +12  $\mu\text{atm}$  higher than the published record [Martínez-Botí *et al.*, 2015b], primarily due to the revised assumption that seawater  $\delta^{11}\text{B}_{\text{sw}}$  was constant at 39.61‰ over the

past 5 Ma (Figure S1), whereas the original publication assumed a lower  $\delta^{11}\text{B}_{\text{sw}}$  ( $\sim 39.2\text{‰}$ ) at the Plio-Pleistocene transition.

For the Plio-Pleistocene (1.97-4.6 Ma) Site 999A *T. sacculifer* dataset, average  $\text{PCO}_2$  is 41  $\mu\text{atm}$  lower than the published record [Bartoli *et al.*, 2011], primarily due to the revised SST record which omits the depth-based dissolution correction (Eq. 4, SST 1.8 K cooler, -15  $\mu\text{atm}$ ) and the application of the pre-industrial disequilibrium value at this site (-21  $\mu\text{atm}$ ). The choice of alkalinity, rather than  $[\text{CO}_3^{2-}]$  as the second parameter of the carbonate system, reduces the glacial-interglacial  $\text{PCO}_2$  amplitude of this record by 25% compared to the original publication (Figure S5). This finding highlights the volatile nature of the pH and  $[\text{CO}_3^{2-}]$  pair in constraining the carbonate system, i.e., a small uncertainty in  $[\text{CO}_3^{2-}]$  translates into a large shift in  $\text{PCO}_2$  when paired with pH. The amplitude reduction is a result of both reducing the interglacial  $\text{PCO}_2$  estimates and increasing the glacial  $\text{PCO}_2$  estimates compared to the original record. All revisions were applied for consistency among calculations; the average  $\text{PCO}_2$  change in all cases is smaller than the average  $2\sigma$  uncertainty reported in the original studies.

#### 4. Discussion

Given that late Pleistocene  $\text{pCO}_2$  levels were closely correlated with both tropical SST [e.g., Lea, 2004; Herbert *et al.*, 2010; Dyez and Ravelo, 2013] and high latitude surface temperatures [Petit *et al.*, 1999; Jouzel *et al.*, 2007], an equivalent relationship could be expected for early Pleistocene glacial-interglacial cycles. Here we add to the growing body of data evidence that a similar first-order relationship between global average temperature and  $\text{pCO}_2$  also existed in the early Pleistocene, specifically in the interval 1.38-1.54 Ma (Figure 4). During interglacial periods  $\delta^{11}\text{B}$  was lower (i.e., lower surface ocean pH and higher atmospheric  $\text{pCO}_2$ ) and during glacial periods  $\delta^{11}\text{B}$  was higher (i.e., higher surface ocean pH and lower atmospheric  $\text{pCO}_2$ ), in line with similar findings for the late Pleistocene period [Hönisch and Hemming, 2005; Henehan *et al.*, 2013; Chalk *et al.*, 2017]. To verify that our data are directly related to variation in atmospheric  $\text{pCO}_2$ , we need to evaluate a range of processes that could have biased our geochemical signals and interpretations.

First of all, ocean upwelling brings cooler and more  $\text{CO}_2$ -rich water to the surface; if upwelling had increased during glacial intervals at this location, we would expect to observe

a larger glacial-interglacial SST amplitude than other open-ocean sites; if upwelling had increased during interglacial intervals, we would expect a smaller SST amplitude. The local temperature amplitude we measure from Mg/Ca values (i.e., average of 4 interglacial SST maxima minus average of 5 glacial SST minima) is 1.4 ( $\pm 0.3$ ) K, equivalent to other early Pleistocene tropical SST records, whether derived from the south China Sea [Site 1146; 1.4 K, *Herbert et al.*, 2010], the western Pacific [Site 806; 1.2 K, *Medina-Elizalde and Lea*, 2005; Site 871; 1.2 K, *Dyez and Ravelo*, 2014], the south Pacific [MD06-3018; 1.3K, *Russon et al.*, 2010], the tropical Atlantic [Site 662; 1.6 K, *Herbert et al.*, 2010], or the Arabian Sea [Site 722; 1.1 K, *Herbert et al.*, 2010]. The similarity of the SST amplitude at Site 668B to other tropical records implies that glacial-interglacial upwelling changes at this site were not substantial and did not preferentially influence either glacial or interglacial  $\delta^{11}\text{B}$  values.

Secondly, shell diagenesis can occur after shells have been deposited on the ocean floor, potentially biasing our paleoenvironmental interpretations. However, in section 2 we already reasoned against potential dissolution at the sediment surface based on the shallow depth of the core tops and the much deeper Atlantic lysocline. Furthermore, the calcite saturation state of bottom water at this site is  $\Omega_{\text{CaCO}_3} = 1.5$  and bottom water  $\Delta[\text{CO}_3^{2-}] = 34.5$ , both of which are higher than any site previously used for  $\delta^{11}\text{B}$ -based  $\text{pCO}_2$  estimates and above the range suggested for the onset of partial dissolution [*de Villiers* 2005; *Dai et al.*, 2016]. If diagenesis lowered  $\delta^{11}\text{B}$  values within the buried sediment, we would expect to also observe lower shell weights and higher planktic  $\delta^{18}\text{O}$  and  $\delta^{13}\text{C}$  values [e.g., *Edgar et al.*, 2015]. We examined the correlations among these values and do not find any significant relationships to support the notion that diagenesis has occurred within the sediment column. Taken together with the expected range of glacial-interglacial SST presented above, we can reasonably infer that the  $\delta^{11}\text{B}$ -based  $\text{PCO}_2$  signal we measure is primary and has not been biased by incomplete preservation.

#### **4.1 Early Pleistocene $\text{pCO}_2$ varied with obliquity-related climate cycles**

To examine the glacial-interglacial linkages between  $\text{pCO}_2$ , temperature, and orbital climate parameters from the period 1.38-1.54 Ma, we created cross-plots of reconstructed  $\text{pCO}_2$  with physiochemical measurements, orbital parameters, and global stacks of temperature and benthic  $\delta^{18}\text{O}$  (Figure 5). In this analysis, only data that are clearly associated with the broad maxima or minima in temperature and marine isotope stage are plotted, as determined by

visual comparison with both a benthic  $\delta^{18}\text{O}$  values [Lisiecki and Raymo, 2005] and a global stack of surface temperatures [Snyder, 2016]. Omitted are intermediate data that fall between these climate extrema and, due to age model uncertainty, cannot be easily associated with a particular stage; the MIS intervals and maximum/minimum  $\text{pCO}_2$  values are listed in Table S2.

With which orbital cycle is  $\text{pCO}_2$  most closely related in the early Pleistocene? Cross-plots show that in the late Pleistocene, periods of peak  $\text{pCO}_2$  are associated with orbital eccentricity, but in the early Pleistocene peak interglacial  $\text{pCO}_2$  is correlated with increased tilt (obliquity) in Earth's rotation axis (Figure 5). The association of  $\text{pCO}_2$  and obliquity supports the notion that  $\text{pCO}_2$  was linked with the orbital insolation cycle and surface temperatures, even in the 41-kyr world before the mid-Pleistocene transition, but that the linkages took a different form, which resulted in climate that was in phase with obliquity. This finding is consistent with previously proposed hypotheses for maintaining ~41-kyr periodicity of glacial-interglacial change in the early Pleistocene, either through meridional temperature gradients or ice dynamics. In the early Pleistocene, the 41-kyr cycle could have been promoted by amplified equator-to-pole temperature gradients that carried additional moisture poleward to build ice sheets [Raymo and Nisancioglu, 2003] and/or by thinner, fast-spreading Laurentide ice sheets [Clark et al., 2006]. The glacial-interglacial temperature perturbations that drive glacial-interglacial climate would likely have been further amplified by obliquity-scale radiative  $\text{pCO}_2$  feedbacks.

#### 4.2 Glacial $\text{pCO}_2$ decreased through the Pleistocene

Site 668B  $\delta^{11}\text{B}_{T. \text{sacculifer}}$  values indicate that early and late Pleistocene maximum interglacial  $\text{pCO}_2$  did not change across the MPT (average interglacial peak  $\text{pCO}_2$  at 1.2-1.8 Ma: 303 ( $\pm 12$ )  $\mu\text{atm}$ , average interglacial peak  $\text{pCO}_2$  at 0-0.5 Ma: 299 ( $\pm 16$ )  $\mu\text{atm}$  (two-tailed t-test of all peak interglacial  $\text{pCO}_2$  values,  $P > 0.7$ ). However, minimum glacial  $\text{pCO}_2$  values declined by ~25  $\mu\text{atm}$  between the early and late Pleistocene (average minimum  $\text{pCO}_2$  at 1.2-1.8 Ma: 213 ( $\pm 10$ )  $\mu\text{atm}$ , average minimum  $\text{pCO}_2$  at 0-0.5 Ma: 187 ( $\pm 10$ )  $\mu\text{atm}$  (two-tailed t-test of glacial minimum values,  $P < 0.05$ ). These  $\text{pCO}_2$  estimates are congruent with proxy records of warmer glacial temperatures in the early Pleistocene than the late Pleistocene and support the initial observation that glacial  $\text{pCO}_2$  declined across the MPT [Hönisch et al., 2009; Chalk et al., 2017]. While the collapse of North Atlantic deep-water formation around 900 ka

coincides with this decrease in glacial pCO<sub>2</sub> [e.g., *Pena and Goldstein, 2014*], our atmospheric estimates do not allow us to determine the cause of the pCO<sub>2</sub> drawdown. However, the covariation of ocean circulation and pCO<sub>2</sub> shifts over the MPT to longer, colder glacial intervals highlights the close association of ocean dynamics, atmospheric circulation, and climate in the Pleistocene [e.g., *Clark et al., 2006*].

Glacial pCO<sub>2</sub> was higher in the early Pleistocene than the late Pleistocene, just as glacial temperatures were also 2-2.2 K warmer in the period 1.2-1.8 Ma than in the period 0-0.5 Ma based on multiple compilations of temperature change between the early and late Pleistocene [*Herbert et al., 2010; Martínez-Botí et al., 2015a; Snyder, 2016*]. If average surface temperature is due to the radiative pCO<sub>2</sub> forcing alone, an equilibrium response of global temperature to such forcing can be calculated. At its most basic, this calculation is commonly given in the form of  $S_{[\text{CO}_2]} = \Delta T / \Delta F_{[\text{CO}_2]}$  where  $\Delta T$  (change in global average surface temperature) and  $\Delta F_{[\text{CO}_2]}$  (change in radiative forcing due to pCO<sub>2</sub>) are millennial-scale averages and all other forcing mechanisms are regarded as internal feedbacks. Here the canonical radiative forcing due to CO<sub>2</sub> is used, where  $\Delta F_{[\text{CO}_2]} = 5.35 * \ln(C/278 \text{ } \mu\text{atm})$  and  $C$  is atmospheric pCO<sub>2</sub> [*Myhre et al., 1998*]. For the early Pleistocene we thus calculate an equilibrium temperature response to radiative CO<sub>2</sub> forcing as  $S_{[\text{CO}_2]} = 0.75 (\pm 0.5) \text{ } ^\circ\text{C}/\text{Wm}^{-2}$ . For the late Pleistocene, the parallel calculation yields  $S_{[\text{CO}_2]} = 1.75 (\pm 0.6) \text{ } ^\circ\text{C}/\text{Wm}^{-2}$  (Figure 6). To the first order, these relationships imply that climate sensitivity to radiative greenhouse gas forcing increased by a factor of ~2 between 1.2 and 0.5 Ma, largely driven by lower glacial-interglacial temperature amplitude in the early Pleistocene.

In reality, however, climate feedbacks such as ice sheets and ocean circulation also amplify the range of global average temperature [e.g., *Köhler et al., 2015; von der Heydt et al., 2016*]. Recent studies have pointed out that in order to project the climate effects of rising pCO<sub>2</sub> levels in a warmer world with smaller ice sheets, climate sensitivity must account for the temperature response to each climate parameter separately (i.e., CO<sub>2</sub>, ice sheets, etc.) [e.g., *Köhler et al., 2015; Schmidt et al., 2017*]. The lower early Pleistocene climate sensitivity calculated above is a result of comparing between time periods in which, at minimum, ice dynamics have changed [*Raymo et al., 2006; Shakun et al., 2016*]. Though this dataset does not allow us to quantify changes in albedo and atmospheric circulation, increased glacial ice volume (and vertical growth of ice sheets) at the MPT is an important change in the earth

system that could have amplified glacial-interglacial temperature variability. Increased ice volume cools global temperature through two pathways: by increasing ice sheet extent, which increased global albedo, and through taller ice sheets, which deflected cold northern hemisphere atmospheric jets southward and compressed the subtropical atmospheric bands [Manabe and Broccoli, 1985; Shinn and Barron, 1989; Clark et al., 1999]. Qualitatively, then, these additional ice sheet and ocean feedbacks, in conjunction with lower atmospheric pCO<sub>2</sub>, worked to cool glacial temperatures across the mid-Pleistocene transition.

### 4.3 Model comparison

We evaluate these reconstructions of early and late Pleistocene pCO<sub>2</sub> with a simple numerical box model that allows for an initial exploration of Pleistocene climate sensitivity given the available surface temperature and pCO<sub>2</sub> data. This model has three coupled components: ice sheets, temperature, and carbon dioxide levels. We force this model with atmospheric insolation over glacial cycles to explore the effect of Laurentide ice sheet changes for climate sensitivity. This model has been documented elsewhere [Schmidt et al., 2017]; briefly, this model includes coupling between ice sheet volume ( $L$ ) and global average surface temperature ( $T$ ) and between surface temperature and carbon dioxide levels ( $C$ ) but does not incorporate 3D geography or topography. The model is initialized at the following mid-glacial values:  $T_0 = 285$  K,  $C_0 = 230$  μatm,  $L_0 = -60$  m (meters of sea level equivalent). The sensitivity of ice sheets to temperature ( $a$ ) and the non-Planck feedback ( $\lambda$ ) are tested via 20x20 experiments (varying  $a = [0,30]$  mSL K<sup>-1</sup> and  $\lambda = [2.8,4.6]$  Wm<sup>-2</sup> K<sup>-1</sup>). These parameters are consistent with the full range of late Pleistocene observations [Köhler et al., 2010].

We use this model to explore the qualitative impact of increasing ice volume on global climate at the MPT. Geochemical evidence and ice sheet models suggest that the Laurentide ice sheet of the early Pleistocene was thinner due to a “slippery” layer of weathered regolith over solid bedrock [Clark and Pollard, 1998; Clark et al., 2006], but that the spatial extent of land ice was similar to the late Pleistocene ice ages [Roy et al., 2004; Balco and Rovey, 2010]. Thus, the radiative forcing due to ice sheet albedo was roughly similar in the early and late Pleistocene, but the ice volume required (in equivalent meters of sea level fall) to acquire that forcing was smaller prior to ~1.0 Ma. We test the effect of radiative albedo forcing per ice sheet volume ( $\mu$ ) at 0.025 Wm<sup>-2</sup> mSL<sup>-1</sup> for the late Pleistocene such that late Pleistocene

ice sheets cooled the global climate by  $1 \text{ Wm}^{-2}$  for each 40 meters of equivalent sea level fall, consistent with what is assumed for ice-albedo cooling at the LGM [Köhler *et al.*, 2010]. If the early Pleistocene Laurentide ice sheet was comparably expansive as in the late Pleistocene, but thinner, it can be thought of as more ‘efficient’ at radiative albedo cooling per unit volume of ice. We investigate this idea by testing the parameter  $\mu$  (defined above) for the early Pleistocene at double and triple the late Pleistocene value: at  $0.05$  and  $0.075 \text{ Wm}^{-2} \text{ mSL}^{-1}$ . This exercise is not meant to fully simulate the climate system, but to explore elemental system sensitivity to a realistic range of radiative  $\text{CO}_2$ , insolation, and ice-sheet albedo forcing.

The results of this model suggest that if the efficiency of ice cooling ( $\mu$ ) were higher in the past, the amplitude of temperature variability and atmospheric  $\text{CO}_2$  variability would also have been higher. When  $\mu$  is doubled (or tripled), which simulates the large, but relatively thinner early Pleistocene northern hemisphere ice sheets, temperature and  $\text{pCO}_2$  amplitude are  $\sim 40$  ( $\sim 80\%$  for tripled  $\mu$ ) larger. However, we do not observe this phenomenon in the early Pleistocene geochemical datasets. Instead we observe lower temperature variability in the early Pleistocene, and a similar amplitude of atmospheric  $\text{CO}_2$  variability as in the late Pleistocene. These observations could be a consequence of only considering northern hemisphere insolation and the impact on Laurentide ice. Out-of-phase insolation in the southern hemisphere could have driven Antarctic ice in the opposite direction and dampened overall atmospheric  $\text{pCO}_2$  levels by modulating the Southern Ocean dynamics [Raymo *et al.*, 2006]. Interhemispheric insolation differences tend to diminish the greater temperature variability that would be implied by greater northern hemisphere ice sheet efficiency in the early Pleistocene.

The simple model described above is also designed to explore the effect of changing Laurentide ice sheet dynamics on climate sensitivity. As the efficiency of ice sheet cooling per unit volume of ice was greater for the early Pleistocene conditions (model  $\mu$  is increased from  $0.025$  to  $0.075 \text{ Wm}^{-2} \text{ mSL}^{-1}$ ) the model suggests that earth system sensitivity (ESS) must be higher as well. This particular example indicates that a three-fold increase in  $\mu$  would increase ESS from  $3.0$  to  $5.1 \text{ K}$  for a doubling of atmospheric  $\text{CO}_2$ . As stated previously, we observe the opposite in geochemical reconstructions of the early Pleistocene: because the early Pleistocene  $\text{pCO}_2$  amplitude is only slightly smaller than the late Pleistocene  $\text{pCO}_2$

amplitude, the associated temperature change with a climate sensitivity of 5.1 K per doubling of CO<sub>2</sub> would predict a temperature amplitude of ~4 K. In contrast, we observe a temperature amplitude of ~3 K and a correspondingly lower ESS in the early Pleistocene than in the late Pleistocene. This result simply suggests that earth's surface temperature in the early Pleistocene is not solely determined by northern hemisphere ice sheets and CO<sub>2</sub> feedbacks. Rather, other forcing factors, which are not explicitly taken into account in this model (e.g., tropical and Southern Ocean dynamics, southern hemisphere insolation, Antarctic ice sheets) must be responsible for helping to dampen glacial-interglacial temperature amplitude in the early Pleistocene.

#### **4.4 Species-specific differences; implications for Plio-Pleistocene pCO<sub>2</sub> drawdown**

As the boron isotope proxy gains maturity and acceptance in the scientific community, the number of δ<sup>11</sup>B-based datasets has increased, offering an opportunity to glean more detailed insight into the interplay between pCO<sub>2</sub> and climate. In Figure 7 we compile new pCO<sub>2</sub> estimates alongside ice-core records of late Pleistocene pCO<sub>2</sub> [Bereiter *et al.*, 2015; Higgins *et al.*, 2015] and six published records of δ<sup>11</sup>B-based pCO<sub>2</sub>. As described above, the δ<sup>11</sup>B-based pCO<sub>2</sub> data [Hönisch *et al.*, 2009; Seki *et al.*, 2010; Bartoli *et al.*, 2011; Henahan *et al.*, 2013; Martínez-Botí *et al.*, 2015a; Chalk *et al.*, 2017], have been recalculated to minimize differences in the chemical and physical boundary conditions estimated for each record (see Section 2.7). It is worth reiterating that the resulting pCO<sub>2</sub> values are primarily dependent on the published δ<sup>11</sup>B measurements and that our minor revisions in boundary condition treatment do not shift average pCO<sub>2</sub> estimates outside of the published 2σ uncertainty bands.

Paleo-pCO<sub>2</sub> estimates based on δ<sup>11</sup>B values of either *T. sacculifer* or *G. ruber* [Bartoli *et al.*, 2011; Martínez-Botí *et al.*, 2015a] suggest that pCO<sub>2</sub> declined by 50-100 μatm between 2.8 and 2.6 Ma (Figure 8). This pCO<sub>2</sub> drawdown, coincident with the onset of northern hemisphere glaciation [Raymo, 1994; Haug *et al.*, 1999] is thought to be the result of increased glacial dust load and greater biological productivity in high-nitrate low-chlorophyll regions [Bailey *et al.*, 2011] or polar stratification which sequestered carbon in the deep ocean in both the north Pacific [e.g., Haug *et al.*, 1999; Sigman *et al.*, 2004] and the Southern Ocean [Hodell and Venz-Curtis, 2006; Waddell *et al.*, 2009; Martínez-García *et al.*, 2011]. The pCO<sub>2</sub> initial drawdown at 2.8-2.6 Ma is implicated in the increased glaciation of Greenland and the northern hemisphere more broadly [Lunt *et al.*, 2008].

Nonetheless, a distinct mismatch exists between the two  $\delta^{11}\text{B}$ -based  $\text{pCO}_2$  estimates from Site 999A (Figures 7, 8) for much of the late Pliocene. Where these two records overlap (from 3.3-2.3 Ma), the *G. ruber*-based  $\text{pCO}_2$  estimates are on average 90  $\mu\text{atm}$  higher than the *T. sacculifer* estimates (Figures 7, 8). This difference is apparent to a small degree even where *G. ruber* and *T. sacculifer* records overlap in the late Pleistocene, and as a mismatch between *G. ruber* and ice core records (Figure S8), although the species difference is larger further back in time. We can rule out discrepancies in environmental temperature as impacting the equilibrium constants because the Mg/Ca-based temperature reconstructions from the two datasets are indistinguishable (Figure S7-B). As we have already precluded inconsistent treatment of the physicochemical boundary conditions, the difference is more likely rooted in the underlying  $\delta^{11}\text{B}$  data of *G. ruber* and *T. sacculifer*, where  $\delta^{11}\text{B}_{G. ruber}$  decreases more strongly between the last glacial cycle and the late Pliocene than  $\delta^{11}\text{B}_{T. sacculifer}$ . It is important to explore this discrepancy, which could be explained a biologically-mediated shift in the  $\delta^{11}\text{B}_{\text{calcite}}$  to  $\delta^{11}\text{B}_{\text{borate}}$  calibration (Figure S9), as differential  $\text{pCO}_2$  results have important implications for Plio-Pleistocene climate research [e.g., Martínez-Botí et al., 2015a].

Differences in the  $\text{pCO}_2$  reconstructions from these two surface dwelling foraminifera could in theory result from diagenetic alteration or incomplete sample cleaning. However, in the specific case of the late Pliocene data, evaluation of these factors is partly constrained by the fact that both species have been analyzed from the same sediment core. The first of these arguments relates to the potential bias due to partial dissolution, which typically lowers the  $\delta^{11}\text{B}$  value by preferential removal of higher- $\delta^{11}\text{B}$  calcite [e.g., Hönisch and Hemming, 2004]. Both Pliocene data sets were measured using material from the same shallow core, so diagenetic alteration due to regional changes in the lysocline can reasonably be excluded. Could dissolution susceptibility be species-specific [e.g., Berger, 1967]? Higher  $\text{pCO}_2$  estimates are based on relatively lower  $\delta^{11}\text{B}$  values, suggesting that *G. ruber* would have to be relatively more dissolved than *T. sacculifer*. Shell-weight evidence indeed suggests that *G. ruber* is slightly more susceptible to partial dissolution than *T. sacculifer* based on *in situ* and laboratory work [e.g., Thunell and Honjo, 1981]. In actuality, however, studies of foraminiferal  $\delta^{11}\text{B}$  from depth transects have suggested that *G. ruber*  $\delta^{11}\text{B}$  values may be more robust and not greatly affected by partial dissolution [Ni et al., 2007; Seki et al., 2010;

*Henehan et al.*, 2013] and that the foraminiferal  $\delta^{11}\text{B}$  signature is preserved even when the shell is visibly recrystallized [*Edgar et al.*, 2015]. Another factor which could lower  $\delta^{11}\text{B}$  values is contamination from pelagic clays, whose  $\delta^{11}\text{B}$  values typically fall in the -7 to +5‰ range [*Ishikawa and Nakamura*, 1993] and are thus much lower than  $\delta^{11}\text{B}$  of foraminiferal calcite. For the *G. ruber* pCO<sub>2</sub> estimates to agree with the *T. sacculifer* estimates, clay contamination would have to explain the -1‰ discrepancy in  $\delta^{11}\text{B}_{G. ruber}$ . This would require the *G. ruber* samples to have contained ~5 wt % clay, which is unlikely given the robust cleaning protocol applied to remove impurities and the careful contaminant screening for aluminum and iron [e.g., *Martínez-Botí et al.*, 2015a; *Chalk et al.*, 2017].

At this point we have reasonably ruled out dissolution differences and clay contamination in addition to differential temperature calibrations,  $\delta^{11}\text{B}_{\text{sw}}$  values, salinity, and alkalinity estimates. It is therefore more likely that the difference is biological. Although both foraminifera species and instrumental techniques have been calibrated using modern cultured and core top specimens and shown to replicate the ice-core pCO<sub>2</sub> record of the last glacial cycle [*Hönisch and Hemming*, 2004; 2005; *Foster*, 2008; *Henehan et al.*, 2013; *Chalk et al.*, 2017], one or both of the studied foraminifer species could have evolved prior to the last glacial cycle. One line of evidence for such an evolutionary shift has been described by *Bartoli et al.* [2011], who could not find enough Pliocene *T. sacculifer* specimens in the >500  $\mu\text{m}$  test size fraction and instead substituted specimens in the 425-500  $\mu\text{m}$  range. *Hönisch and Hemming* [2004] observed no significant difference in  $\delta^{11}\text{B}_{T. sacculifer}$  between the 425-500 and >500  $\mu\text{m}$  test size fraction, suggesting that the depth habitat and ecology is the same for both of the large size fractions. Indeed, if the overall smaller specimens of the largest size fraction in the early Pleistocene sediments had inhabited a deeper water depth, *T. sacculifer* should have recorded lower  $\delta^{11}\text{B}$ , which would imply lower pH and elevated pCO<sub>2</sub>. Instead, we observe the opposite pattern: *T. sacculifer* pCO<sub>2</sub> estimates are lower than those based on *G. ruber* [*Seki et al.*, 2010; *Martínez-Botí et al.*, 2015a; *Chalk et al.*, 2017].

Could the response of *G. ruber* to ocean pH have evolved over the Plio-Pleistocene? Interestingly, in the modern Caribbean the pink variety of *G. ruber* is quite abundant, whereas the culture and global core top calibration of *Henehan et al.* [2013] is based on the white variety. The canonical *G. ruber* morphospecies represents up to five genetically distinct varieties each with non-unique ecological and biogeographic preferences. In contrast, *T.*

*sacculifer* does not exhibit such cryptic diversity [Darling and Wade, 2008; André *et al.*, 2012]. Confidence in the  $\delta^{11}\text{B}$  proxy of  $\text{pCO}_2$  in the Pliocene and early Pleistocene is strengthened by good proxy replication of  $\text{pCO}_2$  with the ice core record (past 800 ka). In comparing the last two glacial cycles, average *G. ruber*  $\delta^{11}\text{B}$  values are  $\sim 0.3\%$  lower in MIS 6 even as  $\text{pCO}_2$  derived from ice cores is nearly identical in MIS 2 and 6 [Chalk *et al.*, 2017]. Using a consistent method for estimating temperature, in this case via Evans and Müller [2012], the  $\text{pCO}_2$  calculated from *G. ruber*  $\delta^{11}\text{B}$  is  $\sim 40 \mu\text{atm}$  higher in MIS 6 than in MIS 2. This result suggests that evolutionary differences in *G. ruber* could be as young as  $\sim 200$  ka. Once again, the Mg/Ca-based temperatures derived from these two species do not diverge in the Plio-Pleistocene (3.3-2.3 Ma), which implies that the difference in reconstructed  $\text{pCO}_2$  is less likely due to changes in habitat depth or seasonal preferences.

Finally,  $\text{pCO}_2$  estimates from other proxy archives are at odds with the highest Pliocene *G. ruber*-based  $\text{pCO}_2$  estimates (Figure 8). For example, evidence from the alkenone  $\delta^{13}\text{C}$  proxy suggests relatively lower ( $< 350 \mu\text{atm}$ ) levels of late Pliocene  $\text{pCO}_2$ , whether derived from Site 999A, (high resolution data:  $270 \pm 40$ ) [Badger *et al.*, 2013], (low resolution data:  $330 \pm 40$ ) [Seki *et al.*, 2010], or from Site 925 in eastern tropical Atlantic ( $320 \pm 40$ ) [Zhang *et al.*, 2013]. While different proxies have different uncertainties, the larger amplitude of Pliocene  $\text{pCO}_2$  change in the *G. ruber*-based record ( $\sim 150 \mu\text{atm}$  as opposed to  $\sim 100 \mu\text{atm}$  in the *T. sacculifer*-based record) is difficult to justify given the smaller amplitude of glacial-interglacial cycles in the Pliocene [Lisiecki and Raymo, 2005]. In summary, although we cannot unequivocally state which species may have changed behavior, it will be important to cross-calibrate the  $\delta^{11}\text{B}$  proxy in the Pliocene with regard to potential physiological distinctions.

Importantly, both *G. ruber* and *T. sacculifer* record a  $\text{pCO}_2$  decline through the Plio-Pleistocene (Figures 7, 8), but the extent of the  $\text{pCO}_2$  decline is larger for *G. ruber* reconstructions and this has critical implications for estimates of climate sensitivity from these two species. If the Pliocene *G. ruber*-based  $\text{pCO}_2$  estimate is correct, then late Pliocene (3.3–2.8 Ma)  $\text{pCO}_2$  levels were relatively high ( $> 350 \mu\text{atm}$ ), and highly variable, and then dramatically declined at the onset of northern hemisphere glaciation. Martínez-Botí *et al.* [2015a] use this data to infer low sensitivity to radiative  $\text{pCO}_2$  forcing in the Pliocene and higher sensitivity in the Pleistocene. They call out increased continental ice-albedo as the

primary mechanism for this change in sensitivity and use, as one line of evidence, the inflection point at  $\sim 275 \mu\text{atm}$  in the relationship between benthic  $\delta^{18}\text{O}$  and forcing due to  $\text{pCO}_2$  changes [Martínez-Botí *et al.*, 2015a]. Here we replot this figure using all available datasets discussed herein, but we also separate the two species (Figure 9). Martínez-Botí *et al.* [2015a] originally excluded the data of Bartoli *et al.* [2011] from their plot to improve clarity, but it now emerges that the change in slope of the relationship observed by Martínez-Botí *et al.* [2015a] is only true for *G. ruber* but not for *T. sacculifer* (Figure 9). Explaining the larger Plio-Pleistocene  $\text{CO}_2$  drawdown inferred by the *G. ruber*  $\delta^{11}\text{B}$  record requires significant increases in ocean stratification, dust fertilization, and/or (potentially) silicate rock weathering since the Pliocene (e.g., Martínez-García *et al.*, 2011).

If, on the other hand, the Pliocene *T. sacculifer*-based  $\text{pCO}_2$  estimates are correct, Pliocene  $\text{pCO}_2$  was less elevated relative to early Pleistocene  $\text{pCO}_2$  values and the linear relationship between benthic  $\delta^{18}\text{O}$  and  $\text{pCO}_2$  forcing extended into the Pliocene (Figure 9A). The *T. sacculifer*-based estimates, with  $\text{pCO}_2$  likely  $< 350\text{--}400 \mu\text{atm}$ , support the evidence for lower Pliocene  $\text{pCO}_2$  from other proxies (Figure 8): alkenone  $\delta^{13}\text{C}$ , stomatal indices, and paleosols [e.g., Badger *et al.*, 2013; Da *et al.*, 2015; Wang *et al.*, 2015] and implies that atmospheric  $\text{pCO}_2$  was relatively similar between the late Pliocene and early Pleistocene, despite the descent into cooler polar temperatures. If correct, this record implies that Arctic temperatures declined at the Plio-Pleistocene transition due to factors other than direct radiative  $\text{pCO}_2$  forcing, such as the thickening of northern-hemisphere ice sheets or reduced poleward oceanic heat transport. Further work is warranted to improve our understanding of foraminiferal vital effects on  $\delta^{11}\text{B}$ , and thereby improve confidence in paleo- $\text{pCO}_2$  estimates from this proxy.

## 5. Conclusions

Glacial-interglacial climate cycles in the early Pleistocene ( $>1 \text{ Ma}$ ) were shorter and less severe than the iconic 100-kyr cycles of the last 0.5 million years. Our new high-resolution record of atmospheric  $\text{pCO}_2$  over three glacial cycles in the early Pleistocene (1.38-1.54 Ma) is closely linked with obliquity pacing, with an average  $\text{pCO}_2$  amplitude of  $92 (\pm 13) \mu\text{atm}$ . Over the MPT, glacial  $\text{pCO}_2$  declined, alongside glacial SST cooling in both the tropics and high latitudes. In contrast to an earlier assessment of climate sensitivity from  $\delta^{11}\text{B}$  in *G. ruber*, our compilation of  $\text{pCO}_2$  estimates from  $\delta^{11}\text{B}$  in *T. sacculifer* suggests apparent

climate sensitivity in the early Pleistocene was lower compared to the late Pleistocene; the difference is likely due to changing ocean or ice sheet dynamics over the mid-Pleistocene. Using a simple model, we suggest that the lower climate sensitivity in the early Pleistocene was not directly related to the thinner, yet extensive, northern-hemisphere terrestrial ice sheets, but is rather a result of changing ocean dynamics in the southern hemisphere or tropics. The observed discrepancy in late Pliocene  $p\text{CO}_2$  estimates based on *G. ruber* and *T. sacculifer* requires further study of potentially evolving species-specific vital effects in the past, so that paleo- $p\text{CO}_2$  estimates from the proxy can be appreciated with confidence.

### Acknowledgements

We thank the International Ocean Drilling Program repository for providing samples for these analyses and Carina Fish, Peter deMenocal and Angela Dial for assistance with the new trace element analyses. This work was funded by the National Science Foundation grant EAR-1349616 to KD and a gift from Gerry Lenfest to BH. Upon publication, all original data from this study will be archived at NOAA's National Center for Environmental Information at <https://www.ncdc.noaa.gov/paleo/study/25490> as a part of the Research Coordination Network grant to BH and Pratigya Polissar (OCE 16-36005).

### References

- Allen, K. A., B. Hönisch, S. M. Eggins, and Y. Rosenthal (2012), Environmental controls on B/Ca in calcite tests of the tropical planktic foraminifer species *Globigerinoides ruber* and *Globigerinoides sacculifer*, *Earth and Planetary Science Letters*, 351-352(C), 270–280, doi:10.1016/j.epsl.2012.07.004.
- Anand, P., H. Elderfield, and M. H. Conte (2003), Calibration of Mg/Ca thermometry in planktonic foraminifera from a sediment trap time series, *Paleoceanography*, 18(2), 1050, doi:10.1029/2002PA000846.
- Anderson, R. F., S. Ali, L. I. Bradtmiller, S. Nielsen, M. Q. Fleisher, B. E. Anderson, and L. H. Burckle (2009), Wind-driven upwelling in the Southern Ocean and the deglacial rise in atmospheric  $\text{CO}_2$ , *Science*, 323(5920), 1443–1448, doi:10.1126/science.1167441.
- Badger, M. P. S., D. N. Schmidt, A. Mackensen, and R. D. Pancost (2013), High-resolution alkenone palaeobarometry indicates relatively stable  $p\text{CO}_2$  during the Pliocene (3.3–2.8 Ma), *Philosophical Transactions of the Royal Society A: Mathematical, Physical and Engineering Sciences*, 371(2001), 20130094–20130094, doi:10.1016/j.gca.2006.06.009.
- Bailey, I., Q. Liu, G. E. A. Swann, Z. Jiang, Y. Sun, X. Zhao, and A. P. Roberts (2011), Iron fertilisation and biogeochemical cycles in the sub-Arctic northwest Pacific during the late

- Pliocene intensification of northern hemisphere glaciation, *Earth and Planetary Science Letters*, 307(3-4), 253–265, doi:10.1016/j.epsl.2011.05.029.
- Balco, G., and C. W. Rovey (2010), Absolute chronology for major Pleistocene advances of the Laurentide Ice Sheet, *Geology*, 38(9), 795–798, doi:10.1130/G30946.1.
- Barker, S., M. Greaves, and H. Elderfield (2003), A study of cleaning procedures used for foraminiferal Mg/Ca paleothermometry, *Geochemistry Geophysics Geosystems*, 4(9), doi:10.1029/2003GC000559.
- Bartoli, G., B. Hönisch, and R. E. Zeebe (2011), Atmospheric CO<sub>2</sub> decline during the Pliocene intensification of Northern Hemisphere glaciations, *Paleoceanography*, 26(4), PA3206, doi:10.1029/2010PA002055.
- Bemis, B. E., H. J. Spero, J. Bijma, and D. W. Lea (1998), Reevaluation of the oxygen isotopic composition of planktonic foraminifera: Experimental results and revised paleotemperature equations, *Paleoceanography*, 13(2), 150–160, doi:10.1029/98PA00070.
- Bereiter, B., S. Eggelston, J. Schmitt, C. Nehrbass-Ahles, T. F. Stocker, H. Fischer, S. Kipfstuhl, and J. Chappellaz (2015), Revision of the EPICA Dome C CO<sub>2</sub> record from 800 to 600kyr before present, *Geophysical Research Letters*, 42(2), 542–549, doi:10.1002/2014GL061957.
- Berger, W. H. (1967), Foraminiferal Ooze - Solution at Depths, *Science*, 156(3773), 383–385, doi:10.1126/science.156.3773.383.
- Bé, A. W. H. (1980), Gametogenic calcification in a spinose planktonic foraminifer, *Globigerinoides sacculifer* (Brady), *Marine Micropaleontology*, 5, 283–310, doi:10.1016/0377-8398(80)90014-6.
- Bibby, T., J. Putkonen, D. Morgan, G. Balco, and D. L. Shuster (2016), Million year old ice found under meter thick debris layer in Antarctica, *Geophysical Research Letters*, doi:10.1002/2016GL069889.
- Bintanja, R., and R. S. W. van de Wal (2008), North American ice-sheet dynamics and the onset of 100,000-year glacial cycles, *Nature*, 454(7206), 869–872, doi:10.1038/nature07158.
- Bird, M. I., and J. A. Cali (1998), A million-year record of fire in sub-Saharan Africa, *Nature*, 394(6695), 767–769, doi:10.1038/29507.
- Bird, M. I., and J. A. Cali (2002), A revised high-resolution oxygen-isotope chronology for ODP-668B: implications for Quaternary biomass burning in Africa, *Global and Planetary Change*, 33(1-2), 73–76, doi:10.1016/S0921-8181(02)00062-0.
- Boyle, E. A. (1988), The Role of Vertical Chemical Fractionation in Controlling Late Quaternary Atmospheric Carbon-Dioxide, *J. Geophys. Res. Oceans*, 93(C12), 15701–15714, doi:10.1029/JC093iC12p15701.
- Boyle, E. A., and L. D. Keigwin (1985), Comparison of Atlantic and Pacific paleochemical records for the last 215,000 years: Changes in deep ocean circulation and chemical

inventories, *Earth and Planetary Science Letters*, 76(1-2), 135–150, doi:10.1016/0012-821X(85)90154-2.

Branson, O., K. Kaczmarek, S. A. T. Redfern, S. Misra, G. Langer, T. Tyliszczak, J. Bijma, and H. Elderfield (2015), The coordination and distribution of B in foraminiferal calcite, *Earth and Planetary Science Letters*, 416(C), 67–72, doi:10.1016/j.epsl.2015.02.006.

Brennan, S. T., T. K. Lowenstein, and D. I. Cendon (2013), The major-ion composition of Cenozoic seawater: The past 36 million years from fluid inclusions in marine halite, *American Journal of Science*, 313(8), 713–775, doi:10.2475/08.2013.01.

Broecker, W. S. (1971), Calcite accumulation rates and glacial to interglacial changes in oceanic mixing, in *The Late Cenozoic glacial ages*, edited by K. K. Turekian, pp. 239–265, Yale University.

Broecker, W. S., and T.-H. Peng (1987), The role of CaCO<sub>3</sub> compensation in the glacial to interglacial atmospheric CO<sub>2</sub> change, *GBC*, 1(1), 15–29, doi:10.1029/GB001i001p00015.

Chalk, T. B. et al. (2017), Causes of ice age intensification across the Mid-Pleistocene Transition, *PNAS*, 114(50), 13114–13119, doi:10.1073/pnas.1702143114.

Clark, P. U., and D. Pollard (1998), Origin of the middle Pleistocene transition by ice sheet erosion of regolith, *Paleoceanography*, 13(1), 1–9, doi:10.1029/97pa02660.

Clark, P. U., D. Archer, D. Pollard, J. D. Blum, J. A. Rial, V. Brovkin, A. C. Mix, N. G. Pisias, and M. Roy (2006), The middle Pleistocene transition: characteristics, mechanisms, and implications for long-term changes in atmospheric pCO<sub>2</sub>, *Quaternary Science Reviews*, 25(23-24), 3150–3184, doi:10.1016/j.quascirev.2006.07.008.

Clark, P. U., R. B. Alley, and D. Pollard (1999), Northern Hemisphere Ice-Sheet Influences on Global Climate Change, *Science*, 286(5442), 1104–1111, doi:10.1126/science.286.5442.1104.

Da, J., Y. G. Zhang, H. Wang, W. Balsam, and J. Ji (2015), An Early Pleistocene atmospheric CO<sub>2</sub> record based on pedogenic carbonate from the Chinese loess deposits, *Earth and Planetary Science Letters*, 426(C), 69–75, doi:10.1016/j.epsl.2015.05.053.

Dai, Y., Yu, J., and Johnstone, H.J.H., 2016, Distinct responses of planktonic foraminiferal B/Ca to dissolution on seafloor: *Geochemistry Geophysics Geosystems*, v. 17, no. 4, p. 1339–1348, doi: 10.1002/2015GC006199.

de Villiers, S., 2005, Foraminiferal shell-weight evidence for sedimentary calcite dissolution above the lysocline: *Deep Sea Research Part I: Oceanographic Research Papers*, v. 52, no. 5, p. 671–680, doi: 10.1016/j.dsr.2004.11.014.

Dekens, P. S., D. W. Lea, D. K. Pak, and H. J. Spero (2002), Core top calibration of Mg/Ca in tropical foraminifera: Refining paleotemperature estimation, *Geochemistry Geophysics Geosystems*, 3, 1022, doi:10.1029/2001GC000200.

- Delaney, M. L., A. W. H. Bé, and E. A. Boyle (1985), Li, Sr, Mg, and Na in foraminiferal calcite shells from laboratory culture, sediment traps, and sediment cores, *Geochimica et Cosmochimica Acta*, doi:10.1016/0016-7037(85)90284-4.
- Dickson, A. G. (1990), Thermodynamics of the dissociation of boric acid in synthetic seawater from 273.15 to 318.15 K, *Deep-Sea Research II*, 37, 755–766, doi:10.1021/je00061a009.
- Dyez, K., and A. C. Ravelo (2013), Late Pleistocene tropical Pacific temperature sensitivity to radiative greenhouse gas forcing, *Geology*, 41(1), 23–26, doi:10.1130/G33425.1.
- Dyez, K., and A. C. Ravelo (2014), Dynamical changes in the tropical Pacific warm pool and zonal SST gradient during the Pleistocene, *Geophysical Research Letters*, 41, 7626–7633, doi:10.1002/2014GL061639.
- Edgar, K. M., E. Anagnostou, P. N. Pearson, and G. L. Foster (2015), Assessing the impact of diagenesis on  $\delta^{11}\text{B}$ ,  $\delta^{13}\text{C}$ ,  $\delta^{18}\text{O}$ , Sr/Ca and B/Ca values in fossil planktic foraminiferal calcite, *Geochimica et Cosmochimica Acta*, 166(C), 189–209, doi:10.1016/j.gca.2015.06.018.
- Evans, D., and W. Müller (2012), Deep time foraminifera Mg/Ca paleothermometry: Nonlinear correction for secular change in seawater Mg/Ca, *Paleoceanography*, 27(4), PA4205, doi:10.1029/2012PA002315.
- Evans, D., C. M. Brierley, M. E. Raymo, J. Erez, and W. Müller (2016), Planktic foraminifera shell chemistry response to seawater chemistry: Pliocene–Pleistocene seawater Mg/Ca, temperature and sea level change, *Earth and Planetary Science Letters*, 438(C), 139–148, doi:10.1016/j.epsl.2016.01.013.
- Fantle, M. S., and D. J. DePaolo (2005), Variations in the marine Ca cycle over the past 20 million years, *Earth and Planetary Science Letters*, 237(1-2), 102–117.
- Fantle, M. S., and D. J. DePaolo (2006), Sr isotopes and pore fluid chemistry in carbonate sediment of the Ontong Java Plateau: Calcite recrystallization rates and evidence for a rapid rise in seawater Mg over the last 10 million years, *Geochimica et Cosmochimica Acta*, 70(15), 3883–3904.
- Farmer, E. C., A. Kaplan, P. B. de Menocal, and J. Lynch-Stieglitz (2007), Corroborating ecological depth preferences of planktonic foraminifera in the tropical Atlantic with the stable oxygen isotope ratios of core top specimens, *Paleoceanography*, 22(3), doi:10.1029/2006PA001361.
- Farmer, J. R., B. Hönisch, and J. Uchikawa (2016), Single laboratory comparison of MC-ICP-MS and N-TIMS boron isotope analyses in marine carbonates, *Chemical Geology*, 1–10, doi:10.1016/j.chemgeo.2016.11.008.
- Farrell, J. W., and W. L. Prell (1991), Pacific CaCO<sub>3</sub> Preservation and  $\delta^{18}\text{O}$  Since 4 Ma: Paleoceanic and Paleoclimatic Implications, *Paleoceanography*, 6(4), 485–498, doi:10.1029/91PA00877.

- Fischer, H. et al. (2010), The role of Southern Ocean processes in orbital and millennial CO<sub>2</sub> variations - A synthesis, *Quaternary Science Reviews*, 29(1-2), 193–205, doi:10.1016/j.quascirev.2009.06.007.
- Fischer, H. et al. (2013), Where to find 1.5 million yr old ice for the IPICS “Oldest Ice” ice core, *Clim. Past Discuss.*, 9(3), 2771–2815, doi:10.5194/cpd-9-2771-2013.
- Foster, G. L. (2008), Seawater pH, pCO<sub>2</sub> and [CO<sub>3</sub><sup>-2</sup>] variations in the Caribbean Sea over the last 130 kyr: A boron isotope and B/Ca study of planktic foraminifera, *Earth and Planetary Science Letters*, 271(1-4), 254–266, doi:10.1016/j.epsl.2008.04.015.
- Foster, G. L., B. Hönisch, G. Paris, G. S. Dwyer, J. W. B. Rae, T. Elliott, J. Gaillardet, N. G. Hemming, P. Louvat, and A. Vengosh (2013), Interlaboratory comparison of boron isotope analyses of boric acid, seawater and marine CaCO<sub>3</sub> by MC-ICPMS and NTIMS, *Chemical Geology*, 358(C), 1–14, doi:10.1016/j.chemgeo.2013.08.027.
- Foster, G. L., P. A. E. Pogge von Strandmann, and J. W. B. Rae (2010), Boron and magnesium isotopic composition of seawater, *Geochemistry Geophysics Geosystems*, 11(8), doi:10.1029/2010GC003201.
- Greenop, R., M. P. Hain, S. M. Sosdian, K. I. C. Oliver, P. Goodwin, T. B. Chalk, C. H. Lear, P. A. Wilson, and G. L. Foster (2017), A record of Neogene seawater δ<sup>11</sup>B reconstructed from paired δ<sup>11</sup>B analyses on benthic and planktic foraminifera, *Climate of the Past*, 13(2), 149–170, doi:10.5194/cp-13-149-2017.
- Groeneveld, J. (2005), Effect of the Pliocene closure of the Panamanian Gateway on Caribbean and east Pacific sea surface temperatures and salinities by applying combined Mg/Ca and, 1–165 pp. Christian Albrechts University, 20 October.
- Hansen, J. et al. (2005), Efficacy of climate forcings, *J. Geophys. Res. Atmos.*, 110(D18), doi:10.1029/2005JD005776.
- Hansen, J., A. Lacis, D. Rind, G. Russell, P. Stone, I. Y. Fung, R. Ruedy, and J. Lerner (1984), Climate sensitivity: Analysis of feedback mechanisms, in *Climate Processes and Climate Sensitivity*, vol. 29, edited by J. E. Hansen and T. Takahashi, American Geophysical Union.
- Haug, G. H., D. M. Sigman, R. Tiedemann, T. F. Pedersen, and M. Sarnthein (1999), Onset of permanent stratification in the subarctic Pacific Ocean, *Nature*, 401(6755), 779–782.
- Hays, J., J. Imbrie, and N. J. Shackleton (1976), Variations in the earth's orbit: pacemaker of the ice ages, *Science*, 194(4270), 1121–1132, doi:10.1126/science.194.4270.1121.
- Hemming, N. G., and G. N. Hanson (1992), Boron isotopic composition and concentration in modern marine carbonates, *Geochimica et Cosmochimica Acta*, 56(1), 537–543.
- Henehan, M. J. et al. (2013), Calibration of the boron isotope proxy in the planktonic foraminifera *Globigerinoides ruber* for use in palaeo-CO<sub>2</sub> reconstruction, *Earth and Planetary Science Letters*, 364, 111–122, doi:10.1016/j.epsl.2012.12.029.

- Herbert, T. D., L. C. Peterson, M. T. Kucera, and Z. Liu (2010), Tropical Ocean Temperatures Over the Past 3.5 Million Years, *Science*, 328, 1530–1534, doi:10.1126/science.1185435.
- Heydt, von der, A. S. et al. (2016), Lessons on climate sensitivity from past climate changes, *Curr Clim Change Rep*, 2(4), 1–11, doi:10.1007/s40641-016-0049-3.
- Higgins, J. A., A. V. Kurbatov, N. E. Spaulding, E. J. Brook, D. S. Introne, L. M. Chimiak, Y. Yan, P. A. Mayewski, and M. L. Bender (2015), Atmospheric composition 1 million years ago from blue ice in the Allan Hills, Antarctica, *PNAS*, 112(22), 6887–6891, doi:10.1073/pnas.1420232112.
- Hodell, D. A., and K. A. Venz-Curtis (2006), Late Neogene history of deepwater ventilation in the Southern Ocean, *Geochemistry Geophysics Geosystems*, 7(9), doi:10.1029/2005GC001211.
- Horita, J., H. Zimmermann, and H. D. Holland (2002), Chemical evolution of seawater during the Phanerozoic: Implications from the record of marine evaporites, *Geochimica et Cosmochimica Acta*, 66(21), 3733–3756, doi:10.1016/S0016-7037(01)00884-5.
- Hönisch, B., and N. G. Hemming (2004), Ground-truthing the boron isotope-paleo-pH proxy in planktonic foraminifera shells: Partial dissolution and shell size effects, *Paleoceanography*, 19(4), PA4010, doi:10.1029/2004PA001026.
- Hönisch, B., and N. G. Hemming (2005), Surface ocean pH response to variations in pCO<sub>2</sub> through two full glacial cycles, *Earth and Planetary Science Letters*, 236(1-2), 305–314, doi:10.1016/j.epsl.2005.04.027.
- Hönisch, B., K. A. Allen, D. W. Lea, H. J. Spero, S. M. Eggins, J. A. Arbuszewski, P. B. deMenocal, Y. Rosenthal, A. D. Russell, and H. Elderfield (2013), The influence of salinity on Mg/Ca in planktic foraminifers - Evidence from cultures, core-top sediments and complementary  $\delta^{18}\text{O}$ , *Geochimica et Cosmochimica Acta*, 121(C), 196–213, doi:10.1016/j.gca.2013.07.028.
- Hönisch, B., N. G. Hemming, D. Archer, M. Siddall, and J. F. McManus (2009), Atmospheric carbon dioxide concentration across the mid-Pleistocene transition, *Science*, 324(5934), 1551, doi:10.1126/science.1171477.
- Huybers, P. (2007), Glacial variability over the last two million years: an extended depth-derived age model, continuous obliquity pacing, and the Pleistocene progression, *Quaternary Science Reviews*, 26(1-2), 37–55, doi:10.1016/j.quascirev.2006.07.013.
- Imbrie, J. et al. (1992), On the structure and origin of major glaciation cycles 1. Linear responses to Milankovitch forcing, *Paleoceanography*, 7(6), 701–738, doi:10.1029/92pa02253.
- Imbrie, J., J. D. Hays, D. G. Martinson, A. McIntyre, A. C. Mix, J. Morley, N. G. Pisias, W. L. Prell, and N. J. Shackleton (1984), The orbital theory of Pleistocene climate: Support from a revised chronology of the marine  $\delta^{18}\text{O}$  record, edited by A. L. Berger, J. Imbrie, J. Hays, G. Kukla, and B. Saltzman, pp. 269–305, Milankovitch and Climate.

- Ishikawa, T., and E. Nakamura (1993), Boron Isotope Systematics of Marine-Sediments, *Earth and Planetary Science Letters*, 117(3-4), 567–580, doi:10.1016/0012-821X(93)90103-G.
- Joannin, S. et al. (2010), Early Pleistocene climate cycles in continental deposits of the Lesser Caucasus of Armenia inferred from palynology, magnetostratigraphy, and  $^{40}\text{Ar}/^{39}\text{Ar}$  dating, *Earth and Planetary Science Letters*, 291(1-4), 149–158, doi:10.1016/j.epsl.2010.01.007.
- Jouzel, J. et al. (2007), Orbital and Millennial Antarctic Climate Variability over the Past 800,000 Years, *Science*, 317(5839), 793–796, doi:10.1126/science.1141038.
- Key, R. M., A. Kozyr, C. L. Sabine, K. Lee, R. Wanninkhof, J. L. Bullister, R. A. Feely, F. Millero, C. Mordy, and T. H. Peng (2004), A global ocean carbon climatology: Results from Global Data Analysis Project (GLODAP), *GBC*, 18(4), doi:10.1029/2004GB002247.
- Klochko, K., A. J. Kaufman, W. Yao, R. H. Byrne, and J. A. Tossell (2006), Experimental measurement of boron isotope fractionation in seawater, *Earth and Planetary Science Letters*, 248(1-2), 276–285, doi:10.1016/j.epsl.2006.05.034.
- Köhler, P., and R. Bintanja (2008), The carbon cycle during the Mid Pleistocene Transition: the Southern Ocean Decoupling Hypothesis, *Climate of the Past*, 4(4), 311–332, doi:10.5194/cp-4-311-2008.
- Köhler, P., B. de Boer, A. S. von der Heydt, L. B. Stap, and R. S. W. van de Wal (2015), On the state dependency of the equilibrium climate sensitivity during the last 5 million years, *Climate of the Past*, 11(12), 1801–1823, doi:10.5194/cp-11-1801-2015.
- Köhler, P., R. Bintanja, H. Fischer, F. Joos, R. Knutti, G. Lohmann, and V. Masson-Delmotte (2010), What caused Earth's temperature variations during the last 800,000 years? Data-based evidence on radiative forcing and constraints on climate sensitivity, *Quaternary Science Reviews*, 29(1-2), 129–145, doi:10.1016/j.quascirev.2009.09.026.
- Kürschner, W. M., J. vanderBurgh, H. Visscher, and D. L. Dilcher (1996), Oak leaves as biosensors of late Neogene and early Pleistocene paleoatmospheric  $\text{CO}_2$  concentrations, *Marine Micropaleontology*, 27(1-4), 299–312, doi:10.1016/0377-8398(95)00067-4.
- Laskar, J., P. Robutel, F. Joutel, M. Gastineau, A. C. M. Correia, and B. Levrard (2004), A long-term numerical solution for the insolation quantities of the Earth, *Astronomy and Astrophysics*, 428(1), 261–285, doi:10.1051/0004-6361:20041335.
- Lawrence, K., T. D. Herbert, C. M. Brown, M. E. Raymo, and A. M. Haywood (2009), High-amplitude variations in North Atlantic sea surface temperature during the early Pliocene warm period, *Paleoceanography*, 24(2), 1–15, doi:10.1029/2008PA001669.
- Lea, D. W. (2004), The 100 000-yr cycle in tropical SST, greenhouse forcing, and climate sensitivity, *Journal of Climate*, 17(11), 2170–2179, doi:10.1175/1520-0442(2004)017<2170:TYCITS>.

- Lee, K., T.-W. Kim, R. H. Byrne, F. J. Millero, R. A. Feely, and Y.-M. Liu (2010), The universal ratio of boron to chlorinity for the North Pacific and North Atlantic oceans, *Geochimica et Cosmochimica Acta*, 74(6), 1801–1811, doi:10.1016/j.gca.2009.12.027.
- Legrande, A. N., and G. A. Schmidt (2006), Global gridded data set of the oxygen isotopic composition in seawater, *Geophysical Research Letters*, 33, doi:10.1029/2006GL026011.
- Lemarchand, D., J. Gaillardet, E. Lewin, and C. J. Allegre (2000), The influence of rivers on marine boron isotopes and implications for reconstructing past ocean pH, *Nature*, 408(6815), 951–954, doi:10.1038/35050058.
- Lisiecki, L. E. (2010), A benthic  $\delta^{13}\text{C}$ -based proxy for atmospheric  $\text{pCO}_2$  over the last 1.5 Myr, *Geophysical Research Letters*, 37(21), L21708, doi:10.1029/2010GL045109.
- Lisiecki, L. E., and M. E. Raymo (2005), A Pliocene-Pleistocene stack of 57 globally distributed benthic  $\delta^{18}\text{O}$  records, *Paleoceanography*, 20, doi:10.1029/2004PA001071.
- Locarnini, R. A. et al. (2013), World Ocean Atlas 2013, Vol. 1: Temperature, in *NOAA Atlas NESDIS 73*, edited by S. Levitus and A. Mishonov, p. 40.
- Lueker, T. J., A. G. Dickson, and C. D. Keeling (2000), Ocean  $\text{pCO}_2$  calculated from dissolved inorganic carbon, alkalinity, and equations for  $K_1$  and  $K_2$ : validation based on laboratory measurements of  $\text{CO}_2$  in gas and seawater at equilibrium, *Marine Chemistry*, 70(1-3), 105–119, doi:10.1016/S0304-4203(00)00022-0.
- Lunt, D. J., G. L. Foster, A. M. Haywood, and E. J. Stone (2008), Late Pliocene Greenland glaciation controlled by a decline in atmospheric  $\text{CO}_2$  levels, *Nature*, 454(7208), 1102–1105, doi:10.1038/nature07223.
- Lüthi, D. et al. (2008), High-resolution carbon dioxide concentration record 650,000–800,000 years before present, *Nature*, 453(7193), 379–382, doi:10.1038/nature06949.
- Manabe, S., and A. J. Broccoli (1985), The Influence of Continental Ice Sheets on the Climate of an Ice-Age, *J. Geophys. Res. Atmos.*, 90(ND1), 2167–2190, doi:10.1029/JD090iD01p02167.
- Martin, P. A., and D. W. Lea (2002), A simple evaluation of cleaning procedures on fossil benthic foraminiferal Mg/Ca, *Geochemistry Geophysics Geosystems*, 3(10), 1–8, doi:10.1029/2001GC000280.
- Martínez-Botí, M. A., G. L. Foster, T. B. Chalk, E. J. Rohling, P. F. Sexton, D. J. Lunt, R. D. Pancost, M. P. S. Badger, and D. N. Schmidt (2015a), Plio-Pleistocene climate sensitivity evaluated using high-resolution  $\text{CO}_2$  records, *Nature*, 518(7537), 49–54, doi:10.1038/nature14145.
- Martínez-Botí, M. A., G. Marino, G. L. Foster, P. Ziveri, M. J. Henehan, J. W. B. Rae, P. G. Mortyn, and D. Vance (2015b), Boron isotope evidence for oceanic carbon dioxide leakage during the last deglaciation, *Nature*, 518(7538), 219–222, doi:10.1038/nature14155.

- Martínez-García, A., A. Rosell-Melé, E. L. McClymont, R. Gersonde, and G. H. Haug (2010), Subpolar link to the emergence of the modern Equatorial Pacific cold tongue, *Science*, 328(5985), 1550, doi:10.1126/science.1184480.
- Martínez-García, A., A. Rosell-Melé, S. L. Jaccard, W. Geibert, D. M. Sigman, and G. H. Haug (2011), Southern Ocean dust-climate coupling over the past four million years, *Nature*, 476(7360), 312–315, doi:10.1038/nature10310.
- Mashiotta, T., D. W. Lea, and H. J. Spero (1999), Glacial-interglacial changes in Subantarctic sea surface temperature and  $\delta^{18}\text{O}$ -water using foraminiferal Mg, *Earth and Planetary Science Letters*, 170(4), 417–432, doi:10.1016/S0012-821X(99)00116-8.
- McClymont, E. L., A. Rosell-Melé, G. H. Haug, and J. M. Lloyd (2008), Expansion of subarctic water masses in the North Atlantic and Pacific oceans and implications for mid-Pleistocene ice sheet growth, *Paleoceanography*, 23(4), PA4214, doi:10.1029/2008PA001622.
- Medina-Elizalde, M., and D. W. Lea (2005), The mid-Pleistocene transition in the Tropical Pacific, *Science*, 310(5750), 1009, doi:10.1126/science.1115933.
- Medina-Elizalde, M., D. W. Lea, and M. S. Fantle (2008), Implications of seawater Mg/Ca variability for Plio-Pleistocene tropical climate reconstruction, *Earth and Planetary Science Letters*, 269(3-4), 585–595, doi:10.1016/j.epsl.2008.03.014.
- Millero, F. J. (1995), Thermodynamics of the carbon dioxide system in the oceans, *Geochimica et Cosmochimica Acta*, 59(4), 661–677, doi:10.1016/0016-7037(94)00354-o.
- Myhre, G., E. J. Highwood, K. P. Shine, and F. Stordal (1998), New estimates of radiative forcing due to well mixed greenhouse gases, *Geophysical Research Letters*, 25(14), 2715–2718, doi:10.1029/98GL01908.
- Ni, Y., G. L. Foster, T. Bailey, T. Elliott, D. N. Schmidt, P. N. Pearson, B. A. Haley, and C. Coath (2007), A core top assessment of proxies for the ocean carbonate system in surface-dwelling foraminifers, *Paleoceanography*, 22(3), PA3212, doi:10.1029/2006PA001337.
- O'Brien, C. L., G. L. Foster, M. A. Martínez-Botí, R. Abell, J. W. B. Rae, and R. D. Pancost (2014), High sea surface temperatures in tropical warm pools during the Pliocene, *Nature Geoscience*, 7(8), 606–611, doi:10.1038/ngeo2194.
- Paillard, D., L. Labeyrie, and P. Yiou (1996), Macintosh Program performs time-series analysis, *Eos Trans. AGU*, 77(39), 379–379, doi:10.1029/96EO00259.
- Pearson, P. N., and M. Palmer (2000), Atmospheric carbon dioxide concentrations over the past 60 million years, *Nature*, 406(6797), 695–699, doi:10.1038/35021000.
- Pena, L. D., and S. L. Goldstein (2014), Thermohaline circulation crisis and impacts during the mid-Pleistocene transition, *Science*, doi:10.1126/science.1249770.
- Perez, F. F., and F. Fraga (1987), The pH measurements in seawater on the NBS scale, *Marine Chemistry*, 21(4), 315–327, doi:10.1016/0304-4203(87)90054-5.

- Petit, J.-R., J. Jouzel, D. Raynaud, N. I. Barkov, J.-M. Barnola, I. Basile, M. L. Bender, J. Chappellaz, M. Davis, and G. Delaygue (1999), Climate and atmospheric history of the past 420,000 years from the Vostok ice core, Antarctica, *Nature*, 399(6735), 429–436.
- Pierrot, D. E. L., D. W. R. Wallace, and E. Lewis (2006), *MS Excel program developed for CO<sub>2</sub> system calculations*, Carbon Dioxide Information Analysis Center.
- Raitzsch, M., and B. Hönisch (2013), Cenozoic boron isotope variations in benthic foraminifers, *Geology*, 41(5), 591–594, doi:10.1130/G34031.1.
- Ravelo, A. C., and R. G. Fairbanks (1992), Oxygen Isotopic Composition of Multiple Species of Planktonic Foraminifera: Recorders of the Modern Photic Zone Temperature Gradient, *Paleoceanography*, 7(6), 815–831, doi:10.1029/92PA02092.
- Raymo, M. E. (1994), The initiation of Northern Hemisphere glaciation, *Annual Review of Earth and Planetary Sciences*, 22(1), 353–383, doi:10.1146/annurev.earth.22.1.353.
- Raymo, M. E., and K. H. Nisancioglu (2003), The 41 kyr world: Milankovitch's other unsolved mystery, *Paleoceanography*, 18(1), 1–6, doi:10.1029/2002PA000791.
- Raymo, M. E., L. E. Lisiecki, and K. Nisancioglu (2006), Plio-Pleistocene ice volume, Antarctic climate, and the global  $\delta^{18}\text{O}$  record, *Science*, 313(5786), 492.
- Regenberg, M., D. Nürnberg, S. Steph, J. Groeneveld, D. Garbe-Schönberg, R. Tiedemann, and W.-C. Dullo (2006), Assessing the effect of dissolution on planktonic foraminiferal Mg/Ca ratios: Evidence from Caribbean core tops, *Geochemistry Geophysics Geosystems*, 7(7), doi:10.1029/2005GC001019.
- Retallack, G. J. (2009), Greenhouse crises of the past 300 million years, *Geological Society of America Bulletin*, 121(9-10), 1441–1455, doi:10.1130/B26341.1.
- Roy, M., P. U. Clark, G. M. Raisbeck, and F. Yiou (2004), Geochemical constraints on the regolith hypothesis for the middle Pleistocene transition, *Earth and Planetary Science Letters*, 227(3), 281–296, doi:10.1016/j.epsl.2004.09.001.
- Ruddiman, W. F., M. E. Raymo, D. G. Martinson, B. M. Clement, and J. Backman (1989), Pleistocene evolution: Northern hemisphere ice sheets and North Atlantic Ocean, *Paleoceanography*, 4(4), 353–412, doi:10.1029/PA004i004p00353.
- Russon, T., M. Elliot, A. Y. Sadekov, G. Cabioch, T. Corrège, and P. De Deckker (2010), Inter-hemispheric asymmetry in the early Pleistocene Pacific warm pool, *Geophysical Research Letters*, 37(11), doi:10.1029/2010GL043191.
- Sanyal, A., J. Bijma, H. J. Spero, and D. W. Lea (2001), Empirical relationship between pH and the boron isotopic composition of *Globigerinoides sacculifer*: Implications for the boron isotope paleo-pH proxy, *Paleoceanography*, 16(5), 515–519, doi:10.1029/2000pa000547.
- Schiebel, R., and C. Hemleben (2005), Modern planktic foraminifera, *Paläontol. Z.*, 79(1), 135–148, doi:10.1007/BF03021758.

- Schlitzer, R. (2000), Electronic atlas of WOCE hydrographic and tracer data now available, *Eos, Transactions American Geophysical Union*, 81(5), 45–45, doi:10.1029/00EO00028.
- Schlitzer, R. (2017), *Ocean Data View*, <http://www.odv.awi.de>, 4 ed.
- Schmidt, G. A. et al. (2017), Overestimate of committed warming, *Nature*, 547(7662), E16–E17, doi:10.1038/nature22803.
- Seki, O., G. L. Foster, D. N. Schmidt, A. Mackensen, K. Kawamura, and R. D. Pancost (2010), Alkenone and boron-based Pliocene pCO<sub>2</sub> records, *Earth and Planetary Science Letters*, 292(1-2), 201–211, doi:10.1016/j.epsl.2010.01.037.
- Shackleton, N. J., A. L. Berger, and W. Peltier (1990), An alternative astronomical calibration of the lower Pleistocene timescale based on ODP Site 677, *Trans. R. Soc. Edinburgh Earth Sci*, 81, 251–261, doi:10.1017/s0263593300020782.
- Shakun, J. D., M. E. Raymo, and D. W. Lea (2016), An early Pleistocene Mg/Ca-<sup>18</sup>O record from the Gulf of Mexico: Evaluating ice sheet size and pacing in the 41-kyr world, 1–17, doi:10.1002/(ISSN)1944-9186.
- Shakun, J. D., P. U. Clark, F. He, S. A. Marcott, A. C. Mix, Z. Liu, B. L. Otto-Bliesner, A. Schmittner, and E. Bard (2012), Global warming preceded by increasing carbon dioxide concentrations during the last deglaciation, *Nature*, 484(7392), 49–54, doi:10.1038/nature10915.
- Shinn, R. A., and E. J. Barron (1989), Climate Sensitivity to Continental Ice-Sheet Size and Configuration, *Journal of Climate*, 2(12), 1517–1537, doi:10.1175/1520-0442(1989)002<1517:CSTCIS>2.0.CO;2.
- Shipboard Scientific Party (1988), Site 668, in *Proceedings of the Ocean Drilling Program, Initial Reports*, vol. 108, edited by W. Ruddiman, M. Sarnthein, J. Baldauf, et al., pp. 931–946, Ocean Drilling Program, College Station, TX.
- Sigman, D. M., S. L. Jaccard, and G. H. Haug (2004), Polar ocean stratification in a cold climate, *Nature*, 428(6978), 59–63, doi:10.1038/nature02357.
- Snyder, C. W. (2016), Evolution of global temperature over the past two million years, *Nature*, 538, 226–228, doi:10.1038/nature19798.
- Spero, H. J., K. M. Mielke, E. M. Kalve, D. W. Lea, and D. K. Pak (2003), Multispecies approach to reconstructing eastern equatorial Pacific thermocline hydrography during the past 360 kyr, *Paleoceanography*, 18(1), doi:10.1029/2002PA000814.
- Stults, D. Z., F. Wagner-Cremer, and B. J. Axsmith (2011), Atmospheric paleo-CO<sub>2</sub> estimates based on *Taxodium distichum* (Cupressaceae) fossils from the Miocene and Pliocene of Eastern North America, *Palaeogeography Palaeoclimatology Palaeoecology*, 309(3-4), 327–332, doi:10.1016/j.palaeo.2011.06.017.
- Takahashi, T. et al. (2009), Climatological mean and decadal change in surface ocean pCO<sub>2</sub>, and net sea–air CO<sub>2</sub> flux over the global oceans, *Deep-Sea Research II*, 56(8-10), 554–577, doi:10.1016/j.dsr2.2008.12.009.

- Thunell, R. C., and S. Honjo (1981), Calcite dissolution and the modification of planktonic foraminiferal assemblages, *Marine Micropaleontology*, 6(2), 169–182, doi:10.1016/0377-8398(81)90004-9.
- Tripati, A. K., C. D. Roberts, R. A. Eagle, and G. Li (2011), A 20 million year record of planktic foraminiferal B/Ca ratios: Systematics and uncertainties in pCO<sub>2</sub> reconstructions, *Geochimica et Cosmochimica Acta*, 75(10), 2582–2610, doi:10.1016/j.gca.2011.01.018.
- Tyrrell, T., and R. E. Zeebe (2004), History of carbonate ion concentration over the last 100 million years, *Geochimica et Cosmochimica Acta*, 68(17), 3521–3530, doi:10.1016/j.gca.2004.02.018.
- Tziperman, E., and H. Gildor (2003), On the mid-Pleistocene transition to 100-kyr glacial cycles and the asymmetry between glaciation and deglaciation times, *Paleoceanography*, 18(1), 1–1–8, doi:10.1029/2001pa000627.
- Waddell, L. M., I. L. Hendy, T. C. Moore, and M. W. Lyle (2009), Ventilation of the abyssal Southern Ocean during the late Neogene: A new perspective from the subantarctic Pacific, *Paleoceanography*, 24(3), 1769–15, doi:10.1029/2008PA001661.
- Wang, Y., A. Momohara, L. Wang, J. Lebreton-Anberrée, and Z. Zhou (2015), Evolutionary History of Atmospheric CO<sub>2</sub> during the Late Cenozoic from Fossilized Metasequoia Needles, edited by W. O. Wong, *PLOS ONE*, 10(7), 1–15, doi:10.1371/journal.pone.0130941.
- Weldeab, S., R. R. Schneider, and M. Kölling (2006), Comparison of foraminiferal cleaning procedures for Mg/Ca paleothermometry on core material deposited under varying terrigenous-input and bottom water conditions, *Geochemistry Geophysics Geosystems*, 7(4), doi:10.1029/2005GC000990.
- Witze, A. (2015), Super-fast drills hunt for oldest ice, *Nature*, 526, 618–619, doi:10.1038/526618a.
- York, D., N. M. Evensen, M. L. Martínez, and J. De Basabe Delgado (2004), Unified equations for the slope, intercept, and standard errors of the best straight line, *American Journal of Physics*, 72(3), 367–375, doi:10.1119/1.1632486.
- Zhang, Y. G., M. Pagani, Z. Liu, S. M. Bohaty, and R. DeConto (2013), A 40-million-year history of atmospheric CO<sub>2</sub>, *Philosophical Transactions of the Royal Society A: Mathematical, Physical and Engineering Sciences*, 371, 20130096–20130096, doi:10.1098/rsta.2013.0096.
- Zweng, M. M. et al. (2013), World Ocean Atlas 2013, Vol. 2: Salinity, in *NOAA Atlas NESDIS 73*, edited by S. Levitus and A. Mishonov, p. 39.

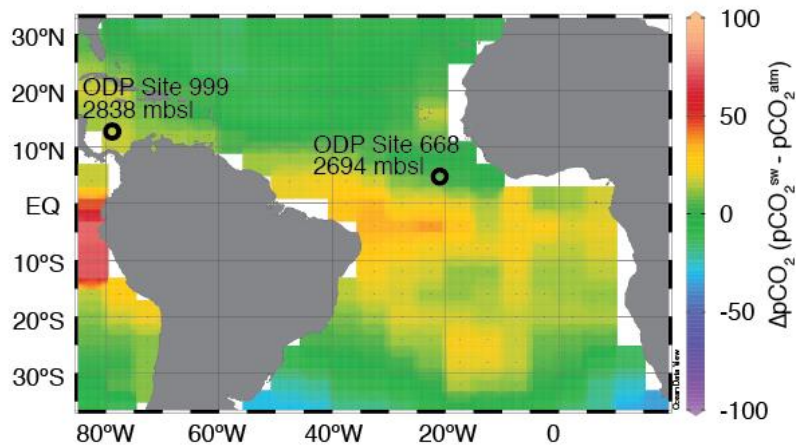


**Figure 1.** New geochemical data presented are from eastern equatorial Atlantic site ODP 668B and from Caribbean site ODP 999A. Background colors are modern mean annual  $\Delta p\text{CO}_2$  (seawater  $p\text{CO}_2$  – atmosphere  $p\text{CO}_2$ ) [Takahashi *et al.*, 2009] and are plotted using Ocean Data View 4 [Schlitzer, 2017]. Today surface water  $p\text{CO}_2$  in these locations is near equilibrium with the atmosphere.

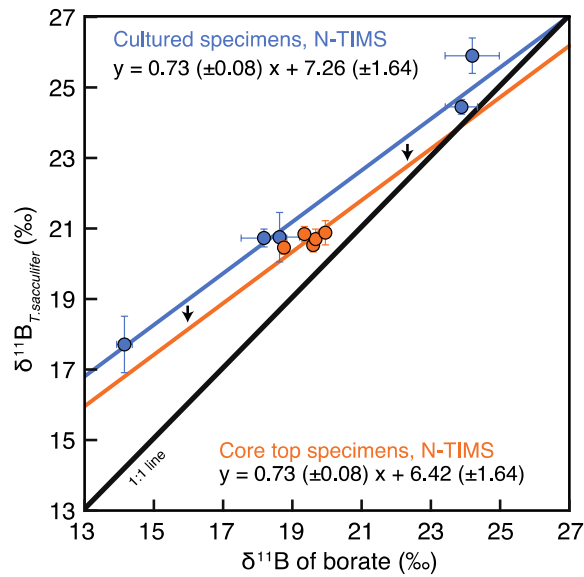


**Figure 2.** Calibration of  $\delta^{11}\text{B}$  of *T. sacculifer* as measured by N-TIMS versus  $\delta^{11}\text{B}$  of borate in seawater (data in Table S1). Culture data [Sanyal *et al.*, 2001 and this study] define the slope of the relationship. Core top  $\delta^{11}\text{B}$  data are offset from the culture relationship, where the offset can be explained by secretion of gametogenic calcite at greater water depth. This offset (0.84‰) is subtracted from the intercept of the culture regression to define the sedimentary calibration of  $\delta^{11}\text{B}_{T.sacculifer}$  calcite to  $\delta^{11}\text{B}$  borate. Linear regression is a York fit [York *et al.*, 2004, Matlab script York\_fit.m] which incorporates x and y uncertainty for each datum; slope and intercept uncertainties are  $2\sigma$ .

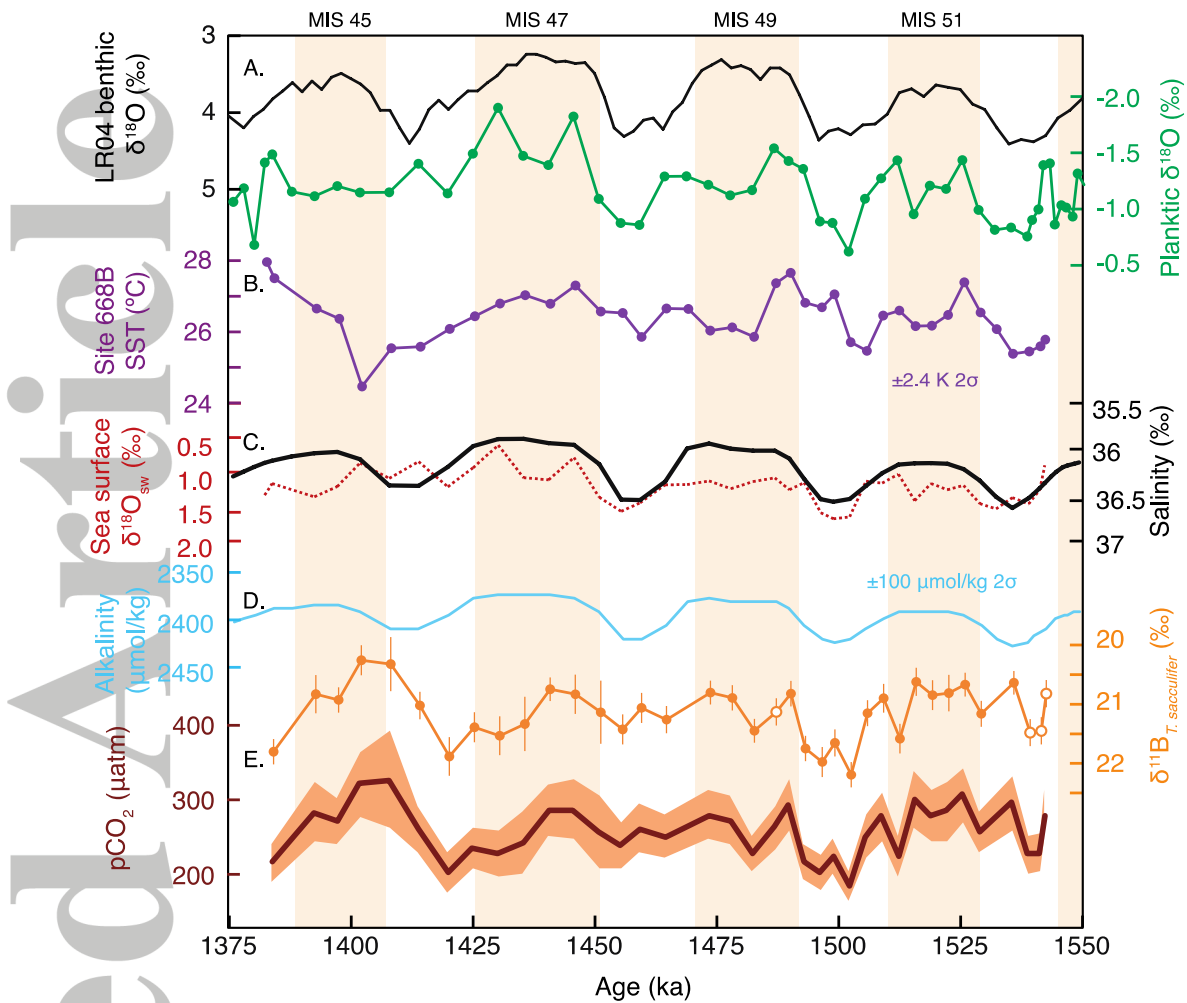


**Figure 3.** Site 668B orbital-scale records of the early Pleistocene from planktic foraminifera. (A) Site 668B planktic  $\delta^{18}\text{O}$  data [green, *Hönisch et al.*, 2009] reflect local temperature and  $\delta^{18}\text{O}_{\text{sw}}$ . (B) SST based on planktic Mg/Ca (purple, uncertainty is  $\pm 2.4\text{ K}$  ( $2\sigma$ )). (C) Calculated  $\delta^{18}\text{O}_{\text{sw}}$  from planktic  $\delta^{18}\text{O}$  and Mg/Ca-based SST (red) and compared with salinity modeled from global sea level [black, *Bintanja and van de Wal*, 2008]. (D) Alkalinity based on local modern relationship with salinity. (E) Planktic  $\delta^{11}\text{B}$  data contain minima and maxima in line with glacial and interglacial periods; uncertainty is  $2\sigma$  and open circles are from *Hönisch et al.* [2009]. Surface ocean  $\text{pCO}_2$  is calculated using pH (as estimated from  $\delta^{11}\text{B}$ , SST, and salinity) and estimated alkalinity; the uncertainty band reflects the propagated  $2\sigma$  uncertainty, the largest source of which is contributed by the analytical uncertainty of  $\delta^{11}\text{B}_{\text{calcite}}$ .

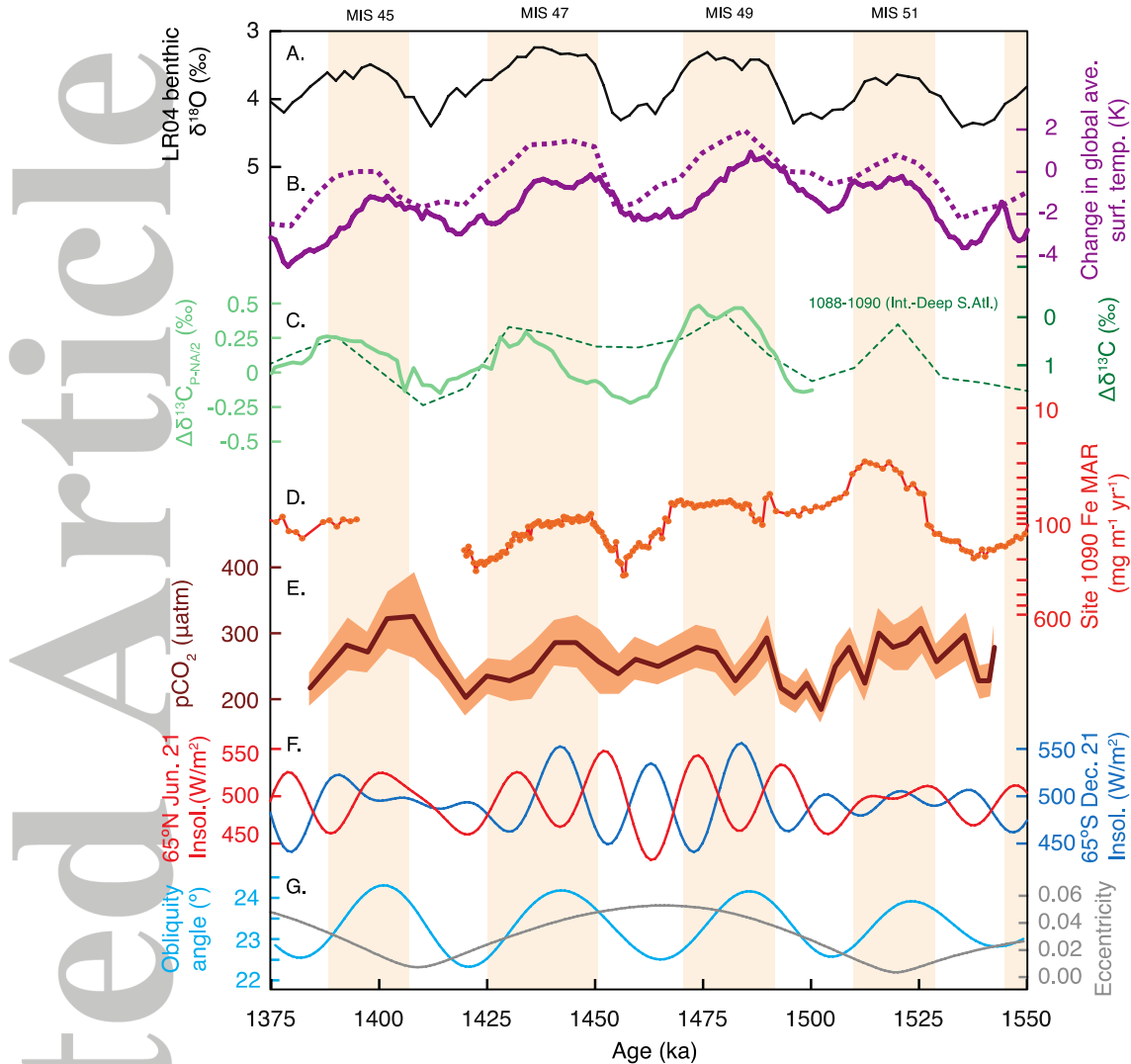


**Figure 4.** Boron-based pCO<sub>2</sub> record compared with orbital-scale records of the early Pleistocene climate. (A) LR04 benthic oxygen isotope stack [black, *Lisiecki and Raymo*, 2005] reflects high-latitude temperature and ice volume changes on the dominant ~41-kyr ice age cycle during this interval. (B) Compilations of sea surface temperature records used to estimate change in global average surface temperature (dashed line from *Martínez-Botí et al.* [2015a] and solid line from *Snyder* [*Snyder*, 2016]). (C) Benthic carbon isotope gradients between Pacific and North Atlantic basins (solid light green line,  $\Delta\delta^{13}\text{C}_{\text{Pacific-(North Atlantic)/2}}$ ) [*Lisiecki*, 2010] and between intermediate and deep water in the south Atlantic (dashed line) [*Hodell and Venz-Curtis*, 2006]. (D) Marine accumulation rate of Fe from ODP Site 1090 (solid line) [*Martínez-García et al.*, 2011]. (E) Calculated  $\delta^{11}\text{B}$ -based surface ocean pCO<sub>2</sub> from Figure 3. (F, G) Summer insolation at 65°N (blue) and 65°S (red) and orbital parameters [*Laskar et al.*, 2004].

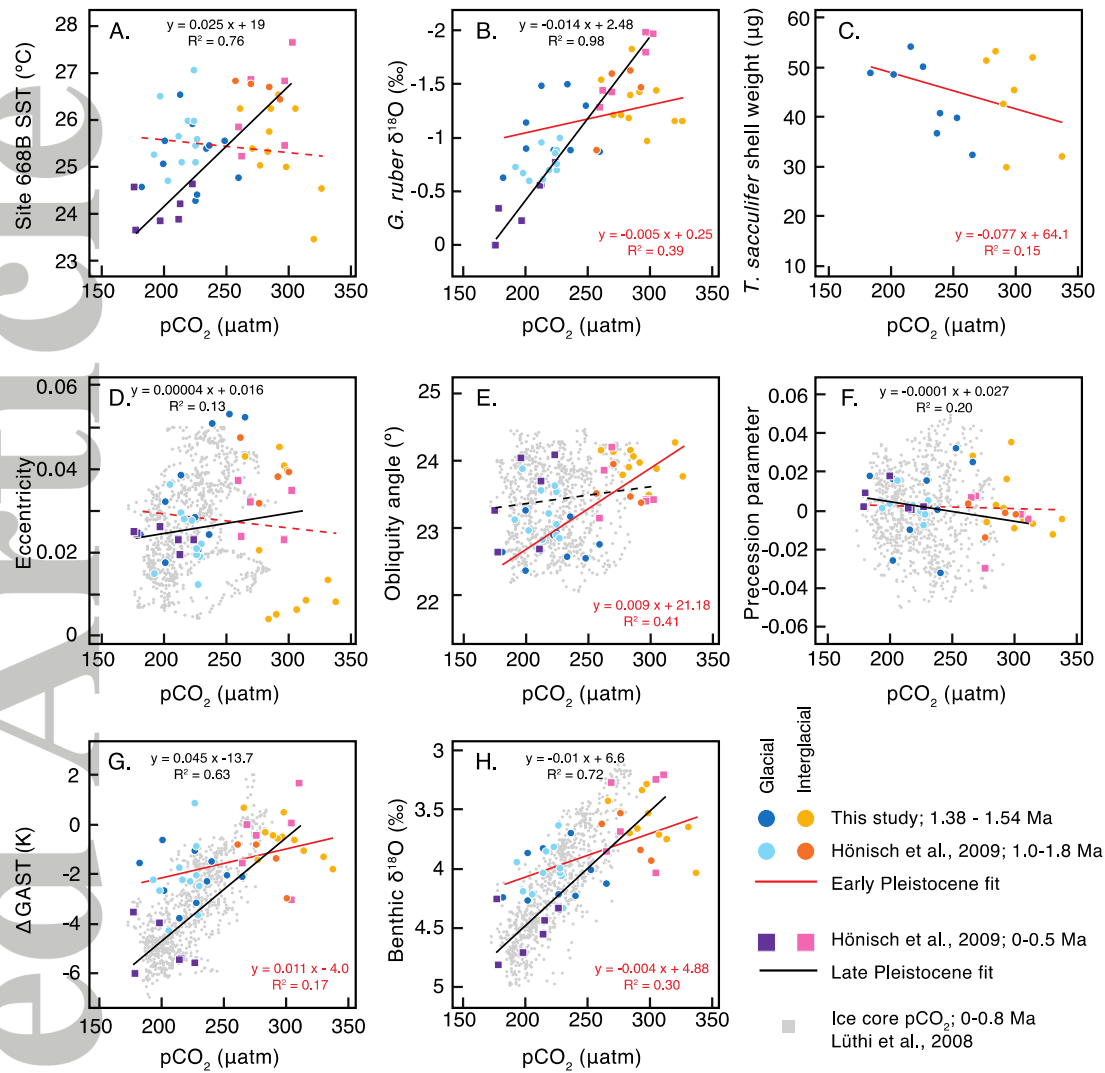


**Figure 5.** Cross plots of Site 668B peak MIS pCO<sub>2</sub> with Mg/Ca-based SST (A), *G. ruber* δ<sup>18</sup>O (B), *T. sacculifer* shell weight (C), coeval orbital parameters (D-F) [Laskar et al., 2004], surface temperature (G) and benthic δ<sup>18</sup>O (H). Late Pleistocene ice core pCO<sub>2</sub> is plotted for reference in gray [Bereiter et al., 2015], but not used for linear regressions. The linear fit of Early Pleistocene values (circles) is in red while the linear fit of late Pleistocene values (squares) is in black. Where R<sup>2</sup> > 0.1, regression equations are plotted and the linear fit is a solid line. Late Pleistocene pCO<sub>2</sub> is correlated with surface temperature and benthic δ<sup>18</sup>O, while early Pleistocene pCO<sub>2</sub> is associated with obliquity forcing. Precession parameter is calculated as the standard definition of precession (i.e., where  $\varpi$  is the angle between perihelion and vernal equinox on the orbital plane, precession is  $e \cdot \sin(\varpi)$ ).

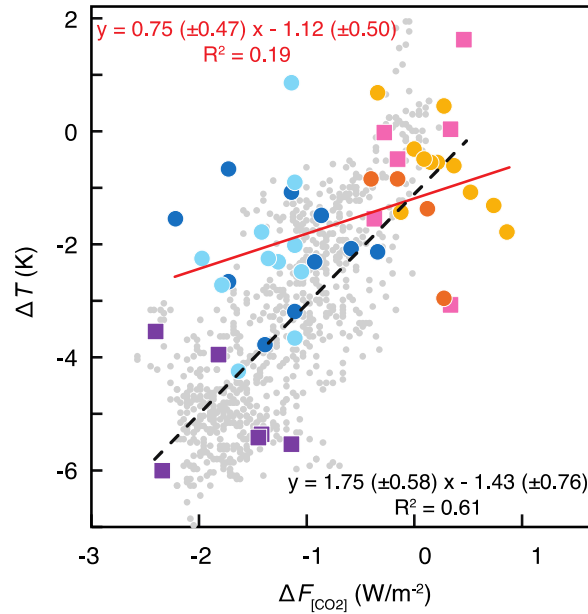


**Figure 6.** Cross plot of the change in global average surface temperature [ $\Delta T$ ; Snyder 2016] with the change in radiative pCO<sub>2</sub> forcing ( $\Delta F_{[\text{CO}_2]}$ ; calculated after Myhre *et al.* [1998], relative to pre-industrial pCO<sub>2</sub> of 278 ppm). Colors are the same as in Figure 5, with fit through early Pleistocene (1.0-1.8 Ma) in red and fit through late Pleistocene data (0-0.8 Ma) in black. Note that this framework considers the contributions of other feedbacks as internal to the Pleistocene climate system.

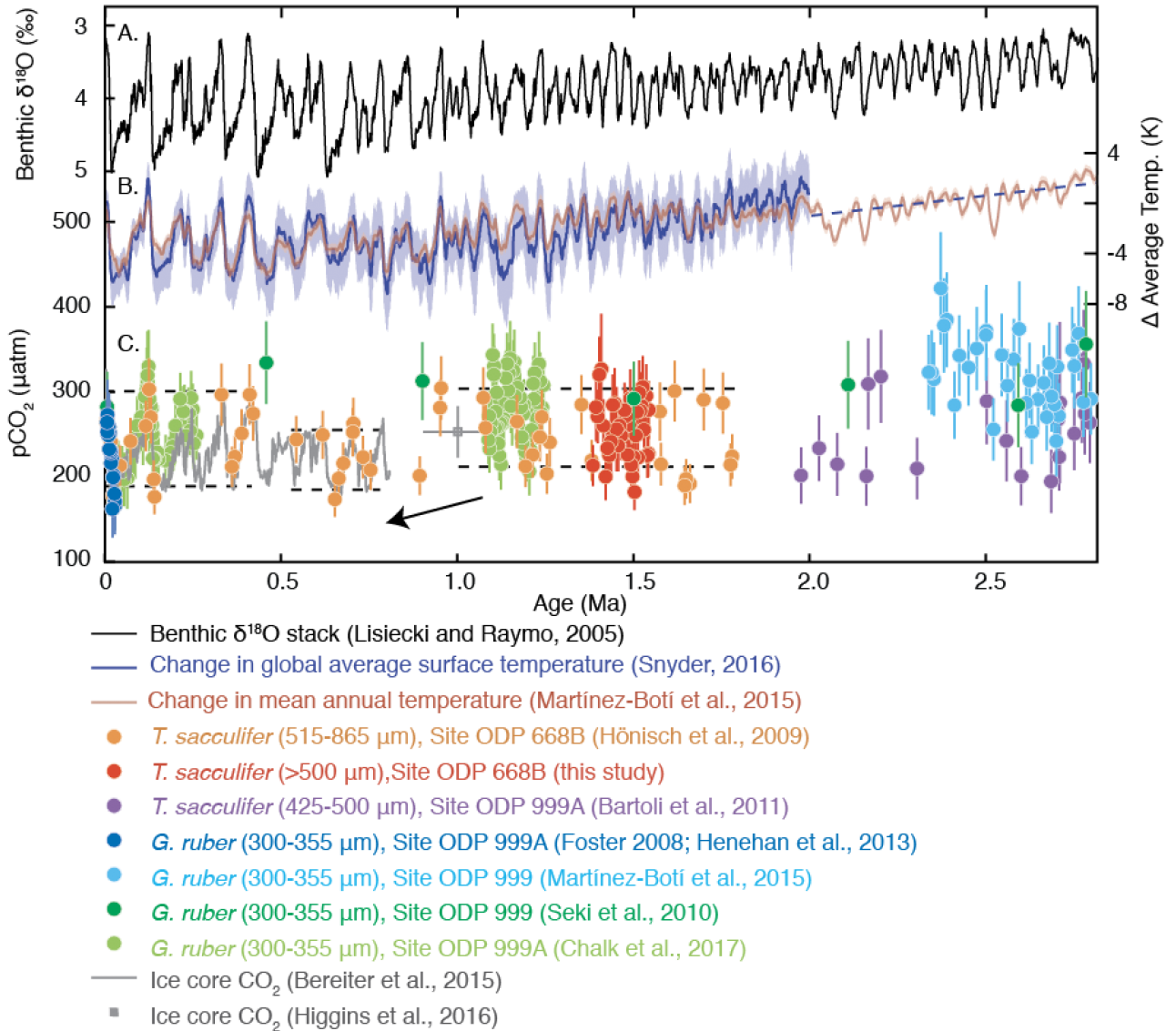


**Figure 7.** (A) Benthic  $\delta^{18}\text{O}$  [Lisiecki and Raymo, 2005] and (B) change in global average surface temperature ( $\Delta\text{GAST}$ ) [Snyder, 2016] compared with (C)  $\text{pCO}_2$  derived from ice cores [Bereiter et al., 2015; Higgins et al., 2015] and boron isotope reconstructions [Hönisch et al., 2009; Seki et al., 2010; Bartoli et al., 2011; Henehan et al., 2013; Martínez-Botí et al., 2015a; Chalk et al., 2017]. Published  $\text{pCO}_2$  records have been recalculated using consistent methods (see Methods) from the original  $\delta^{11}\text{B}$  data. Late Pleistocene boron-based  $\text{pCO}_2$  records from Sites 999A and 668B are in the same range as ice-core-based  $\text{pCO}_2$  measurements. The largest resulting difference is the record of Bartoli et al. [2011], to which new temperature data have been applied and  $\text{pCO}_2$  is calculated by pairing pH with alkalinity estimates rather than  $[\text{CO}_3^{2-}]$ .

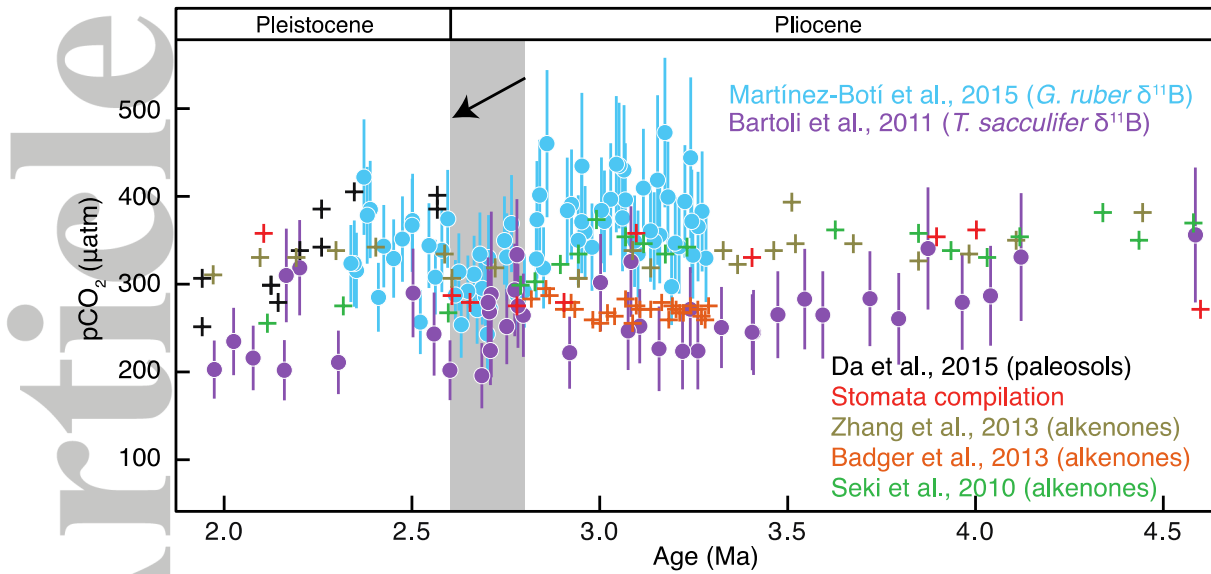


**Figure 8.** Revised pCO<sub>2</sub> values using δ<sup>11</sup>B from *T. sacculifer* [Bartoli et al., 2011] (purple) compared with pCO<sub>2</sub> from *G. ruber* [Martínez-Botí et al., 2015a] (blue). In the interval 2.8-2.6 Ma, *G. ruber*-based pCO<sub>2</sub> declines by >100 μatm, coincident with the onset of northern hemisphere glaciation (gray band, black arrow). Throughout the Pliocene, the *T. sacculifer*-based pCO<sub>2</sub> record is lower than *G. ruber*-based pCO<sub>2</sub> but also shifts to lower values at 2.7 Ma. The text discusses potential offsets due to evolutionary changes in foraminiferal physiology and consequent species-differences between pH and pCO<sub>2</sub> reconstructions. Paleo-pCO<sub>2</sub> reconstructions from paleosols [Da et al., 2015], stomatal indices [Kürschner et al., 1996; Retallack, 2009; Stults et al., 2011; Wang et al., 2015], and alkenone δ<sup>13</sup>C [Seki et al., 2010; Badger et al., 2013; Zhang et al., 2013] are intermediate between the estimates of Martínez-Botí et al. [2015a] and Bartoli et al. [2011].

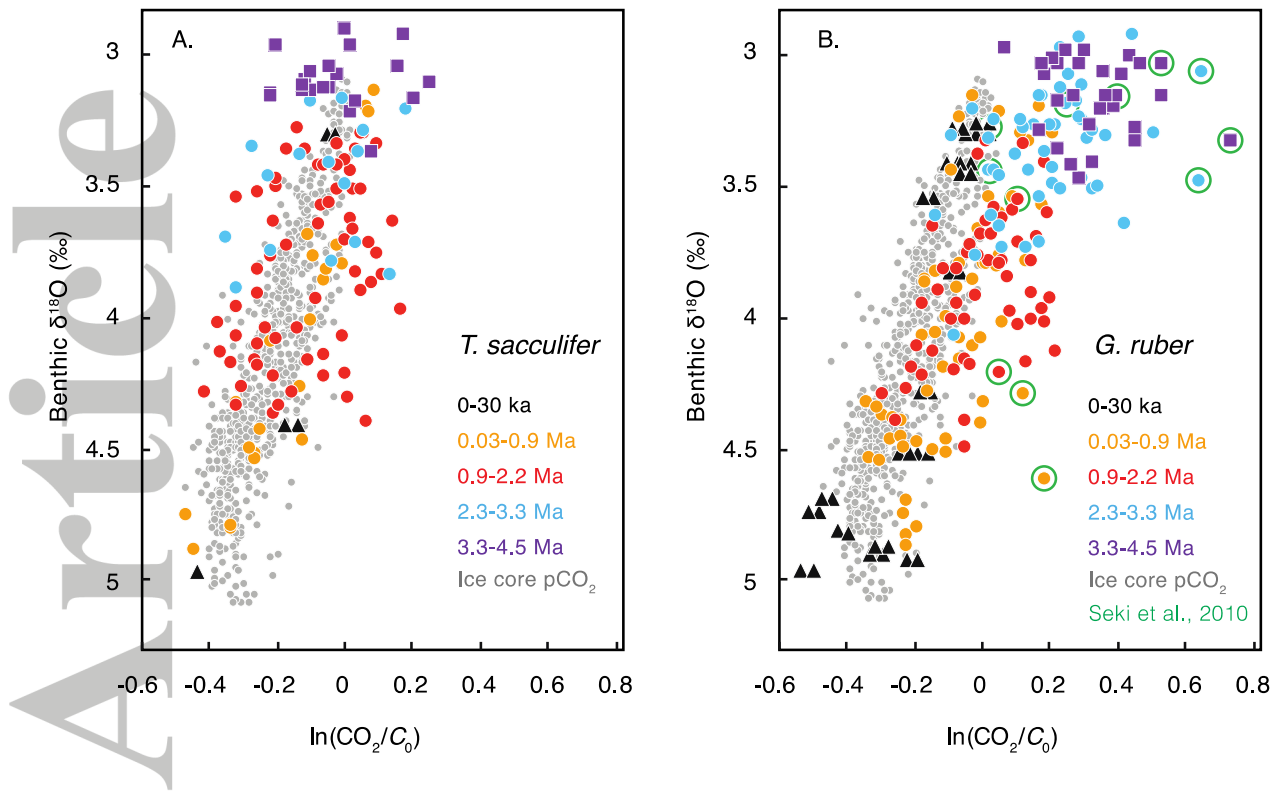


**Figure 9.** Relationship between benthic  $\delta^{18}\text{O}$  and climate forcing due to radiative  $\text{CO}_2$  forcing ( $\ln(\text{CO}_2/C_0)$ , where  $C_0$  is  $278 \mu\text{atm}$ ), including all six  $\delta^{11}\text{B}$ -based  $\text{pCO}_2$  records presented in Figure 7. (A) Forcing derived from  $\delta^{11}\text{B}_{T. sacculifer}$ -based  $\text{pCO}_2$  compared with forcing from  $\text{pCO}_2$  values derived from ice cores (gray). Time periods are coded by color, yet the overall benthic  $\delta^{18}\text{O}$ -to- $\ln(\text{CO}_2/C_0)$  relationship for boron-based  $\text{pCO}_2$  data falls along the same relationship for  $\text{pCO}_2$  as that derived from ice cores. (B) The corresponding relationship of boron-based  $\text{CO}_2$  forcing compared with  $\text{pCO}_2$  values from ice cores, this time using  $\delta^{11}\text{B}$  values from *G. ruber*. Although Holocene and LGM  $\text{pCO}_2$  values based on the foraminifer *G. ruber* are consistent with the ice-core  $\text{pCO}_2$ , the estimates deviate in earlier time periods, when  $\text{pCO}_2$  values are higher than expected based on the general benthic  $\delta^{18}\text{O} : \ln(\text{CO}_2/C_0)$  relationship derived from ice cores. This gives rise to the question of whether *G. ruber* and its vital effects evolved over time. Values derived from one early study are circled in green; these data are based on unusually low boron isotope values [Seki et al., 2010].

Supporting Information for

**Early Pleistocene obliquity-scale pCO<sub>2</sub> variability at ~1.5 million years ago**

Kelsey A. Dyez<sup>1\*</sup>, Bärbel Hönisch<sup>1,2</sup>, Gavin A. Schmidt<sup>3</sup>

<sup>1</sup>Lamont-Doherty Earth Observatory, Columbia University, Palisades, NY, USA.

<sup>2</sup>Department of Earth and Environmental Sciences of Columbia University, New York, NY, USA

<sup>3</sup>NASA Goddard Institute for Space Studies, New York, NY, USA

\*kdyez@umich.edu

**Contents of this file**

Introduction  
Figures S1 to S9  
Tables S1 to S2

**Additional data files**

Tables S3 and S4 (xlsx),  
data also archived at NOAA (NCEI)

**Introduction**

The supplemental appendix contains additional supporting information, figures, and tables, in the same order as each is discussed in the main text. These figures provide supporting information for the choice of the  $\delta^{11}\text{B}_{\text{sw}}$  value (Figure S1), alkalinity (Figure S2), and the chronology for Site 668B (Figure S3). They provide additional comparisons with previous work (Figures S4, S5), and plots of supplemental data (Figures S6, S7, S8).

Pliocene salinity estimates

In section 2.7, Plio-Pleistocene salinity was estimated from a model of sea level changes and assumed to be constant for samples prior to 3 Ma. An alternative method for estimating salinity is via  $\delta^{18}\text{O}_{\text{calcite}}$  and SST estimates [Bemis *et al.*, 1998]. For Site 999A, this alternative relies on planktic  $\delta^{18}\text{O}$  measurements [Schmidt *et al.*, 2004] and Mg/Ca-based SST [Schmidt *et al.*, 2004; Martínez-Botí *et al.*, 2015], via the following equations:

$$\delta^{18}\text{O}_{\text{sw}} = (\text{SST} - 16.5)/4.8 + \delta^{18}\text{O}_{\text{calcite}} + 0.27 \text{ [Bemis et al., 1998]}$$

$$\text{Salinity} = (\delta^{18}\text{O}_{\text{sw Caribbean}} + 10.511) / 0.319 \text{ [Steph et al., 2006]}$$

This alternative method results in salinity that is on average within  $\pm 0.5\%$  of the method used in the manuscript, but exhibits larger swings in salinity ( $>2\%$ ) that are difficult to reconcile with

the smaller amplitude of sea level change (<25 m) in the Pliocene [*Hansen et al.*, 2013]. In practice, salinity variations have only a small impact on the pH estimate from boron isotopes (salinity  $\pm 1\text{‰} = \pm 0.006$  pH units). To account for the glacial-interglacial uncertainty on this estimate, a salinity uncertainty of  $\pm 2\text{‰}$  is propagated through the pH and pCO<sub>2</sub> uncertainty calculations.

### Model equations

In section 4.3, a simple box model is presented to relate ice volume, temperature, and carbon dioxide levels. This model does not have explicit geography, topography, or circulation; the governing equations are as follows:

$$\begin{aligned}\tau_L \frac{dL}{dt} &= F_I + (aT - L) \\ \tau_C \frac{dC}{dt} &= bT - C \\ \frac{dT}{dt} &= \mu L + F_{CO_2}(C) + \lambda T - P(T, T_0) + \varepsilon\end{aligned}$$

where, in the first equation,  $F_I$  is the forcing of ice sheets and  $\tau_L$  is a time constant for the ice sheet response. Similarly, in the second equation,  $b$  is the carbon cycle sensitivity to temperature and  $\tau_C$  is the response time. In the third equation,  $\mu$  is the radiative forcing associated with the ice sheets,  $\lambda$  is the non-Planck feedback and  $\varepsilon$  is a small source of random noise. For further documentation and discussion of this model, see the supplementary material of *Schmidt et al.* [2017].

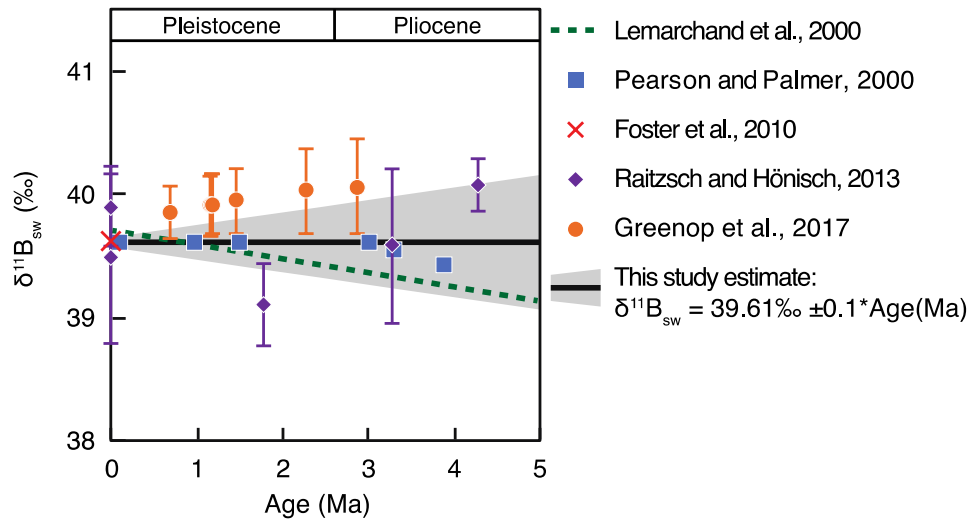


**Figure S1.** Compilation of  $\delta^{11}\text{B}_{\text{sw}}$  estimates from previous work. Seawater  $\delta^{11}\text{B}$  has been reconstructed from a model from river inputs [Lemarchand *et al.*, 2000], benthic foraminiferal  $\delta^{11}\text{B}$  alongside modeled ocean pH [Raitzsch and Hönisch, 2013], and multi-species foraminiferal  $\delta^{11}\text{B}$  measurements in the water column coupled with the water column pH gradient [Pearson and Palmer, 2000; Greenop *et al.*, 2017]. The estimates of Pearson and Palmer [2000] have been offset by +0.51‰ so that modern  $\delta^{11}\text{B}_{\text{sw}}$  is equal to 39.61‰ [Foster *et al.*, 2010]. The  $\delta^{11}\text{B}_{\text{sw}}$  value used in this study is the solid line (constant at the modern value) with uncertainty increasing with time ( $\pm 0.1\text{‰/Myr}$ ), which is depicted by the gray band.

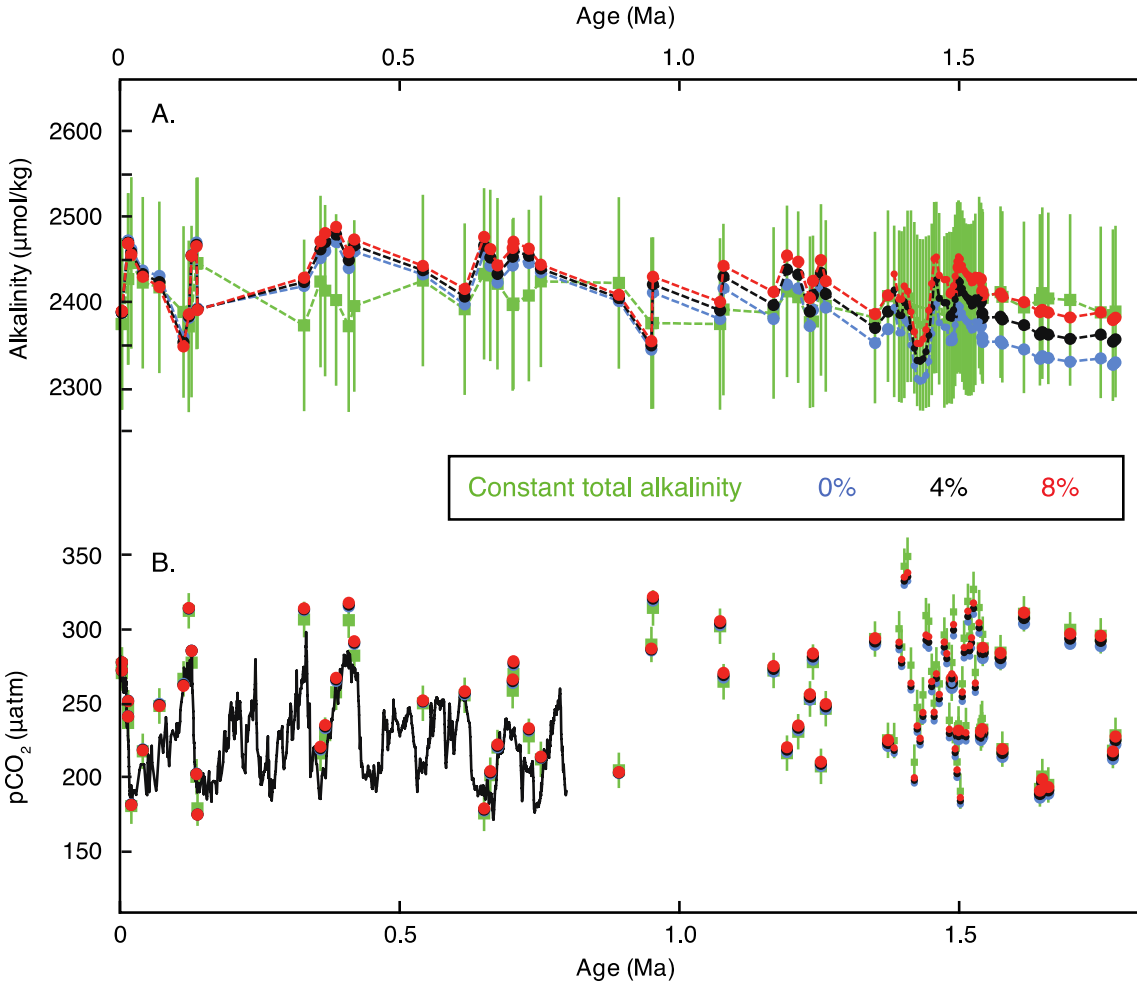


**Figure S2.** Comparison of various alkalinity scenarios used to estimate  $\text{pCO}_2$  from Site 668B. (A) Alkalinity estimates for 4 scenarios; green squares represent ‘constant total alkalinity’ in which alkalinity is scaled as a function of sea level; the uncertainty band is  $\pm 100 \mu\text{mol/kg}$ . Blue, black, and red circles represent scenarios in which continental weathering, calcite production, and seafloor dissolution impact ocean alkalinity after the geochemical model of *Clark et al.* [2006]. Alkalinity was estimated from this same model in the study of *Hönisch et al.* [2009], although the time axis of the model alkalinity output was erroneously reversed in that study. The  $\text{pCO}_2$  estimates we derive here are nearly the same as the original publication, which reflects the small influence alkalinity has on the  $\text{pCO}_2$  estimate when alkalinity differs by less than  $200 \mu\text{mol/kg}$ . The difference between the other estimates reflects the relative contribution of Canadian Shield weathering to global weathering rates (blue = 0%, black = 4%, red = 8%). The average absolute value of the difference between the 0% scenario and the constant alkalinity scenario is  $33 \mu\text{mol/kg}$ . (B) Comparison of  $\text{pCO}_2$  calculated via the different alkalinity scenarios compared to ice core  $\text{pCO}_2$  [Bereiter et al., 2015]. The impact of the varying alkalinity scenarios on calculated  $\text{pCO}_2$  values is smaller than the uncertainty in the constant total alkalinity scenario ( $\pm 100 \mu\text{mol/kg}$ ); the largest difference in calculated  $\text{pCO}_2$  between any varying alkalinity scenario and the ‘constant total alkalinity’ scenario is  $12 \mu\text{atm}$ . Uncertainty in the lower panel is only due to alkalinity in the constant total alkalinity scenario ( $2\sigma$ ).

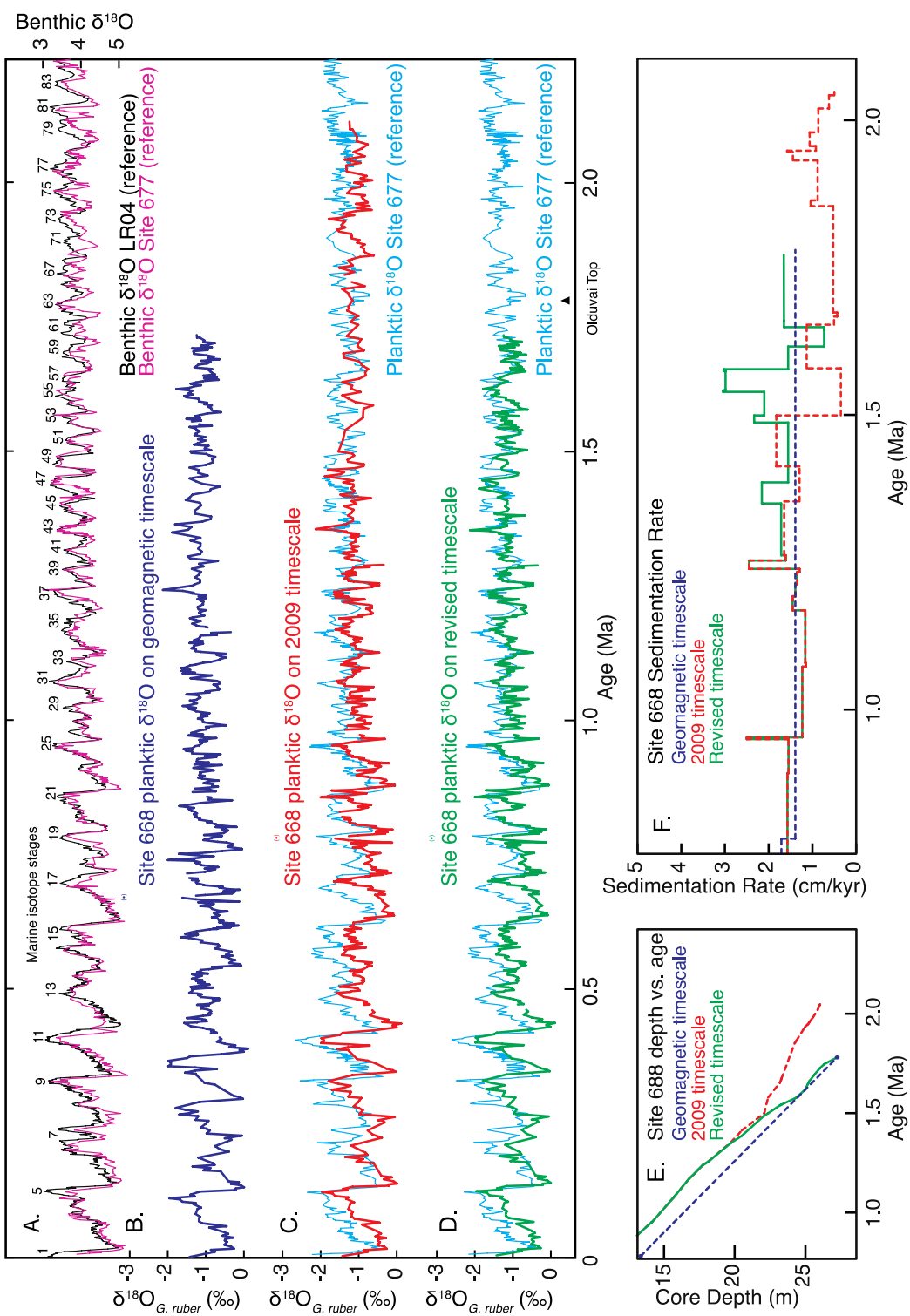


**Figure S3.** Comparison of published and revised age model for Site 668B. (A) Reference curves are the benthic  $\delta^{18}\text{O}$  stack (black line) [Lisiecki and Raymo, 2005] and benthic  $\delta^{18}\text{O}$  from Site 677 (magenta line) [Shackleton et al., 1990]. (B) Site 668B planktic  $\delta^{18}\text{O}$  plotted using the

original timescale from ODP initial reports, which relied on geomagnetic estimates and microfossil appearances [*Shipboard Scientific Party*, 1988]. (C) Site 688B planktic  $\delta^{18}\text{O}$  plotted using the published '2009 timescale' (red line) [*Hönisch et al.*, 2009], which was based on visual alignment of the Site 668B planktic  $\delta^{18}\text{O}$  record with both the Site 677 planktic  $\delta^{18}\text{O}$  record (light blue line) [*Shackleton et al.*, 1990] and the LR04 benthic  $\delta^{18}\text{O}$  stack [*Lisiecki and Raymo*, 2005]. (D) Site 668B planktic  $\delta^{18}\text{O}$  plotted using the revised timescale (green line), which remains the same as the previously published '2009 timescale' for ages 0-1.3 Ma and is only adjusted for ages prior to 1.3 Ma. Revisions are made in AnalySeries [*Paillard et al.*, 1996] based on visual alignment of the Site 668B planktic  $\delta^{18}\text{O}$  record with the Site 677 planktic  $\delta^{18}\text{O}$  record and using the top of the Olduvai magnetic reversal as an additional tie point (core depth 27.2-27.3 m; 1.78 Ma [*Shipboard Scientific Party*, 1988]). (E) The depth vs. age comparison for the revised timescale for Site 668B. (F) Using the revised timescale, sedimentation rate for Site 668B varied between 0.7 and 3.0 cm/kyr.

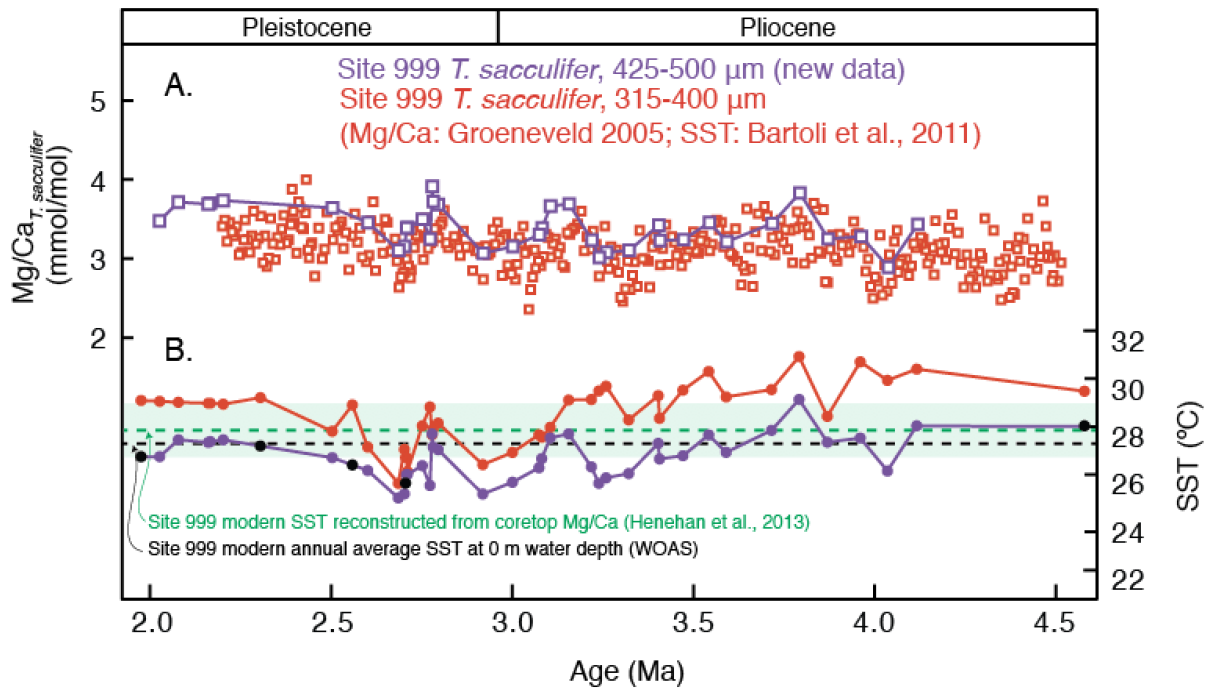


**Figure S4.** (A) Site 999A *T. sacculifer* (425-500 μm) measured Mg/Ca values (open purple squares) from the same or adjacent samples to those with boron isotope measurements from *Bartoli et al.* [2011]. The original *T. sacculifer* Mg/Ca record [*Groeneveld, 2005*] used by *Bartoli et al.* [2011] is plotted for reference (open red squares). The new Mg/Ca data are slightly higher and from the same larger size fraction also used for  $\delta^{11}\text{B}$ . (B) The new SST estimate (filled purple circles) is then calculated using the new Mg/Ca data and applying an upward adjustment by +10% due to our use of the reductive cleaning step, which has been reported to lower the Mg/Ca value by 10% [*Martin and Lea, 2002*]. The new SST record is corrected for changes in  $\text{Mg}/\text{Ca}_{\text{sw}}$  using the approach of *Medina-Elizalde et al.* [2008] and a modern  $\text{Mg}/\text{Ca}_{\text{sw}}$  value of 5.2 mmol/mol [*Evans and Müller, 2012*]. Because the correction for changing  $\text{Mg}/\text{Ca}_{\text{sw}}$  is not linear, we include the species-specific power-law exponential H-value of 0.41 [*Delaney et al., 1985; Evans and Müller, 2012; Evans et al., 2016*].  $\text{Mg}/\text{Ca}_{\text{sw}}$  data are from *Fantle and dePaolo* [2006], which is consistent with  $\text{Mg}/\text{Ca}_{\text{sw}}$  estimates from marine evaporite fluid inclusions [*Horita et al., 2002; Brennan et al., 2013*]. Sediment was not available for 5 out of the 42 samples in the record; SST was estimated by extrapolation from new *T. sacculifer* measurements (filled black circles). The correction for dissolution with depth [*Dekens et al., 2002*] is omitted in favor of the calibration of *Anand et al.* [2003] as water depth at this core location (2839 m) is well above the tropical Atlantic lysocline (4200 m) and bottom waters are supersaturated with respect to calcite ( $\Omega = 1.5$ ). The original SST record (red circles) was based on *T. sacculifer* from a smaller size fraction (315-400 μm), a modern  $\text{Mg}/\text{Ca}_{\text{sw}}$  value of 4.96 mmol/mol, and the depth-based dissolution correction of *Dekens et al.* [2002], which resulted in ~1.8 K warmer calculated SST. Modern SST reconstructed from core top material [*Henehan et al., 2013*] and from annual average climatology (WOAS) is plotted for comparison.

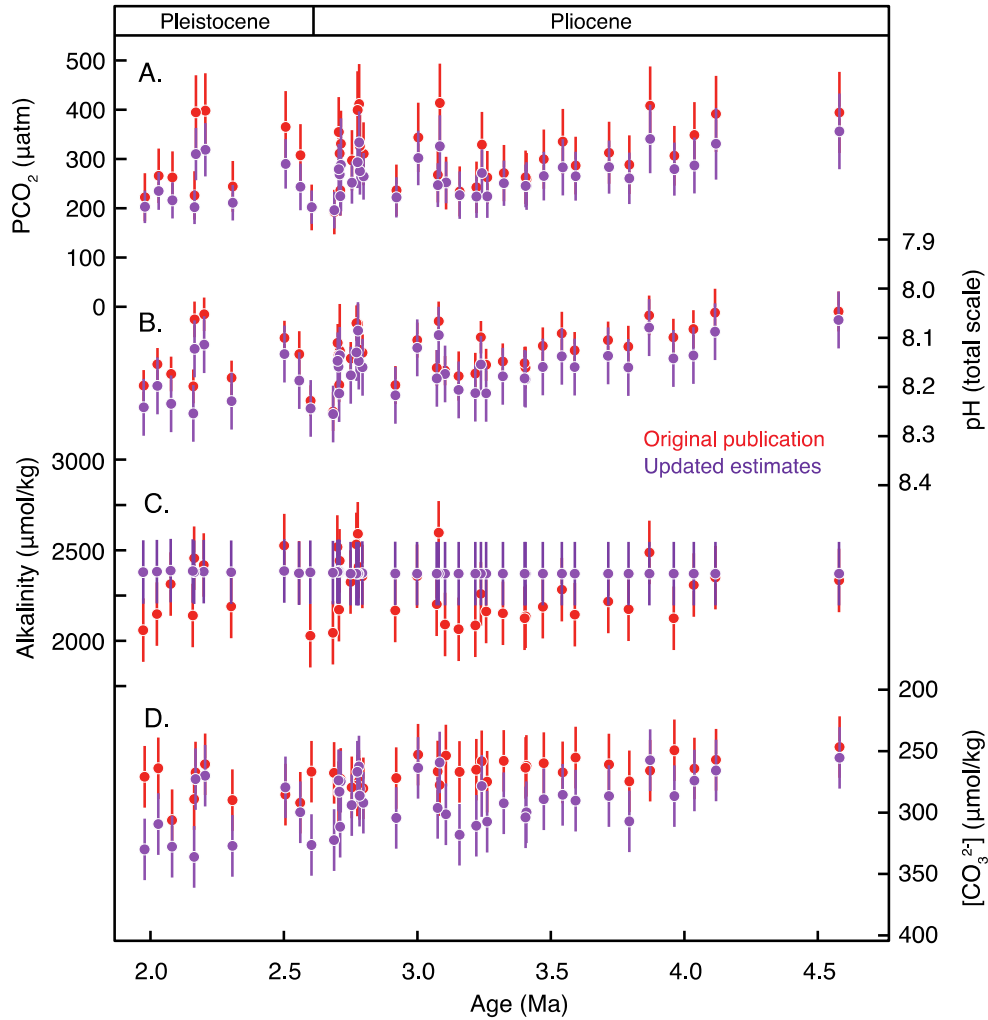


**Figure S5.** Original paleoceanographic estimates (red symbols) from *Bartoli et al.* [2011] compared with updated estimates (purple symbols) for (A)  $\text{PCO}_2$ , (B) pH, (C) total alkalinity, and (D) carbonate ion concentration,  $[\text{CO}_3^{2-}]$ . The original publication paired pH with carbonate ion concentration estimates as input parameters for the carbonate system whereas this study uses estimates of total alkalinity as the second parameter. Using pH and alkalinity as inputs reduces the  $\text{PCO}_2$  variability compared to the original estimate. Furthermore, if  $\text{PCO}_2$  is calculated using  $[\text{CO}_3^{2-}]$  as the second parameter, the corresponding alkalinity widely varies over a range of  $\sim 800$   $\mu\text{mol/kg}$ , which highlights the greater sensitivity of calculated  $\text{PCO}_2$  in (A) to small uncertainties in  $[\text{CO}_3^{2-}]$ . Such a large variability in alkalinity is unreasonable given geochemical modelling constraints [*Tyrrell and Zeebe, 2004; Ridgwell, 2005*] and the limited range of late Pleistocene alkalinity ( $\sim 120$   $\mu\text{mol/kg}$ ) [*Clark et al., 2006*] due to the stabilizing effect on alkalinity from the distribution of calcium carbonate accumulation in the deep sea.

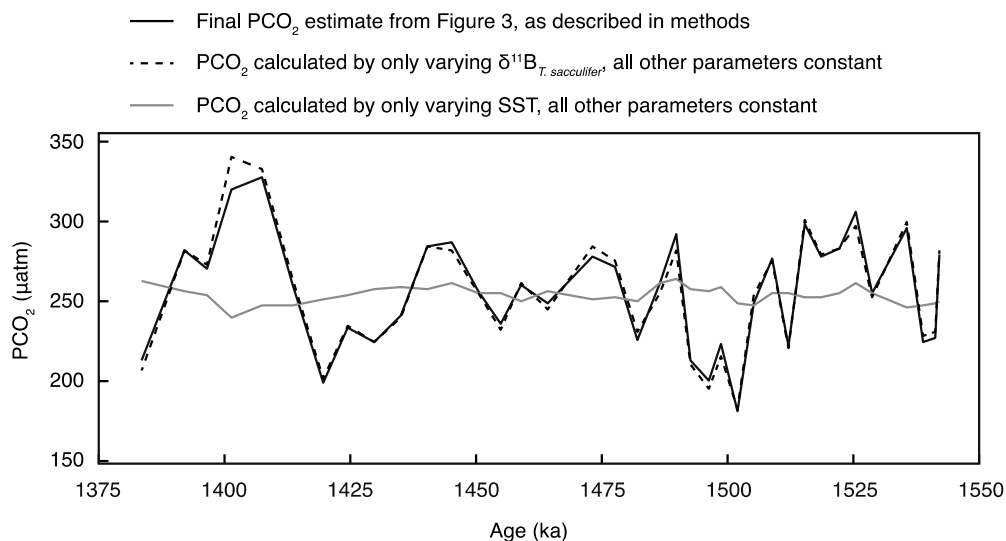


**Figure S6.** Sensitivity study of contributing factors to  $\text{PCO}_2$  calculations (Site 668B, this study). (A) The primary component of calculated  $\text{PCO}_2$  is the initial  $\delta^{11}\text{B}$  measurement input. Here the final  $\text{PCO}_2$  estimate (from Figure 3) is plotted alongside  $\text{PCO}_2$  calculated by varying only the measured  $\delta^{11}\text{B}_{T. \text{sacculifer}}$  values and keeping all other parameters constant (dashed line). The second greatest contributor to calculated  $\text{PCO}_2$  uncertainty is SST. However, if  $\text{pCO}_2$  is calculated by only varying SST, the maximum  $\text{pCO}_2$  range is minimized to only  $\sim 24 \mu\text{atm}$  (grey solid line).

Site ODP 668B (Hönisch et al., 2009)  
 $\delta^{11}\text{B}$ : *T. sacculifer* (515-865  $\mu\text{m}$ ), Mg/Ca: *G. ruber* (250-300  $\mu\text{m}$ )

Site ODP 668B (this study)  
 $\delta^{11}\text{B}$ : *T. sacculifer* (>500  $\mu\text{m}$ ), Mg/Ca: *G. ruber* (300-355  $\mu\text{m}$ )

Site ODP 999A (Bartoli et al., 2011) *T. sacculifer* (425-500  $\mu\text{m}$ )

Site ODP 999A (Foster 2008; Henehan et al., 2013) *G. ruber* (300-355  $\mu\text{m}$ )

Site ODP 999A (Martínez-Botí et al., 2015) *G. ruber* (300-355  $\mu\text{m}$ )

Site ODP 999A (Seki et al., 2010), *G. ruber* (300-355  $\mu\text{m}$ ), SST from  $\text{U}^{\text{K}}_{37}$  index

Site ODP 999A (Chalk et al., 2017), *G. ruber* (300-355  $\mu\text{m}$ )

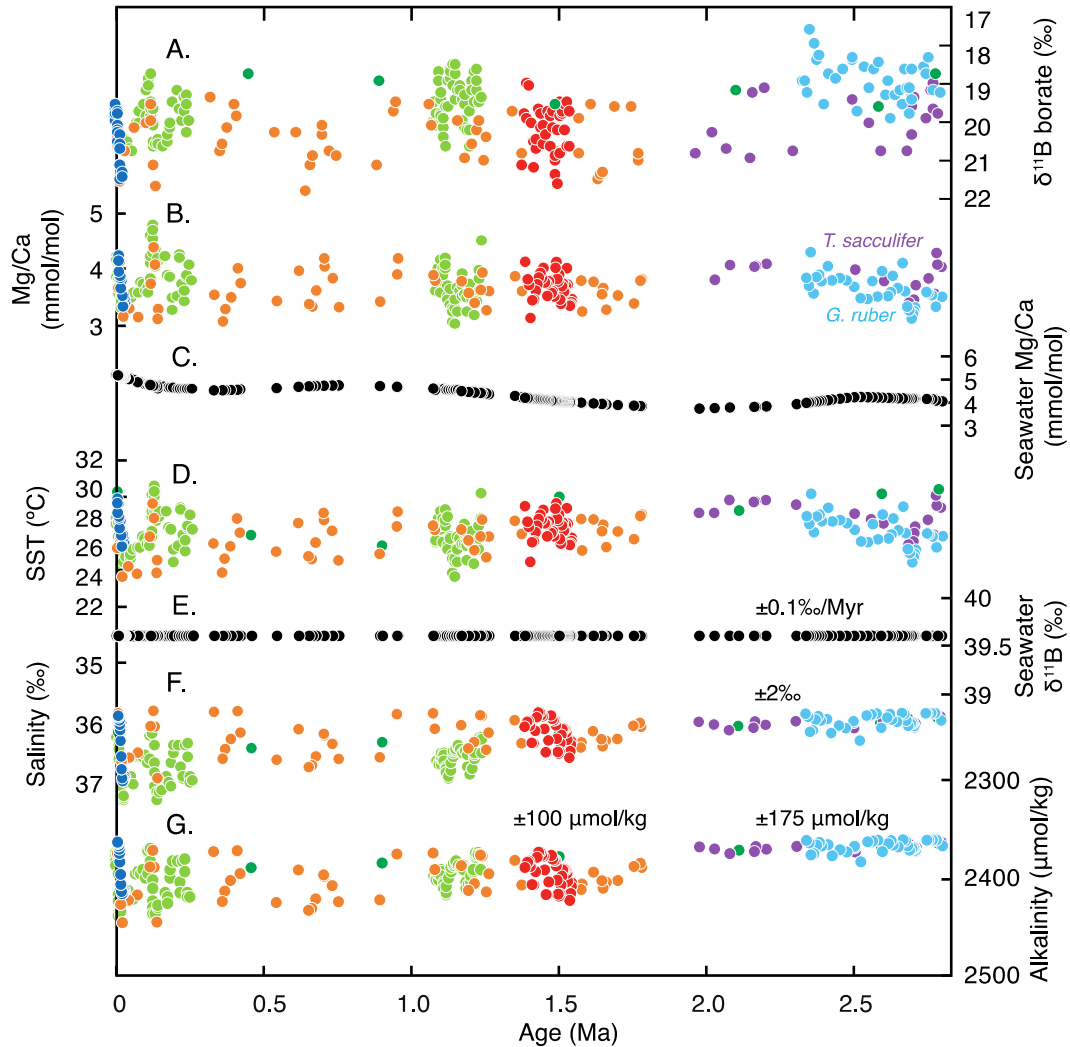


**Figure S7.** Supplemental data for  $\text{pCO}_2$  calculations in Figure 4, differentiated by  $\delta^{11}\text{B}$  source: dark blue [Henehan et al., 2013], orange [Hönisch et al., 2009], red (this study), purple [Bartoli et al., 2011], light blue [Martínez-Botí et al., 2015] and green [Seki et al., 2010]. (A) Borate  $\delta^{11}\text{B}$  calculated from foraminiferal  $\delta^{11}\text{B}$  of foraminifera and analytical technique-specific calibrations (see Methods for details). (B) Mg/Ca data are used for SST reconstructions and are based on *G. ruber*, 250-300  $\mu\text{m}$  (orange), *G. ruber*, 300-355  $\mu\text{m}$  (red), *T. sacculifer*, 425-500  $\mu\text{m}$  (purple) and *G. ruber*, 300-355  $\mu\text{m}$  [Henehan et al., 2013; Martínez-Botí et al., 2015]. (C) The Mg/Ca value

of seawater (used for correcting Mg/Ca-based SST) is taken from *Fantle and DePaolo* [2006], which for this time period is consistent with Mg/Ca<sub>sw</sub> estimates from marine evaporite fluid inclusions [*Horita et al.*, 2002; *Brennan et al.*, 2013]. (D) SST is based on Mg/Ca data and corrected for changes in Mg/Ca<sub>sw</sub> [*Evans and Müller*, 2012] in all cases, except *Seki et al.* [2010] who based their SST estimates on the alkenone unsaturation index (U<sup>k</sup><sub>37</sub>). (E) The δ<sup>11</sup>B value of seawater is assumed to have been constant over the past 5 Ma (F) Salinity at Site 668B is derived from the modeled sea level estimates of *Bintanja and van de Wal* [2008] as described in the text, with an uncertainty of ±2‰. (G) Alkalinity calculated using local S:ALK relationship of TA<sub>668B</sub> = 65.62\*S+22.84 and TA<sub>999A</sub> = 59.19 + 229.08 [*Foster*, 2008], based on modern surface WOCE and GLODAP data. Alkalinity uncertainty is ±100 μmol/kg for the past 1.9 Ma and ±175 for samples older than 1.9 Ma.

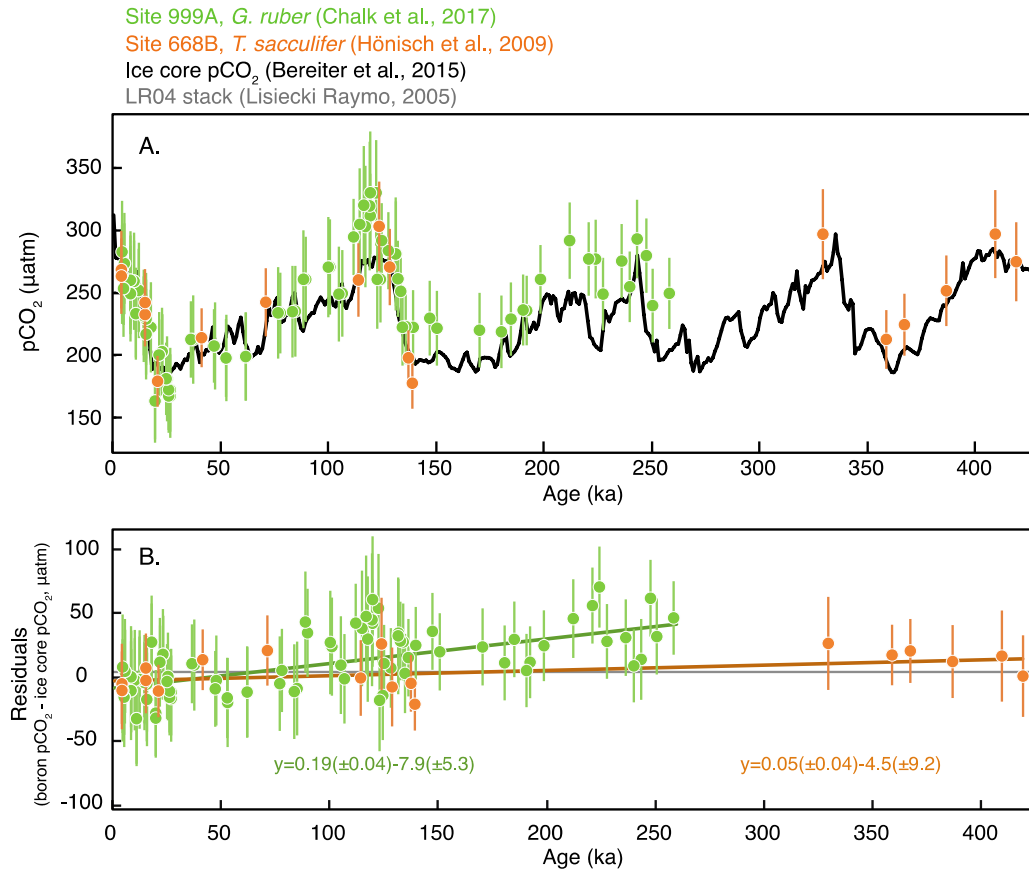


**Figure S8.** (A) Expanded view of boron-based pCO<sub>2</sub> from Figure 7, as calculated using the published  $\delta^{11}\text{B}$  measurements [Hönisch et al., 2009; Chalk et al., 2017] and the boundary conditions set forth in the Methods, compared with pCO<sub>2</sub> from ice core measurements [Bereiter et al., 2015]. (B) Difference between boron-based pCO<sub>2</sub> and ice core pCO<sub>2</sub>. Over the past 260 ka, the difference between *G. ruber*-based pCO<sub>2</sub> and ice core pCO<sub>2</sub> is larger further back in time, which we suggest is most likely due to small evolutionary changes in *G. ruber* ecology or habitat over time.

Based on Martínez-Botí et al., 2015 (*G. ruber*  $\delta^{11}\text{B}$ ), various  $\delta^{11}\text{B}_{\text{calcite}}$  to  $\delta^{11}\text{B}_{\text{borate}}$  calibration slopes (m) and intercepts (b)  
 Based on Bartoli et al., 2011 (*T. sacculifer*  $\delta^{11}\text{B}$ ), as presented in text

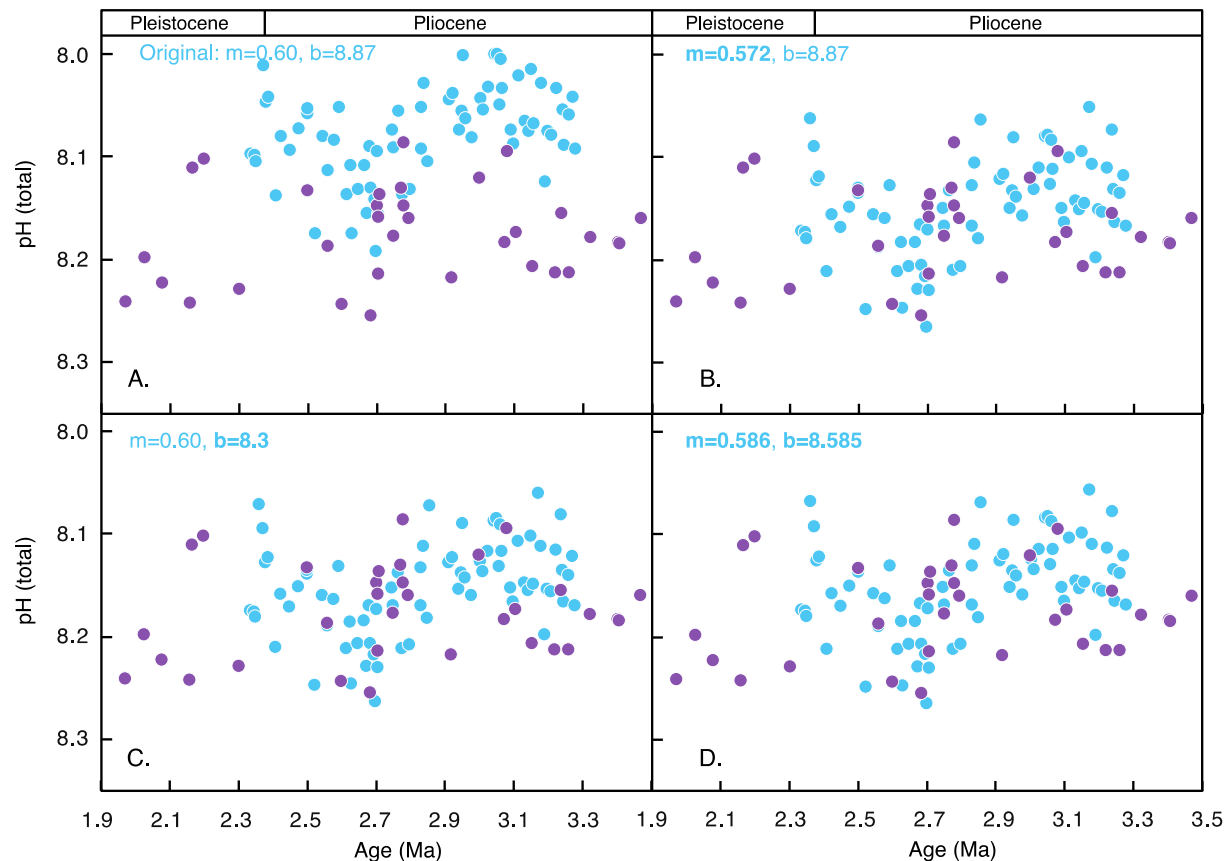


**Figure S9.** If we assume that the *T. sacculifer*-based pH record from Site 999 is correct for the early Pleistocene-late Pliocene, the pH offset of the *G. ruber*-based pH record from Site 999 from the same time period could be due to a biologically-mediated change in the slope and/or intercept of the *G. ruber*  $\delta^{11}\text{B}_{\text{calcite}}$  to  $\delta^{11}\text{B}_{\text{borate}}$  relationship. The modern *G. ruber*  $\delta^{11}\text{B}_{\text{calcite}}$  to  $\delta^{11}\text{B}_{\text{borate}}$  calibration has a slope of 0.60 and intercept of 8.87 [Henehan et al., 2013]; if the *G. ruber* calibration slope is modified to force the two pH records to match, then the new Plio-Pleistocene slope for *G. ruber* samples would become 0.572 (panel B). If instead the intercept is modified to force a match, the new intercept is 8.3 (panel C). A number of potential matches can be made by changing both the calibration slope and intercept; a third example of one of these potential solutions is given in panel D.

**Table S1.** Data from Figure 2. Calibration of  $\delta^{11}\text{B}$  of *T. sacculifer* (>450  $\mu\text{m}$ ) to  $\delta^{11}\text{B}$  of seawater borate ion as measured via N-TIMS for down-core records.

<b>Culture</b>							
pH <sup>1</sup>	$\delta^{11}\text{B}$ (‰)	$\delta^{11}\text{B}$ 2se	$\delta^{11}\text{B}$ borate (‰) <sup>3</sup>	$\delta^{11}\text{B}$ borate uncertainty <sup>4</sup>	Temp. (°C)	Sal.	Reference
7.49	17.68	0.8	14.18	0.22	27	35.4	<i>Sanyal et al.</i> , 2001 <sup>2</sup>
8.03	20.69	0.25	18.20	0.66	27	35.4	<sup>5</sup>
8.07	20.71	0.7	18.65	0.58	27	35.4	<i>Sanyal et al.</i> , 2001 <sup>2</sup>
8.45	24.40	0.21	23.89	0.47	27	35.4	<sup>5</sup>
8.47	25.85	0.5	24.20	0.78	27	35.4	<i>Sanyal et al.</i> , 2001 <sup>2</sup>

<b>Core top</b>							
pH <sup>1</sup>	$\delta^{11}\text{B}$ (‰)	$\delta^{11}\text{B}$ 2se	$\delta^{11}\text{B}$ borate (‰) <sup>3</sup>	$\delta^{11}\text{B}$ borate uncertainty <sup>4</sup>	Temp. (°C)	Sal.	Reference
8.17	20.84	0.34	19.97	0.04	27.72	35.25	ODP 668B, <i>Hönisch et al.</i> , 2009
8.12	20.80	0.22	19.36	0.04	25.8	40.02	GeoB 5810 <sup>6</sup>
8.14	20.66	0.28	19.69	0.04	29.14	34.3	RC10-139, <i>Hönisch and Hemming</i> , 2004
8.14	20.49	0.19	19.61	0.04	28.45	34.42	V34-54, <i>Hönisch and Hemming</i> , 2004
8.07	20.42	0.19	18.77	0.03	27.63	35.82	ODP 999A <sup>6</sup>

<b>Core top details</b>				
Core	Latitude	Longitude	Sample	<i>T. sacculifer</i> size fraction ( $\mu\text{m}$ )
GeoB 5810	29.56°N	35.02°E	10-20 cm	450-500
ODP 999A	12.75°N	78.73°W	1-1, 3-5 cm	515-865

<sup>1</sup> All pH values on the total scale.

<sup>2</sup> Culture studies corrected for  $\delta^{11}\text{B}_{\text{sw}}$  where  $\delta^{11}\text{B}_{\text{sw}}$  was different from 39.61‰. *Sanyal et al.* [2001]. In addition, *T. sacculifer*  $\delta^{11}\text{B}$  data from an old NBS 6<sup>3</sup> radius of curvature NTIMS at SUNY Stony Brook corrected by -1.1‰ to be equivalent with  $\delta^{11}\text{B}$  measured on the Triton at LDEO [*Hönisch et al.*, 2009].

<sup>3</sup>  $\delta^{11}\text{B}$  of borate calculated using  $\alpha_{\text{B3-B4}}$  after *Klochko et al.* [2006] and T, S effects on pK\*B after *Dickson* [1990] and *Millero* [1995], with constants corrected after *Rae et al.* [2011] and the isotopic composition of borate calculated using the revised boron isotope mass balance of *Rae* [2018].

<sup>4</sup> The uncertainty in  $\delta^{11}\text{B}_{\text{borate}}$  is based on the pH uncertainty only and does not take into account uncertainties in temperature and salinity.

<sup>5</sup> New cultured *T. sacculifer* data are based on specimens cultured in Puerto Rico in 2010 using methods identical to *Allen et al.* [2012]. Both samples were analyzed on the Triton TIMS at LDEO using established analytical [*Hönisch et al.*, 2009] and cleaning methods [*Russell et al.*, 2004].

<sup>6</sup> Core top  $\delta^{11}\text{B}$  measurements are carried out with the same technique as described in the text, section 2.1. Core locations and samples are described above.

**Table S2.** Summary of peak marine isotope stages (MIS) used to define average data for cross plots and maximum and minimum pCO<sub>2</sub> estimated for each stage.

MIS	Start age (ka)	End age (ka)	Age (ka)	Glacial pCO <sub>2</sub> (μatm)	Interglacial pCO <sub>2</sub> (μatm)	Comment
44	1370	1385	1384	214		MIS 44 min
45	1395	1410	1397		271	MIS 45 max
			1402		320	
			1408		327	
46	1415	1426	1420	201		MIS 46 min
			1425	234		
47	1436	1450	1441		285	MIS 47 max
			1446		287	
48	1454	1467	1456	237		MIS 48 min
			1459	261		
			1465	249		
49	1485	1491	1487		262	MIS 49 max
			1490		292	
50	1495	1504	1496	201		MIS 50 min
			1499	224		
			1502	183		
51	1514	1527	1516		299	MIS 51 max
			1519		278	
			1522		284	
			1526		306	
52	1537	1542	1539	226		MIS 52 min
			1541	228		

## Supporting Information Reference List

- Allen, K. A., B. Hönisch, S. M. Eggins, and Y. Rosenthal (2012), Environmental controls on B/Ca in calcite tests of the tropical planktic foraminifer species *Globigerinoides ruber* and *Globigerinoides sacculifer*, *Earth and Planetary Science Letters*, 351-352(C), 270–280, doi:10.1016/j.epsl.2012.07.004.
- Anand, P., H. Elderfield, and M. H. Conte (2003), Calibration of Mg/Ca thermometry in planktonic foraminifera from a sediment trap time series, *Paleoceanography*, 18(2), 1050, doi:10.1029/2002PA000846.
- Bartoli, G., B. Hönisch, and R. E. Zeebe (2011), Atmospheric CO<sub>2</sub> decline during the Pliocene intensification of Northern Hemisphere glaciations, *Paleoceanography*, 26(4), PA3206, doi:10.1029/2010PA002055.
- Bemis, B. E., H. J. Spero, J. Bijma, and D. W. Lea (1998), Reevaluation of the oxygen isotopic composition of planktonic foraminifera: Experimental results and revised paleotemperature equations, *Paleoceanography*, 13(2), 150–160, doi:10.1029/98PA00070.
- Bereiter, B., S. Eggleston, J. Schmitt, C. Nehrbass-Ahles, T. F. Stocker, H. Fischer, S. Kipfstuhl, and J. Chappellaz (2015), Revision of the EPICA Dome C CO<sub>2</sub> record from 800 to 600kyr before present, *Geophysical Research Letters*, 42(2), 542–549, doi:10.1002/2014GL061957.
- Bintanja, R., and R. S. W. van de Wal (2008), North American ice-sheet dynamics and the onset of 100,000-year glacial cycles, *Nature*, 454(7206), 869–872, doi:10.1038/nature07158.
- Brennan, S. T., T. K. Lowenstein, and D. I. Cendon (2013), The major-ion composition of Cenozoic seawater: The past 36 million years from fluid inclusions in marine halite, *American Journal of Science*, 313(8), 713–775, doi:10.2475/08.2013.01.
- Chalk, T. B. et al. (2017), Causes of ice age intensification across the Mid-Pleistocene Transition, *PNAS*, 114(50), 13114–13119, doi:10.1073/pnas.1702143114.
- Clark, P. U., D. Archer, D. Pollard, J. D. Blum, J. A. Rial, V. Brovkin, A. C. Mix, N. G. Pisias, and M. Roy (2006), The middle Pleistocene transition: characteristics, mechanisms, and implications for long-term changes in atmospheric pCO<sub>2</sub>, *Quaternary Science Reviews*, 25(23-24), 3150–3184, doi:10.1016/j.quascirev.2006.07.008.
- Dekens, P. S., D. W. Lea, D. K. Pak, and H. J. Spero (2002), Core top calibration of Mg/Ca in tropical foraminifera: Refining paleotemperature estimation, *Geochemistry Geophysics Geosystems*, 3, 1022, doi:10.1029/2001GC000200.
- Delaney, M. L., A. W. H. Bé, and E. A. Boyle (1985), Li, Sr, Mg, and Na in foraminiferal calcite shells from laboratory culture, sediment traps, and sediment cores, *Geochimica et Cosmochimica Acta*, doi:10.1016/0016-7037(85)90284-4.
- Dickson, A. G. (1990), Thermodynamics of the dissociation of boric acid in synthetic seawater from 273.15 to 318.15 K, *Deep-Sea Research II*, 37, 755–766, doi:10.1021/je00061a009.

- Evans, D., and W. Müller (2012), Deep time foraminifera Mg/Ca paleothermometry: Nonlinear correction for secular change in seawater Mg/Ca, *Paleoceanography*, 27(4), PA4205, doi:10.1029/2012PA002315.
- Evans, D., C. M. Brierley, M. E. Raymo, J. Erez, and W. Müller (2016), Planktic foraminifera shell chemistry response to seawater chemistry: Pliocene–Pleistocene seawater Mg/Ca, temperature and sea level change, *Earth and Planetary Science Letters*, 438(C), 139–148, doi:10.1016/j.epsl.2016.01.013.
- Fantle, M. S., and D. J. DePaolo (2006), Sr isotopes and pore fluid chemistry in carbonate sediment of the Ontong Java Plateau: Calcite recrystallization rates and evidence for a rapid rise in seawater Mg over the last 10 million years, *Geochimica et Cosmochimica Acta*, 70(15), 3883–3904.
- Foster, G. L. (2008), Seawater pH, pCO<sub>2</sub> and [CO<sub>3</sub><sup>2-</sup>] variations in the Caribbean Sea over the last 130 kyr: A boron isotope and B/Ca study of planktic foraminifera, *Earth and Planetary Science Letters*, 271(1-4), 254–266, doi:10.1016/j.epsl.2008.04.015.
- Foster, G. L., P. A. E. Pogge von Strandmann, and J. W. B. Rae (2010), Boron and magnesium isotopic composition of seawater, *Geochemistry Geophysics Geosystems*, 11(8), doi:10.1029/2010GC003201.
- Greenop, R., M. P. Hain, S. M. Soshian, K. I. C. Oliver, P. Goodwin, T. B. Chalk, C. H. Lear, P. A. Wilson, and G. L. Foster (2017), A record of Neogene seawater  $\delta^{11}\text{B}$  reconstructed from paired  $\delta^{11}\text{B}$  analyses on benthic and planktic foraminifera, *Climate of the Past*, 13(2), 149–170, doi:10.5194/cp-13-149-2017.
- Groeneveld, J. (2005), Effect of the Pliocene closure of the Panamanian Gateway on Caribbean and east Pacific sea surface temperatures and salinities by applying combined Mg/Ca and, 1–165 pp. Christian Albrechts University, 20 October.
- Hansen, J., M. Sato, G. Russell, and P. Kharecha (2013), Climate sensitivity, sea level and atmospheric carbon dioxide, *Philosophical Transactions of the Royal Society A: Mathematical, Physical and Engineering Sciences*, 371(2001), 20120294–20120294, doi:10.1666/0094-8373(2000)26[259:GCCANA]2.0.CO;2.
- Henehan, M. J. et al. (2013), Calibration of the boron isotope proxy in the planktonic foraminifera *Globigerinoides ruber* for use in palaeo-CO<sub>2</sub> reconstruction, *Earth and Planetary Science Letters*, 364, 111–122, doi:10.1016/j.epsl.2012.12.029.
- Horita, J., H. Zimmermann, and H. D. Holland (2002), Chemical evolution of seawater during the Phanerozoic: Implications from the record of marine evaporites, *Geochimica et Cosmochimica Acta*, 66(21), 3733–3756, doi:10.1016/S0016-7037(01)00884-5.
- Hönisch, B., and N. G. Hemming (2004), Ground-truthing the boron isotope-paleo-pH proxy in planktonic foraminifera shells: Partial dissolution and shell size effects, *Paleoceanography*, 19(4), PA4010, doi:10.1029/2004PA001026.

- Hönisch, B., N. G. Hemming, D. Archer, M. Siddall, and J. F. McManus (2009), Atmospheric carbon dioxide concentration across the mid-Pleistocene transition, *Science*, 324(5934), 1551, doi:10.1126/science.1171477.
- Klochko, K., A. J. Kaufman, W. Yao, R. H. Byrne, and J. A. Tossell (2006), Experimental measurement of boron isotope fractionation in seawater, *Earth and Planetary Science Letters*, 248(1-2), 276–285, doi:10.1016/j.epsl.2006.05.034.
- Lemarchand, D., J. Gaillardet, E. Lewin, and C. J. Allegre (2000), The influence of rivers on marine boron isotopes and implications for reconstructing past ocean pH, *Nature*, 408(6815), 951–954, doi:10.1038/35050058.
- Lisiecki, L. E., and M. E. Raymo (2005), A Pliocene-Pleistocene stack of 57 globally distributed benthic  $\delta^{18}\text{O}$  records, *Paleoceanography*, 20, doi:10.1029/2004PA001071.
- Martin, P. A., and D. W. Lea (2002), A simple evaluation of cleaning procedures on fossil benthic foraminiferal Mg/Ca, *Geochemistry Geophysics Geosystems*, 3(10), 1–8, doi:10.1029/2001GC000280.
- Martínez-Botí, M. A., G. L. Foster, T. B. Chalk, E. J. Rohling, P. F. Sexton, D. J. Lunt, R. D. Pancost, M. P. S. Badger, and D. N. Schmidt (2015), Plio-Pleistocene climate sensitivity evaluated using high-resolution  $\text{CO}_2$  records, *Nature*, 518(7537), 49–54, doi:10.1038/nature14145.
- Medina-Elizalde, M., D. W. Lea, and M. S. Fantle (2008), Implications of seawater Mg/Ca variability for Plio-Pleistocene tropical climate reconstruction, *Earth and Planetary Science Letters*, 269(3-4), 585–595, doi:10.1016/j.epsl.2008.03.014.
- Millero, F. J. (1995), Thermodynamics of the carbon dioxide system in the oceans, *Geochimica et Cosmochimica Acta*, 59(4), 661–677, doi:10.1016/0016-7037(94)00354-o.
- Paillard, D., L. Labeyrie, and P. Yiou (1996), Macintosh Program performs time-series analysis, *Eos Trans. AGU*, 77(39), 379–379, doi:10.1029/96EO00259.
- Pearson, P. N., and M. Palmer (2000), Atmospheric carbon dioxide concentrations over the past 60 million years, *Nature*, 406(6797), 695–699, doi:10.1038/35021000.
- Rae, J. W. B. (2018), Boron Isotopes in Foraminifera: Systematics, Biomineralisation, and  $\text{CO}_2$  Reconstruction, in *Boron Isotopes*, vol. 55, pp. 107–143, Springer International Publishing, Cham, Switzerland.
- Rae, J. W. B., G. L. Foster, D. N. Schmidt, and T. Elliott (2011), Boron isotopes and B/Ca in benthic foraminifera: Proxies for deep ocean carbonate system, *Earth and Planetary Science Letters*, 302(3-4), 403–413, doi:10.1016/j.epsl.2010.12.034.
- Raitzsch, M., and B. Hönisch (2013), Cenozoic boron isotope variations in benthic foraminifers, *Geology*, 41(5), 591–594, doi:10.1130/G34031.1.

- Ridgwell, A. (2005), A Mid Mesozoic Revolution in the regulation of ocean chemistry, *Marine Geology*, 217(3-4), 339–357, doi:10.1016/j.margeo.2004.10.036.
- Russell, A.D., Hönisch, B., Spero, H.J., and D. W. Lea (2004), Effects of seawater carbonate ion concentration and temperature on shell U, Mg, and Sr in cultured planktonic foraminifera, *Geochimica et Cosmochimica Acta*, 68(21), 4347–4361, doi: 10.1016/j.gca.2004.03.013.
- Sanyal, A., J. Bijma, H. J. Spero, and D. W. Lea (2001), Empirical relationship between pH and the boron isotopic composition of *Globigerinoides sacculifer*: Implications for the boron isotope paleo-pH proxy, *Paleoceanography*, 16(5), 515–519, doi:10.1029/2000pa000547.
- Schmidt, M., H. J. Spero, and D. W. Lea (2004), Links between salinity variation in the Caribbean and North Atlantic thermohaline circulation, *Nature*, 428, 160–163, doi:10.1038/nature02346.
- Schmidt, G. A. et al. (2017), Overestimate of committed warming, *Nature*, 547(7662), E16–E17, doi:10.1038/nature22803.
- Seki, O., G. L. Foster, D. N. Schmidt, A. Mackensen, K. Kawamura, and R. D. Pancost (2010), Alkenone and boron-based Pliocene pCO<sub>2</sub> records, *Earth and Planetary Science Letters*, 292(1-2), 201–211, doi:10.1016/j.epsl.2010.01.037.
- Shackleton, N. J., A. L. Berger, and W. Peltier (1990), An alternative astronomical calibration of the lower Pleistocene timescale based on ODP Site 677, *Trans. R. Soc. Edinburgh Earth Sci*, 81, 251–261, doi:10.1017/s0263593300020782.
- Shipboard Scientific Party (1988), Site 668, in *Proceedings of the Ocean Drilling Program, Initial Reports*, vol. 108, edited by W. Ruddiman, M. Sarnthein, J. Baldauf, et al., pp. 931–946, Ocean Drilling Program, College Station, TX.
- Steph, S., R. Tiedemann, M. Prange, J. Groeneveld, D. Nürnberg, L. Reuning, M. Schulz, and G. H. Haug (2006), Changes in Caribbean surface hydrography during the Pliocene shoaling of the Central American Seaway, *Paleoceanography*, 21(4), 1–25, doi:10.1029/2004PA001092.
- Tyrrell, T., and R. E. Zeebe (2004), History of carbonate ion concentration over the last 100 million years, *Geochimica et Cosmochimica Acta*, 68(17), 3521–3530, doi:10.1016/j.gca.2004.02.018.